Synthesis and Characterization of Ammonium Ionenes Containing Hydrogen Bonding Functionalities

Mana Tamami

Dissertation submitted to the faculty of the Virginia Polytechnic Institute and State University in partial fulfillment of the requirements for the degree of

Doctor of Philosophy
in
Chemistry

Timothy E. Long, Chair

Garth L. Wilkes

Robert B. Moore

S. Richard Turner

Susan E. Duncan

December 6, 2012

Blacksburg, Virginia

Keywords: Segmented ionenes, non-segmented ionenes, nucleobase, hydrogen bonding, Michael addition, self-healing, bio-adhesion, molecular recognition, step-growth polymerization, non-covalent interactions

Synthesis and Characterization of Ammonium Ionenes Containing Hydrogen Bonding Functionalities

Mana Tamami

Abstract

Ammonium ionenes are polycations that have quaternary nitrogens in their macromolecular backbone and are synthesized via step-growth polymerization technique. They offer interesting coulombic properties, and the synthetic design provides control over charge density. Non-covalent interactions including nucleobase hydrogen bonding and electrostatics were studied in ammonium ionenes. The non-covalent interactions are expected to increase the effective molecular weight of polymeric precursors and induce microphase separation due to intermolecular associations. The influence of non-covalent interactions on structure-property relationships of ammonium ionenes were studied regarding mechanical (tensile, DMA), thermal (DSC, TGA), and morphological (AFM, SAXS) properties.

Hydrogen bonding interaction (10-40 kJ/mol) was introduced using DNA nucleobase pairs such as adenine and thymine. Novel adenine and thymine functionalized segmented and non-segmented ammonium ionenes were successfully synthesized using Michael addition chemistry. In non-segmented systems, we investigated the influence of spacer length on homoassociation and heteroassociation of complementary nucleobase-containing ionenes. Based on DSC analyses, complementary non-segmented ionenes made miscible blends. The T_gs of ionene blends with shorter spacer length (4 bonds between the nucleobase and secondary amine in the

polymer backbone) followed the Fox equation, which indicated no intermolecular interactions. The longer alkyl spacer (9 bonds between nucleobase and secondary amine in the polymer backbone) provided efficient flexibility for the self-assembly process to occur. Thus, increasing the spacer length from 4-bonds to 9-bonds, the T_gs of the blends deviated from both Fox and Gordon-Taylor equations and demonstrated the presence of hydrogen bonding interactions.

In segmented systems, we investigated the association between nucleobase-containing ionenes and their complementary guest molecules. Job's method revealed a 1:1 stoichiometry for the hydrogen-bonded complexes. These association constants for the 1:1 complexes, based on the Benesi-Hildebrand model were 94 and 130 M^{-1} respectively, which were in agreement with literature values for adenine and thymine nucleobase pairs (10-100 M^{-1}). DSC thermograms confirmed no macrophase separation for 1:1 [ionene-A/T]:[guest molecule] complexes based on the disappearance of the melting peak of the guest molecule. Morphological studies including atomic force microscopy (AFM) demonstrated a reduced degree of microphase separation for the 1:1 complexes due to the disruption of adenine-adenine or thymine-thymine interactions.

Poly(dimethyl siloxane)-based ammonium ionenes having various hard segment contents were synthesized. The charge density or hard segment content was tuned for appropriate application using low molecular weight monomer. The change in hard segment content had a profound effect on thermal, mechanical, rheological, and gas permeability. Microphase separation was confirmed using DSC and DMA in these systems. DMA showed that the rubbery plateau modulus extended to higher temperatures with increasing hard segment content. Tensile analysis demonstrated systematic increase in modulus of PDMS-ionenes with increasing hard segment content. Oxygen transmission rates decreased linearly as the wt% hard segment increased.

Acknowledgements

I would like to thank my advisor, Prof. Timothy E. Long, for his guidance, encouragement, and support over the course of my graduate career. I am grateful to work under his supervision; he taught me polymer science, to be a good researcher, presenter, and a teacher. I would also like to thank my committee members for their participation and support. I would like to express my special thanks to Prof. Garth Wilkes for his helpful discussions and constant guidance. He has been an insightful and helpful committee member and teacher during my graduate career. I would never forget his kindness and support throughout my graduate career. I would also like to thank Prof. S. Richard Turner for his helpful guidance and helping me with job opportunities in industry. I would like to thank Prof. Robert B. Moore for his guidance and close research collaboration. I would also like to thank Prof. Susan Duncan for her helpful guidance and direction during the MILES program. I would like to thank Victoria Long for teaching me technical writing skills and organizing summer group meeting events. I would also like to thank Naya Sou, Valerie Owens, Laurie Good, and Tammy Jo Hiner. The staffs at Virginia Tech have been a great resource. I would especially like to acknowledge Steve McCartney and John McIntosh for their help with AFM and TEM imaging. Geno Iannacone, Hugo Azurmendi, and John Burleson have also been very helpful with NMR spectroscopy.

I would like to thank my manager, Dr. Guiru Zhang during the three-month summer internship program at Proctor & Gamble in Cincinnati, OH in 2010. He was a knowledgeable scientist and a great mentor. I also would like to thank our collaborators in SHIELD project including Dr. Vishnu Baba Sundaresan and Andrew Morgan from Virginia Commonwealth University. I would like to thank collaborations with Prof. Karen Winey and David Salas-de la

Cruz from University of Pennsylvania. I acknowledge the funding source from Kimberly-Clark and special thanks to Dr. Clay Bunyard from Kimberly-Clark and Prof. Michael Rubinstein from the University of North Carolina as a consultant on the project.

I would like to thank all my group members, previous and present, for their advice, encouragement, discussions, time, and support including Dr. Sharlene Williams, Dr. Rebecca Huyck, Erika Borgerding, Dr. Gozde Ozturk, Dr. Tomonori Saito, Dr. Akshay Kokil, Dr. Sean Ramirez, Dr. Matthew Hunley, Dr. Mathew Green, Dr. Mathew Cashion, Dr. Askim Senyurt, Dr. Bill Heath, Dr. Emily Anderson, Dr. Andy Duncan, Dr. Steve June, Dr. Shijing Cheng, Tianyu Wu, Nancy Zhang, Dr. Renlong Gao, Ali Nebipasagil, Dr. Philippe Bissel, Dr. Takeo Suga, Dr. John Layman, Mike Allen, Sean Hemp, Dr. Adam Smith, Keren Zhang, Chanika Jangu, Ashley Nelson, Alex Fersner, Dan Buckwalter, Dr. Daisuke Yamamato, Dr. Erin Murphy, Evan Margaretta, David Inglefield, and Alison Schultz.

Finally, I am forever grateful to my family: Afsaneh, Bahman, and Mehrnaz for their continued love and support in my life endeavors. I am deeply thankful to my father, Prof. Bahman Tamami, he is my role model, a great mentor and a true scientist. Words cannot express my love for him. With all my heart I would like to make him proud and thank him for all his support throughout the years. I cannot ever forget my parents' sacrifices to provide me encouragement and motivation to pursue my goals. I would be nothing without them on the journey of life. Finally, I would like to thank my very dear friend Dr. Anton Sizovs for his help and support during the hardest times of my graduate career, he was my inspiration.

TABLE OF CONTENTS

LIST OF FIGURES

LIST OF SCHEMES

LIST OF TABLES

Chapter 1. Introduction

1.1. Dissertation Overview

The effect of non-covalent interactions, electrostatics and hydrogen bonding on structure-property relationships of ammonium ionenes was studied in this dissertation. Following this chapter, the role of hydrogen bonding interactions and supramolecular assembly on the design of adhesives was reviewed. The third chapter describes the synthesis and characterization of non-segmented adenine- and thymine-containing ionenes having various side-chain spacer lengths. The spacer length is the distance between ionene backbone and nucleobase in the side chain. In the beginning, the synthesis of novel ditertiary amine monomers containing vinyl side groups, their subsequent polymerization with an alkyl dihalide, followed by the post-polymerization functionalization with nucleobases is discussed. Following the functionalization, the effect of spacer length on the complementary hydrogen bonding interaction in the blends was investigated. This investigation was mainly on studying the trend in glass transition temperatures of blends containing various molar ratios of complementary ionene components.

The fourth chapter illustrates the synthesis and characterization of segmented poly(ethylene glycol)-based ammonium ionenes functionalized with adenine and thymine nucleobases. In the beginning of this chapter the synthesis of PEG-based ionene followed by the post-polymerization functionalization with nucleobases is explained. Due to enhanced solubility of the segmented systems (compared to non-segmented) in nonpolar solvents such as chloroform, an extensive ^{1}H NMR titration studies were performed in $CDCl_3$. Using ^{1}H NMR titatrion results, the stoichiometry of 1:1 complexes between nucleobase-containing ionenes and complementary guest molecules was measured by Job's method. In addition, association constants were

calculated for 1:1 complexes and compared with current literature values for adenine-thymine association.

The fifth chapter focuses on the synthesis and structure-property relationships of poly(dimethyl siloxane)-based ionene copolymers. The thermomechanical properties as well as gas permeability were evaluated as a function of hard segment content. This project was based on collaboration between Virginia CommonWealth University and Astro Terra Corp. One of the project objectives was to synthesize PDMS-based ionenes for self-healing inflatable modules as an alternative to Surlyn®. This project was funded through NASA STTR program administered by Johnson Space Center under the Contract No. NNX11CI22P for the project titled "Self-healing Inflatable Extraterrestrial shieLD (SHIELD)"

The sixth chapter summarizes the dissertation accomplishments and the seventh chapter describes potential future work.

Chapter 2. Role of Intermolecular Interactions in Adhesive Design

Mana Tamami and Timothy E. Long*

Macromolecules and Interfaces Institute, Department of Chemistry, Virginia Tech, Blacksburg, VA 24061, USA

*E-mail address: telong@vt.edu

2.1. Abstract

Adhesion involves molecular interactions at the interface between two surfaces. The focus of this review article is on physical adhesion that involves the use of non-covalent interactions. These interactions include van der Waals, electrostatics, hydrogen bonding, and supramolecular associations. Herein, we briefly discuss the gecko feet inspired high adhesive superhydrophobic surface properties. We then mainly summarize the recent work in the use of polymers having supramolecular interactions and hydrogen bonding interactions for adhesion applications. In the end, we cover adhesive polymers that are applicable to biomedical areas.

2.2. Definition of adhesion

Adhesion involves the tendency of dissimilar atoms or molecules to stick to each other and cohesion relates to like materials sticking together. The area of adhesion focuses on formation of adhesion or cohesion, characterization of the adhesive or cohesive interfaces, destruction of the interfaces, and the failure analysis of interfaces.[1] Based on the type of bonding (physical, chemical, mechanical) across the interface, the adhesion or cohesion is categorized. The physical adhesion is the weakest interfacial force and is due to van der Waals forces, electrostatic interactions, supramolecular interactions, and hydrogen bonding. Chemical adhesion involves covalent, metallic, and chelation bonding. Mechanical adhesion is the strongest among all, is

very common, and involves the adhesive penetrating into the adherent and become mechanically interlocked, for example, dental cements that fill in the coarseness of the castings and help to retain them.[2, 3]

2.3. Physical adhesion

2.3.1. Adhesion using van der Waals interactions

Geckos are lizards that possess unique adhesive characteristic known in nature. Geckos along with many other small insects use seta or fibrillar structures on their feet to adhere to different surfaces (Figure 2.1).[4, 5] Setal adhesion has unique properties compared to other common adhesives like pressure sensitive adhesives (PSAs). These properties include; adhesion surfaces remaining clean and reusable, adhesion being directional, and adhesion having controlled "lift-off mechanism".[6, 7] Many experiments have been performed to investigate the possible mechanism behind setal adhesion. The hypotheses were secretion of a glue, suction, electrostatics, and intermolecular forces. However, enough evidence demonstrates that setal adhesion mainly uses van der Waals interactions which are as a result of the size and shape of tips and the adhesion is not governed by surface chemistry.[8] The van der Waals forces are strong enough to allow the gecko to climb vertical walls. This type of adhesion has inspired many researchers to develop synthetic materials that show unique properties similar to setal or fibrillar adhesives.

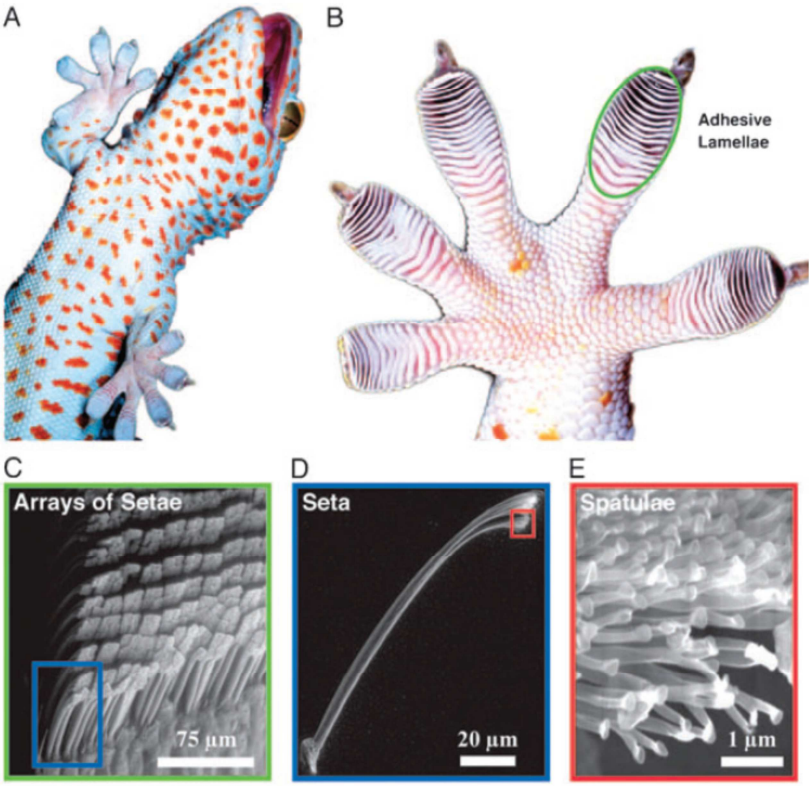

Figure 2.1. Fibrillar structure on the bottom of gecko's foot. A) Ventral view of tokay gecko while climbing on the glass B) Ventral view of gecko's foot with adhesive lamellae C) Single lamellae with an array of individual setaes D)Single seta with branched structure at the end E) Spatular tips at the ends of seta.[9]

Inspired by the high adhesive ability of gecko's feet, Choi et al.[10] prepared hairy hard poly(dimethyl siloxane) (PDMS) films containing nanopillars with controllable lengths using nanoporous anodic aluminum oxide membranes as templates. They coated the glass surface with nanostructured hairy PDMS and showed that the water droplets can adhere strongly to the glass surface. The adhesive properties was due to the densely packed nanopillars by generating large van der Waals forces between the large surface area and water molecules that are in close contact.

2.3.2. Adhesion using supramolecular interactions

Hydrogen bonding in contrast to nondirectional interactions such as electrostatics, demonstrate lower enthalpies (10-40 kj/mol) with greater specificity which induces molecular recognition. The strength of hydrogen bonding interactions is highly dependent on the temperature, solvent, humidity, and pH. Therefore, these interactions enable us to synthesize novel architectures that are responsive to environmental parameters. Hydrogen bond containing polymers have many advantages such as enhanced rheological properties due to decrease in melt-viscosity, increase in modulus, tensile strength, polarity, and adhesion.

Recently hydrogen bonding interactions have been used to design supramolecular structures.[11, 12] Supramolecular chemistry in polymers involves the synthesis of macromolecules using secondary interactions between small molecules (monomers) to develop polymer-like structures.[13-15] These secondary interactions can be hydrogen bonding,[16] π-π interactions,[17] metal coordination,[18] electrostatics, and van der Waals interactions. Many researchers have used supramolecular hydrogen bonded polymers[19-30] for various applications; including formation of large vesicles,[12] attach functional small molecules on polymers,[31] and reversibly adhere polymers on to surfaces.[32]

In this section, we will mainly focus on supramolecular polymers that have application in adhesion. Surprisingly, they are few reports on the use of supramolecular chemistry for application in adhesion. One area of adhesives that supramolecuar chemistry can be applied is pressure sensitive adhesives (PSAs). PSAs are usually made from lightly crosslinked polymer networks with a low glass transition temperature (T_g),[7, 33, 34] and bond to many substrates upon applying very low pressure.[35]

Courtois et al.[36] investigated the influence of supramolecular interactions on adhesive properties of functionalized polyisobutene on steel and silicone surfaces. They prepared polyisobutene with a bis-urea moiety in the middle of the chain (PIBUT) (Figure 2.2a). The hydrogen bonding between bis-urea moieties induced supramolecular assembly leading to ordered pattern. They showed that supramolecular polymers modified the rheological properties of low T_g polyisobutene and have promising adhesive applications. PIBUT polymers can dissipate energy upon adhesive debonding and make stronger interactions with substrates such as silicone compared to acrylic-based PSAs.[37]

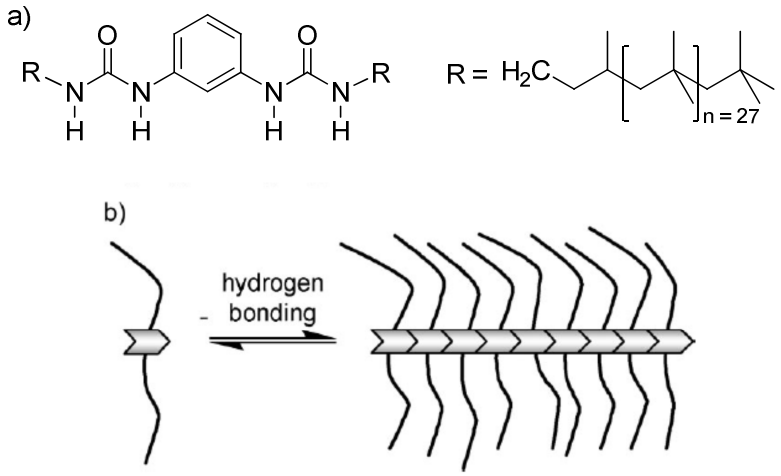

Figure 2.2. a) Structure of polyisobutylene (PIBUT) containing bis-urea moiety. b) Supramolecular structure of PIBUT in solution[36]

Supramolecular interactions are also present in systems containing complementary hydrogen bonding moieties. One category of bio-inspired complementary units include DNA nucleobases such as adenine, thymine, cytosine, and guanine. Long et al.[38] synthesized acrylic nucleobase-containing copolymers using radical polymerization (Figure 2.3). They synthesized novel acrylic adenine and thymine monomers using aza-Michael addition and then copolymerized with *n*-butyl acrylate. Adenine-containing polyacrylates demonstrated unique morphologies due to adenine-adenine π-π interactions. The adenine and thymine polymer blend showed the presence of

complementary hydrogen bonding leading to supramolecular structures. In order to measure peel and shear strengths, a strip of PET film was coated with the hydrogen-bonded polymer (adenine or thymine) and adhered to the same or complementary polymer coated on stainless steel substrate. The hydrogen-bonded supramolecular polymers showed enhanced peel and shear strengths (3-4 times) compared to acrylic acid- and 4-vinylpyridine- based polymer analogues.

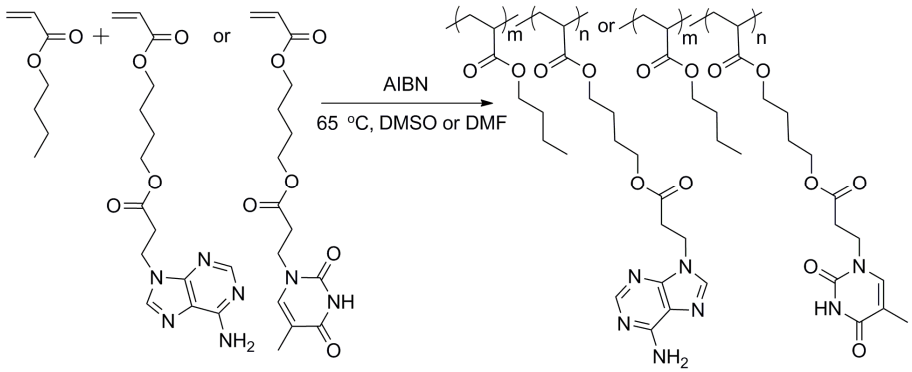

Figure 2.3. Synthesis of adenine- and thymine-containing poly(*n*-butyl acrylate) copolymers[38]

In addition, a limited number of studies referred to supramolecular interactions on surfaces using nucleobase pairs.[39] Long et al.[40] were first to report the modification of silicone surfaces with adenine-containing triethoxysilane (ADPTES). They demonstrated the specific and reversible adhesion of ADPTES silicon surface with complementary thymine-functionalized polystyrene (PS-thymine). The reversibility of adhesion was examined using hydrogen bond disruptive solvent (DMSO). The hydrogen bonding interactions were disrupted while rinsing the surface with aprotic DMSO and were reformed following the removal of DMSO and addition of chloroform (Figure 2.4). This behavior demonstrated the reversibility nature of the adenine and thymine association. These polymers that show reversible interactions with solid surfaces have potential application in releasable coatings and smart adhesives.

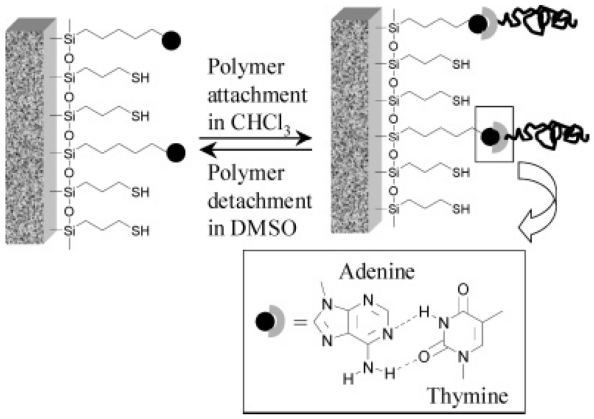

Figure 2.4. Molecular recognition between adenine-functionalized silicone surface and thymine-containing polystyrene[40]

2.3.3. Adhesion using hydrogen bonding interactions

Hydrogen bonding association provides strategies to increase the apparent molecular weight after application. These interactions are used to design adhesives and prevent creep and cohesive failure. Poly(acrylic acids) (PAAs) contain hydrogen bonding functionalities and are applied in PSA formulations. However, one limitation in PAAs is that they can undergo thermal crosslinking above 150 °C and form intermolecular anhydrides.[41] In hot melt pressure sensitive adhesives (HMPSAs), crosslinking during processing is problematic, therefore PAAs have limited utility. Long et al.[42] synthesized low T_g acrylic copolymers that were functionalized with hydrogen bonding (urethane) groups and photo-reactive (cinnamate) functionalities for HMPSAs application (Figure 2.5). The synergy of these groups resulted in higher peel values. In addition the isothermal rheological studies showed that at 150 °C the copolymer was stable with no crosslinking and therefore has potential in HMPSA application.

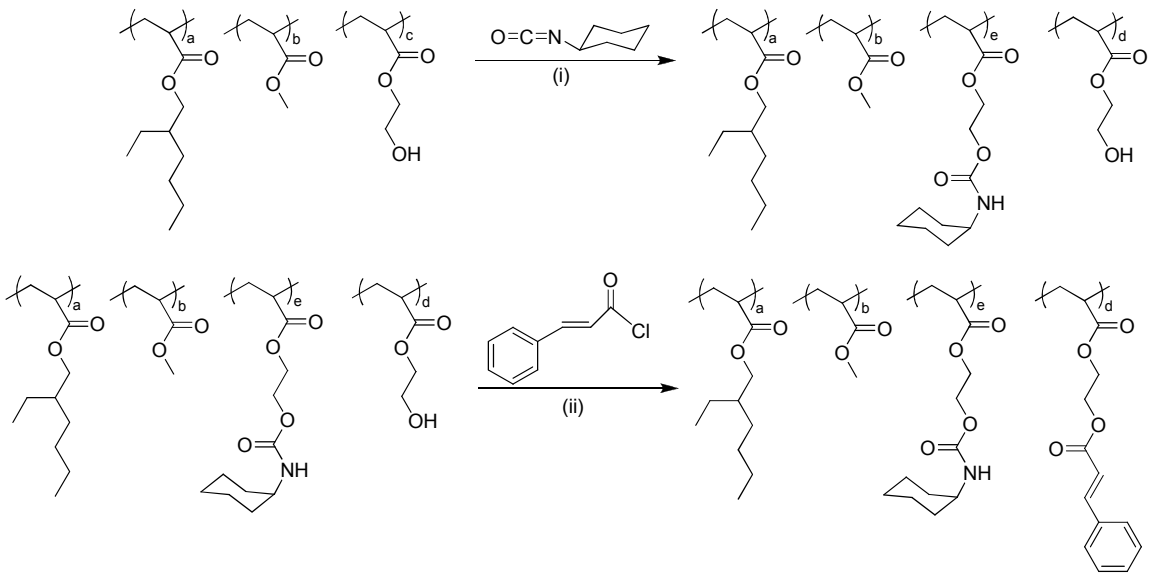

Figure 2.5. Synthesis of photo-curable acrylic copolymer containing hydrogen bonding functionality[42]

Another hot topic in adhesive research is the development of reversible adhesives. In some applications we require debonding of adhesive from adherent when the adhesion is not required at the time.[43] These applications can be removable labels, surface protection films, easily placeable and removable notepaper. Researchers used many strategies to develop reversible adhesives such as using fibrillar structure of a gecko foot,[44] and shape memory effect to induce microscopic or macroscopic change for "self-peel".[45-47] Another strategy is to use theromosensitive polymer to achieve reversible adhesion properties. Hu et al.[48] synthesized poly(vinyl alcohol)-*g*-*N*-isopropylacrylamide PVA-*g*-NIPAM as a novel thermosensitive copolymer membrane with thermally induced adhesion around the lower critical solution temperature (LCST) of 31 °C. At temperatures below LCST, the copolymer becomes more hydrophilic and enhances the adhesion effect and at temperatures above LCST, the copolymer became hydrophobic with decreased adhesion. The adhesive strength of PVA-g-NIPAM was measured for the T-type peel adhesion toward the paper. The adhesive ability of the copolymer was mainly due to the hydrogen bonding interaction between the PVA and cellulose of the paper.

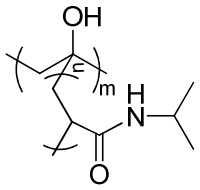

Figure 2.6. Chemical structure of PVA-*g*-NIPAM[48]

Another reversible adhesive system was designed by Xie et al.[49] where they prepared hydrogen bonding-based epoxy thermosets (Figure 2.7). In order to have good adhesion at a solid interface, interfacial contact and good molecular interactions are required. Xie et al. demonstrated that the epoxy thermosets are ideal candidates for reversible adhesion. Firstly, the modulus of epoxy thermosets would drop two orders of magnitude upon glass transition temperature, which would lead to an effective interfacial contact with solid surface.[47] Secondly, the hydrogen bonding moieties will provide the reversibility for adhesion. The adhesion between two identical polymer surfaces was through interfacial hydrogen bonding interaction between the free hydroxyl groups (H-bond doner) and oxygen atoms (H-bond acceptor) in the epoxy.

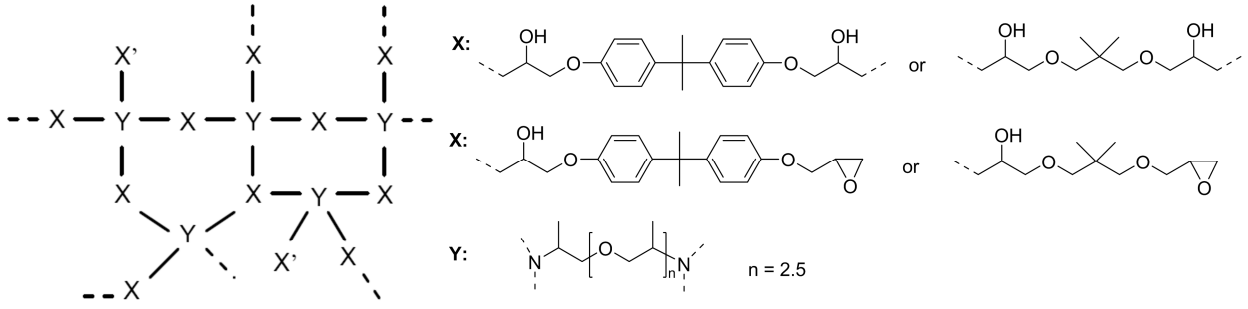

Figure 2.7. Representation of crosslinked epoxy network. Solid line represents covalent bonds and dotted lines represent continuation of covalent bonds[47]

A popular area of adhesion is based on bio-inspired hydrogen-bonded polymers. It has been shown that Mussels can adhere to many organic and inorganic surfaces by producing 3,4-

dihydroxyphenyl-L-alanine which contains catechol groups.[50-53] Although the adhesion mechanism is still not completely understood, but it is hypothesized that adhesion is due to hydrogen bonding interactions between catechol groups and OH-containing substrates. Kaneko et al.[54] synthesized Mussel-mimetic adhesive resin from copolymerization of 3,4-dihydroxycinnamic acid (DHCA) and 4-hydroxycinnamic acid (4HCA) and confirmed it's adhesive properties. The chain-ends of the hyperbranched polymer resin contain catechol moieties which are hydrogen bond donors and can strongly adhere to organic/inorganic surfaces. Since this novel adhesive resin is made from biomass monomers, it is environmentally friendly and non-toxic.

2.4. Adhesive polymers in bio-related fields

2.4.1. Polymers used as substrates for cell adhesion

One of the requirements in the design of many medical devices is to have patterned adhesion of human or animal cells on artificial substrates. There are two routes to perform this process; one way is to attach photoactive proteins or peptides to the substrate and the other way is to either chemically modify the substrate or deposit thiols or silanes on the substrate to adhere biomolecules. Both routes would lead to structured substrates that act as adhesion sites and cells will attach to them via ligand/receptor interactions. Polymers have become unique substrates due to the simplicity of cell adhesion process on to them and also have lower cost.

Welle and Gottwald[55] used commercially available polycarbonate, poly(methyl methacrylate) (PMMA), and polystyrene as substrates for cell adhesion. They exposed the polymeric surfaces to UV light and modified their physical behavior and chemical composition. This led to strong adhesion of hepatocyte and fibroblast cells.

Most implant materials such as polymers, carbon fibers, and metals are nontoxic, biocompatible, and do not degrade in the organism. However, their lifetime can be short due to the improper mechanical contact between implant surface and the regenerating cells. Therefore it is necessary to coat implant surfaces with cell-adhesive molecules or macromolecules to obtain strong mechanical contact between cells and the surface. Kessler et al.[56] showed that functionalization of PMMA surface coated with integrin-selected peptides effectively bind to osteoblast murine and human cells compared to uncoated PMMAs. Ohashi and Dauskardt[57] studied the debonding behavior of prosthetic-PMMA interface. They demonstrated that precoating the surface of the implant with PMMA at higher temperatures would drastically enhance the adhesion and fatigue resistance in both air and physiological conditions.

In order for the biomaterial to be used clinically, not only it needs to have excellent bulk properties, but also surface properties play a major role as well. The initial response of body organisms depends on biomaterial's surface property. Poor adhesion between the biomaterial and the tissue causes numerous complications including infection. However, most polymers need surface modification to be used as biomaterials. One of the ways to do surface modification is by grafting. Grafting can either be through coupling reaction between reactive polymers and functionalized substrate polymer surface or it can be through graft polymerization of monomers. Ikada[58] reviewed surface modification of polymers using different grafting techniques to obtain lubricous, blood compatible or physiologically bioactive polymer surfaces (Figure 2.8).

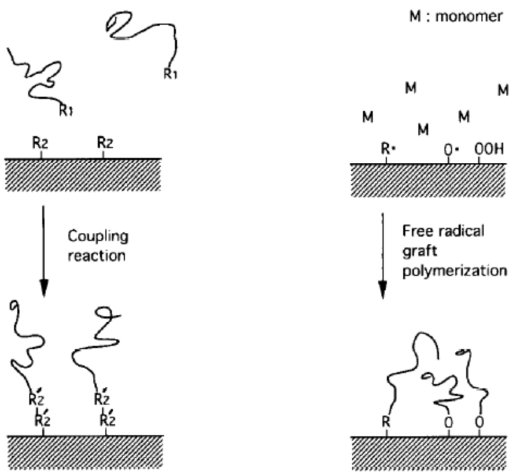

Figure 2.8. Representation of coupling reaction and graft polymerization[58]

Surface modification is also applied to the area of gene delivery. DNA is usually condensed into nanoparticle-sized complexes and is introduced to the culture media (liquid gene transfection or LGT method). However, studies have shown that localized gene delivery to the targeted cells using LGT method is not favorable.[59, 60] Another strategy is to use substrate-mediated delivery, where DNA is attached to the surface of substrate and selective adhesion between the substrate-supported DNA and adherent cells would occur.[61, 62] Liu et al.[63] designed high-strength hydrogels with both hydrogen bonding and thermoresponsive characteristics. The hydrogels were synthesized from copolymerization of N-isopropylacrylamide (NIPAM) and 2-vinyl-4,6-diamino-1,3,5-triazine (VDT) and crosslinked with poly(ethylene glycol) diacrylate. The VDT functionalities contributed to the formation of complementary hydrogen bonding interactions between the substrate and nucleobase pairs.[64-66] The NIPAM components of the hydrogels contributed to the thermoresponsiveness behavior and allowed the adhesion and detachment of cells by temperature change.[67, 68]

2.4.2. Polymers used for mucosal adhesion

When polymeric materials adhere to mucosal tissues is called mucoadhesion. The mucoadhesive polymers have been used to deliver drugs in a controlled-release dosage forms and enhance the bioavailability of the drug for various mucosal tissues such as nasal, gastrointestinal, vaginal, rectal, and ocular.[69-73] Mucoadhesive polymers need to have certain structural properties as listed here; hydrogen bonding groups (hydroxyl, carboxyl, amino, sulphate), ionically charged, high molecular weight, chain flexibility, higher surface energy to spread on mucos. From mucoadhesive polymers, we can name poly(acrylic acid), poly(methacrylic acid), chitosan, cellulose ethers, and sodium alginate. Park et al.[74] illustrated that poly(acrylic acid) hydrogel interacts with mucin glycoproteins using hydrogen bonding interactions. At lower pHs the carboxylic groups are protonated and show strong mucoadhesion, however, at higher pHs the mucoadhesion decreases due to deprotonation of carboxylic groups.

2.5. Conclusions

In this review, we discussed the recent developments in the use of supramolecular chemisty and hydrogen bonding interactions for application in adhesion. Although there were not many reports on the use of supramolecular chemistry for application in adhesion, however, few examples were reported on the use of complementary hydrogen bonding moieties to generate reversible and smart adhesives. Several studies demonstrated the use of hydrogen bonding interactions for adhesion on the surface. We also reviewed reports that studied polymers with unique properties to adhere to cells. These adhesive polymers played a major role in the design of implant materials.

2.6. References

(1) Marshall, S. J.; Bayne, S. C.; Baier, R.; Tomsia, A. P.; Marshall, G. W. *Dent. Mater.* **2010,** 26, e11-6.
(2) Bayne, S.; Taylor, D.; Zardiackas, L., *Biomaterials science*. Brightstar Publishing: Chapel Hill, NC, 1992.
(3) Marshall, G.; Marshall, S., *Biomaterials science for restorative dentistry*. San Francisco: UCSF, 1999.
(4) Arzt, E.; Gorb, S.; Spolenak, R. *Proc. Natl. Acad. Sci. U. S. A.* **2003,** 100, 10603-10606.
(5) Scherge, M.; Gorb, S. N., *Biological micro and nanotribology: Nature's solutions*. Springer: Berlin, 2001.
(6) Autumn, K.; Liang, Y. A.; Hsleh, S. T.; Zesch, W.; Chan, W. P.; Kenny, T. W.; Fearilng, R.; Full, R. J. *Nature (London)* **2000,** 405, 681-686.
(7) Creton, C. *MRS Bull.* **2003,** 28, 434-439.
(8) Autumn, K.; Sitti, M.; Liang, Y. A.; Peattie, A. M.; Hansen, W. R.; Sponberg, S.; Kenny, T. W.; Fearing, R.; Israelachvili, J. N.; Full, R. J. *Proc. Natl. Acad. Sci. U. S. A.* **2002,** 99, 12252-12256.
(9) Liu, K.; Yao, X.; Jiang, L. *Chem. Soc. Rev.* **2010,** 39, (8), 3240-3255.
(10) Cho, W. K.; Choi, I. S. *Adv. Funct. Mater.* **2008,** 18, 1089-1096.
(11) Brunsveld, L.; Folmer, B. J. B.; Meijer, E. W.; Sijbesma, R. P. *Chem. Rev* **2001,** 101, 4071-4097.
(12) Ilhan, F.; Galow, T. H.; Gray, M.; Clavier, G.; Rotello, V. M. *J. Am. Chem. Soc.* **2000,** 122, 5895-5896.
(13) Bosman, A. W.; Brunsveld, L.; Folmer, B. J. B.; Sijbesma, R. P.; Meijer, E. W. *Macromol. Symp.* **2003,** 201, 143-154.
(14) Shimizu, L. S. *Polym. Int.* **2007,** 56, 444-452.
(15) Fox, J. D.; Rowan, S. J. *Macromolecules (Washington, DC, U. S.)* **2009,** 42, 6823-6835.
(16) Sijbesma, R. P.; Beijer, F. H.; Brunsveld, L.; Folmer, B. J. B.; Hirschberg, J. H. K. K.; Lange, R. F. M.; Lowe, J. K. L.; Meijer, E. W. *Science* **1997,** 278, 1601-1604.
(17) Adam, D.; Schuhmacher, P.; Simmerer, J.; Haeussling, L.; Siemensmeyer, K.; Etzbach, K. H.; Ringsdorf, H.; Haarer, D. *Nature (London)* **1994,** 371, 141-3.
(18) Michelsen, U.; Hunter, C. A. *Angew. Chem., Int. Ed.* **2000,** 39, 764-767.
(19) Keeling, D. L.; Oxtoby, N. S.; Wilson, C.; Humphry, M. J.; Champness, N. R.; Beton, P. H. *Nano Lett.* **2003,** 3, 9-12.
(20) De, F. S.; Miura, A.; Yao, S.; Chen, Z.; Wuerthner, F.; Jonkheijm, P.; Schenning, A. P. H. J.; Meijer, E. W.; De, S. F. C. *Nano Lett.* **2005,** 5, 77-81.
(21) Kihara, H.; Kato, T.; Uryu, T.; Frechet, J. M. J. *Chem. Mater.* **1996,** 8, 961-8.
(22) Kato, T.; Frechet, J. M. J. *Macromolecules* **1989,** 22, 3818-19.
(23) MacDonald, J. C.; Whitesides, G. M. *Chem. Rev. (Washington, D. C.)* **1994,** 94, 2383-420.
(24) Schwiebert, K. E.; Chin, D. N.; MacDonald, J. C.; Whitesides, G. M. *J. Am. Chem. Soc.* **1996,** 118, 4018-29.
(25) Fouquey, C.; Lehn, J. M.; Levelut, A. M. *Adv. Mater. (Weinheim, Fed. Repub. Ger.)* **1990,** 2, 254-7.
(26) Kotera, M.; Lehn, J. M.; Vigneron, J. P. *J. Chem. Soc., Chem. Commun.* **1994**, 197-9.

(27) Sijbesma, R. P.; Beijer, F. H.; Brunsveld, L.; Folmer, B. J. B.; Hirschberg, J. H. K. K.; Lange, R. F. M.; Lowe, J. K. L.; Meijer, E. W. *Science (Washington, D. C.)* **1997,** 278, 1601-1604.
(28) Ligthart, G. B. W. L.; Ohkawa, H.; Sijbesma, R. P.; Meijer, E. W. *J. Am. Chem. Soc.* **2005,** 127, 810-811.
(29) Shenhar, R.; Sanyal, A.; Uzun, O.; Nakade, H.; Rotello, V. M. *Macromolecules* **2004,** 37, 4931-4939.
(30) Park, T.; Zimmerman, S. C.; Nakashima, S. *J. Am. Chem. Soc.* **2005,** 127, 6520-6521.
(31) Ilhan, F.; Gray, M.; Rotello, V. M. *Macromolecules* **2001,** 34, 2597-2601.
(32) Norsten, T. B.; Jeoung, E.; Thibault, R. J.; Rotello, V. M. *Langmuir* **2003,** 19, 7089-7093.
(33) Zosel, A. *Colloid Polym. Sci.* **1985,** 263, 541-53.
(34) Zosel, A. In *Fracture energy and tack of pressure-sensitive adhesives*, 1992; Satas Assoc.: 1992; pp 92-127.
(35) Benedek, I., *Pressure-sensitive adhesives and applications*. Marcel Dekker: New York, 2004.
(36) Courtois, J.; Baroudi, I.; Nouvel, N.; Degrandi, E.; Pensec, S.; Ducouret, G.; Chaneac, C.; Bouteiller, L.; Creton, C. *Adv. Funct. Mater.* **2010,** 20, 1803-1811.
(37) Gower, M. D.; Shanks, R. A. *J. Polym. Sci., Part B: Polym. Phys.* **2006,** 44, 1237-1252.
(38) Cheng, S.; Zhang, M.; Dixit, N.; Moore, R. B.; Long, T. E. *Macromolecules* **2012,** 45, 805-812.
(39) Park, J. S.; Lee, G. S.; Lee, Y.-J.; Park, Y. S.; Yoon, K. B. *J. Am. Chem. Soc.* **2002,** 124, 13366-13367.
(40) Viswanathan, K.; Ozhalici, H.; Elkins, C. L.; Heisey, C.; Ward, T. C.; Long, T. E. *Langmuir* **2006,** 22, 1099-1105.
(41) Maurer, J. J.; Eustace, D. J.; Ratcliffe, C. T. *Macromolecules* **1987,** 20, 196-202.
(42) Cashion, M. P.; Park, T.; Long, T. E. *J. Adhes.* **2009,** 85, 1-17.
(43) Creton, C.; Papon, E. *MRS Bull.* **2003,** 28, 419-421.
(44) del, C. A.; Arzt, E. *Macromol. Biosci.* **2007,** 7, 118-127.
(45) Kim, S.; Sitti, M.; Xie, T.; Xiao, X. *Soft Matter* **2009,** 5, 3689-3693.
(46) Reddy, S.; Arzt, E.; del, C. A. *Adv. Mater. (Weinheim, Ger.)* **2007,** 19, 3833-3837.
(47) Xie, T.; Xiao, X. *Chem. Mater.* **2008,** 20, 2866-2868.
(48) Yang, J.; Hu, D.-D.; Zhang, H. *React. Funct. Polym.* **2012,** 72, 438-445.
(49) Wang, R.; Xie, T. *Langmuir* **2010,** 26, 2999-3002.
(50) Waite, J. H.; Tanzer, M. L. *Science (Washington, D. C., 1883-)* **1981,** 212, 1038-40.
(51) Lin, Q.; Gourdon, D.; Sun, C.; Holten-Andersen, N.; Anderson, T. H.; Waite, J. H.; Israelachvili, J. N. *Proc. Natl. Acad. Sci. U. S. A.* **2007,** 104, 3782-3786.
(52) Yu, M.; Deming, T. J. *Macromolecules* **1998,** 31, 4739-4745.
(53) Yu, M.; Hwang, J.; Deming, T. J. *J. Am. Chem. Soc.* **1999,** 121, 5825-5826.
(54) Kaneko, D.; Wang, S.; Matsumoto, K.; Kinugawa, S.; Yasaki, K.; Chi, D. H.; Kaneko, T. *Polym. J. (Tokyo, Jpn.)* **2011,** 43, 855-858.
(55) Welle, A.; Gottwald, E. *Biomed. Microdevices* **2002,** 4, (1), 33-41.
(56) Kantlehner, M.; Schaffner, P.; Finsinger, D.; Meyer, J.; Jonczyk, A.; Diefenbach, B.; Nies, B.; Hölzemann, G.; Goodman, S. L.; Kessler, H. *ChemBioChem* **2000,** 1, (2), 107-114.
(57) Ohashi, K. L.; Dauskardt, R. H. *J. Biomed. Mater. Res.* **2000,** 51, (2), 172-183.
(58) Ikada, Y. *Biomaterials* **1994,** 15, 725-36.

(59) Bonadio, J. *Adv. Drug Delivery Rev.* **2000,** 44, 185-194.
(60) De, L. L.; Lei, Y. A.; Shea, L. D. *Biomaterials* **2009,** 30, 2361-2368.
(61) Erfle, H.; Neumann, B.; Liebel, U.; Rogers, P.; Held, M.; Walter, T.; Ellenberg, J.; Pepperkok, R. *Nat. Protoc.* **2007,** 2, 392-399.
(62) Rea, J. C.; Gibly, R. F.; Davis, N. E.; Barron, A. E.; Shea, L. D. *Biomacromolecules* **2009,** 10, 2779-2786.
(63) Tang, L.; Liu, W.; Liu, G. *Adv. Mater. (Weinheim, Ger.)* **2010,** 22, 2652-2656.
(64) Asanuma, H.; Ban, T.; Gotoh, S.; Hishiya, T.; Komiyama, M. *Macromolecules* **1998,** 31, 371-377.
(65) Fujimori, A.; Sato, N.; Kanai, K.; Ouchi, Y.; Seki, K. *Langmuir* **2009,** 25, 1112-1121.
(66) Janssen, P. G. A.; van, D. J. L. J.; Meijer, E. W.; Schenning, A. P. H. J. *Chem.--Eur. J.* **2009,** 15, 352-360.
(67) Hou, Y.; Matthews, A. R.; Smitherman, A. M.; Bulick, A. S.; Hahn, M. S.; Hou, H.; Han, A.; Grunlan, M. A. *Biomaterials* **2008,** 29, 3175-3184.
(68) Alexander, C.; Shakesheff, K. M. *Adv. Mater. (Weinheim, Ger.)* **2006,** 18, 3321-3328.
(69) Edsman, K.; Hagerstrom, H. *J. Pharm. Pharmacol.* **2005,** 57, 3-22.
(70) Grabovac, V.; Guggi, D.; Bernkop-Schnuerch, A. *Adv. Drug Delivery Rev.* **2005,** 57, 1713-1723.
(71) Harding, S. E. *Biochem. Soc. Trans.* **2003,** 31, 1036-1041.
(72) Jung, Y. J.; Lee, J. S.; Kim, Y. M. *J. Pharm. Sci.* **2000,** 89, 594-602.
(73) Smart, J. D. *Adv. Drug Delivery Rev.* **2005,** 57, 1556-1568.
(74) Park, H.; Robinson, J. R. *Pharm. Res.* **1987,** 4, 457-64.

Chapter 3. Effect of Spacer Length on Association of Nucleobase-Containing Ammonium Ionenes

Mana Tamami, Keren Zhang, Ninad Dixit, Amanda Hudson, Robert B. Moore, and Timothy E. Long*

Macromolecules and Interfaces Institute, Department of Chemistry, Virginia Tech, Blacksburg, VA 24061, USA

*E-mail address: telong@vt.edu

3.1. Abstract

Adenine and thymine functionalized ammonium ionenes having shorter (4-bonds) and longer (9-bonds) side chain spacer lengths were successfully synthesized using Michael addition chemistry. Herein, we investigated the influence of spacer length on homoassociation and heteroassociation of complementary nucleobase-containing ionenes. The films of ionene homopolymers and blends having various side chain spacer lengths showed a single glass transition temperature. Higher glass transition temperatures were observed for the shorter spacer films of ionene homopolymers and the blends. The hydrogen bonding interaction in the blends of adenine-containing ionene (ionene-A) and thymine-containing ionene (ionene-T) having shorter spacer length as well as the blends of ionene-A with ionene-T having longer spacer length was studied using differential scanning calorimetry (DSC), fourier-transform infrared (FT-IR) spectroscopy and atomic force microscopy (AFM). DSC analyses showed no hydrogen bonding interactions in the ionene blends with shorter spacer length. The longer spacer length ionene blends showed the presence of hydrogen bonding interaction and demonstrated that the homoassociation is stronger than heteroassociation. FT-IR confirmed hydrogen bonding interactions for the longer spacer ionene blends.

Keywords: non-segmented ionenes, nucleobases, hydrogen bonding, miscibility, spacer length

3.2. Introduction

Ionenes are polyelectrolytes that have regularly placed quaternary nitrogen atoms in their macromolecular backbone. Gibbs et al.[1] were first to synthesize this type of polycations from dimethylamino-*n*-alkyl halides. Ionenes are usually synthesized from a reaction of a ditertiary amine and a dihalide called a Menschutkin reaction.[2] The ionene is named from the number of methylene spacers, which correspond to the diamine and dihalide monomers, respectively (i.e. x,y-ionene).

The introduction of non-covalent interactions such as hydrogen bonding has recently received increasing attention due to the construction and design of supramolecular polymers.[3, 4] Hydrogen bonding provides thermoreversible characteristics for macromolecules through non-covalent intermolecular interactions.[5] Herein, we introduced hydrogen bonding interactions into ionenes through complementary hetereocyclic DNA nucleobases such as adenine and thymine. The association strength for DNA base pairs is in the order of 10^2 M^{-1} magnitude.[6, 7] However, structural design of hydrogen-bonded polymers influences the strength of complementary hydrogen bonding interactions.

There are many reports on the effect of the placement of hydrogen bonding motifs on either the chain ends of polymers[8-11] or polymer side chains.[12-14] Chang et al.[15] utilized the Michael addition reaction to functionalize poly(ε-caprolactone) chain ends with adenine and uracil heteronucleobases. They studied the self-assembly behavior of the functionalized pol(ε-caprolactone) on solution and solid state properties. Long et al.[16] also synthesized four-arm, star-shaped poly(D,L-lactide) (PDLLA) functionalized with complementary adenine (A) and thymine (T) nucleobase pairs to obtain PDLLA-A and PDLLA-T. They demonstrated a 1:1

stoichiometry and an association constant (K_a) of 84 M^{-1} for the A-T complexes. Rowan et al.[17] reported the supramolecular polymerization of adenine and cytosine-terminated poly(tetrahydrofuran) macromonomers. These macromonomers self-assembeled in the solid-state and yielded film and fiber-forming materials. Long et al.[12] synthesized and characterized nucleobase-functionalized triblock copolymers having styrene outer blocks and a *n*-butyl acrylate center block. These copolymers had nucleobase functionalities as side groups on the styrene outer blocks.

Recently Meijer et al.[18] prepared poly(*n*-butyl acrylate) (P*n*BA) functionalized with ureido-pyrimidinone (UPy) units using ATRP. They investigated the effect of side chain spacer length on the homoassociation and heteroassociation of UPy-containing P*n*BA. The homoassociation and hetereassociation of UPy-containing P*n*BA decreased for the shorter spacer (C_2) due to competitive non-covalent intramolecular interactions and no change in the association strength was observed for the longer aliphatic spacer (C_6).

Herein, we synthesized non-segmented ionenes and functionalized the side chains with adenine and thymine units using Michael addition. We investigated the effect of spacer length (4-bond spacer versus 9-bond spacer) on the association of complementary ionene chains. In these systems, the spacer is the length of aliphatic unit between the ionene backbone and the nucleobase. The influence of complementary hydrogen bond interactions for the ionene blends having 9-bond spacer was clearly observed on thermal and morphological properties. Infrared spectroscopy monitored the thermoreversibility of ionene blends using variable temperature (30 °C to 170 °C).

3.3. Experimental

3.3.1. Materials

Adenine (A, 99%), thymine (T, 99%), potassium tert-butoxide (99.99%), sodium bicarbonate (99.7%), magnesium sulfate (99.5%), γ- butyrolactone (+99%) and diisobutylalumium hydride 1.0 M solution in toluene were purchased from Sigma-Aldrich and used without further purification. 3,3-Iminobis(N,N-dimethylpropylamine) (97%), acryloyl chloride (97%), triethylamine (TEA, 99%) were purchased from Aldrich and vacuum distilled. 1,12-Dibromododecane (98%) was purchased from Sigma-Aldrich and sublimed before use. Dichloromethane (DCM, HPLC grade), tetrahydrofuran (THF, HPLC grade), dimethyl formamide (DMF, HPLC grade) were passed through columns packed with alumina and molecular sieves before use. Chloroform ($CHCl_3$, HPLC grade) and ethyl acetate (EtOAc, HPLC grade) were purchased from Fischer Scientific and were used as received.

3.3.2. Instrumentation

^{1}H NMR spectra was collected in $CDCl_3$ or CD_3OD using a Varian Advance 500 MHz spectrometer to confirm the monomer and polymer composition at ambient temperature. Fast Atom Bombardment Mass Spectrometry (FAB-MS) was conducted in positive ion mode on a JEOL HX110 dual focusing mass spectrometer. FT-IR experiments were carried out using a Varian 670-IR spectrometer (DTGS detector) equipped with Pike Technologies variable temperature GladiATRTM attachment (Diamond crystal). The spectra were collected at 4 cm^{-1} resolution and as an average of 32 scans. The samples were subjected to a temperature ramp of 1 °C/min, starting from 30 °C to 170 °C and FT-IR spectra was collected at every 10 °C beginning from 30 °C. Differential scanning calorimetry (DSC) was performed on a TA Instrument Q100 under nitrogen with a flow rate of 50 mL/min and a heating rate of 10 °C/min. The glass

transition temperatures were measured as the midpoint of the transition in the second heating scan. Thermogravimetric analysis (TGA) was conducted on a TA Instruments Hi-Res TGA 2950 under nitrogen at a heating rate of 10 °C/min. Atomic force microscopy (AFM) was performed using a Veeco MultiMode AFM equipped with nanosensor silicon tips having a spring constant of 42 N/m. SAXS was performed using a Rigaku S-Max 3000 3 pinhole SAXS system, equipped with a rotating anode emitting X-ray with a wavelength of 0.154 nm (Cu Kα). Scattering from a Silver behenate standard was used to calibrate the sample-to-detector distance. For SAXS, the sample-to-detector distance was 1603 mm. Two-dimensional SAXS patterns were obtained using a fully integrated 2D multiwire, proportional counting, gas-filled detector, with an exposure time of 1 hour. All SAXD data were analyzed using the SAXSGUI software package to obtain radically integrated SAXS intensity versus the scattering vector q (SAXS), where $q=(4\pi/\lambda)\sin(\theta)$, θ is one half of the scattering angle and λ is the wavelength of X-ray profiles.

3.3.3. Synthesis of 4-(bis(3-(dimethylamino)propyl)amino)-4-oxobutyl acrylate

The acrylic monomer was synthesized via two steps. In the first step a flame-dried, 2000 mL, three-neck, round-bottomed flask was attached to a 250 mL addition funnel and a condenser. Round-bottomed flask was charged with 50 mL (1.00 eq) of 3,3-iminobis(N,N-dimethylpropylamine) and 700 mL tetrahydrofuran (THF), and nitrogen was purging through the glassware. 225 mL (1.00 eq) of diisobutylalumium hydride 1.0 M solution in toluene was added to the addition funnel and subsequently added to the reaction flask in a drop-wise fashion. The reaction was allowed 7 h at 0 °C. After 7 hours, the reaction flask was warmed to room temperature and 17 mL (1.00 eq) of γ- butyrolactone was added to the reaction mixture and refluxed for 12 h. Water (10 mL) was added slowly to a cooled reaction flask and THF was evaporated under reduced pressure. 100 mL solution of 15% sodium hydroxide was added and

stirred for an hour. The reaction mixture was poured into a separatory funnel and organic layer was separated from aqueous layer and extracted 3x (100 mL) with chloroform. The solvent was evaporated and the product was purified using Kugel-rohr distillation. Evaporation of the total eluent gave a yellow oil with an overall yield of 70%. ^{1}H NMR (500 MHz, $CDCl_3$): 1.71 (m, 4H, H_c), 1.90 (m, 2H, H_f), 2.21 (d, 12H, H_a), 2.26 (t, 4H, H_b), 2.52 (t, 2H, H_e), 3.35 (m, 4H, H_d), 3.67 (t, 2H, H_g), 3.45 (s, 1H, H_i). HRMS (ES+): m/z calcd for [M+H+] 273.24 g/mol, found 274.17 g/mol. (Figure S 3.1). In the second step, a flame-dried, 100 mL, round-bottomed flask was connected to a 50-mL addition funnel and was charged with dichloromethane (DCM) and 1.00 eq of hydroxyl-containing ditertiary amine monomer that was synthesized from the first step. The flask was cooled to 0 °C and acryloyl chloride (1.20 eq) was added to the addition funnel containing DCM and the solution was drop-wise added to the reaction flask. The reaction was allowed to proceed for 12 h. Upon reaction completion, DCM was evaporated and the salt was dissolved in a mixture of saturated $NaHCO_3$ (aq) and saturated Na_2CO_3 (aq). The aqueous solution was introduced to a separatory funnel and extracted 6x with DCM. Solvent was evaporated and the product was purified using column chromatography. Evaporation of the total eluent gave a yellow oil with an overall yield of 30%. ^{1}H NMR (500 MHz, $CDCl_3$): 1.68 (m, 4H, H_c), 2.02 (m, 2H, H_f), 2.19 (d, 12H, H_a), 2.24 (t, 4H, H_b), 2.42 (t, 2H, H_e), 3.31 (m, 4H, H_d), 4.20 (t, 2H, H_g), 5.78-5.83 (dd, 1H, H_{J1}), 6.05-6.14 (m, 1H, H_k), 6.35-6.42 (dd, 1H, H_{J2}) (Figure S 3.2).

3.3.4. Synthesis of N,N-bis(3-(dimethylamino)propyl)acrylamide

A flame-dried, 100 mL, round-bottomed flask was charged with 20 mL 3,3-iminobis(N,N-dimethylpropylamine), 14 mL of anhydrous triethylamine (TEA) (1.1 eq) and 150 mL of dichloromethane (DCM). The system was then purged with nitrogen and cooled to 0 °C. 8 mL of

acryloyl chloride (1.1 eq) was diluted with 80 mL of DCM and cooled to 0 °C. Acryloyl chloride solution was then added to the flask through a cannula in a drop-wise fashion over 2 h at 0 °C. The reaction was then warmed up to room temperature and stirred for 3 h. A short alumina column was used to remove the TEA salt and DCM in the filtrate was then evaporated under reduced pressure. Diethyl ether was used to dissolve any remaining solid and evaporated after filtered through alumina column and a yellow oil was obtained. Product was purified by Kugel-rohr distillation with 30% yield. ^{1}H NMR (500 MHz, $CDCl_3$): 1.74 (m, 4H, H_b), 2.21 (d, 12H, H_a), 2.26 (m, 4H, H_c), 3.41(m, 4H, H_d), 5.64-5.68 (dd, 1H, H_{f2}), 6.31-6.38 (dd, 1H, H_{f1}), 6.60-6.69 (m, 1H, H_e) (Figure S 3.6).

3.3.5. Synthesis of non-segmented acrylate- and acrylamide-based ionene precursor

A 1:1 ratio of acrylate- or acrylamide- containing ditertiary amine and 1,12-dibromododecane monomers were polymerized in DMF for 24 h at 80 °C in the presence of catalytic amount of BHT. The polymer was stored in DMF solution until the post-polymerization functionalization. ^{1}H NMR (400 MHz, CD_3OD) for acrylate-ionene: 1.27-1.47 (m, 16H, H_b), 1.71-1.86 (m, 4H, H_c), 1.97-2.17 (m, 6H, H_{d1-3}), 2.57 (t, 2H, H_g), 3.08-3.20 (d, 12H, H_a), 3.32-3.56 (m+t, 12H, e_{1-6}), 4.24 (t, 2H, H_f), 5.87-5.93 (dd, 1H, H_{j2}), 6.12-6.23 (m, 1H, H_h), 6.36-6.42 (dd, 1H, H_{j1}) (Figure S 3.3). ^{1}H NMR (400 MHz, CD_3OD) for acrylamide-ionene: 1.37 (m, 16H, H_a), 1.79 (m, 4H, $H_{b+b'}$), 2.11 (m, 4H, $H_{c+c'}$), 3.12 (d, 12H, H_{d1-4}), 3.32-3.51 (m, 8H, H_{e1-4}), 3.52-3.68 (m, 4H, $H_{f+f'}$), 5.78-5.84 (dd, 1H, H_{h1}), 6.26-6.35 (dd, 1H, H_{h2}), 6.80-6.93 (m, 1H, H_g) (Figure S 3.7).

3.3.6. Synthesis of non-segmented nucleobase-containing ionene (9-bond spacer)

Upon reaction completion acrylate-cotaining ionene solution in DMF was charged with 1.01 eq of adenine or thymine and 0.15 eq of tBuOK for 24 h. The nucleobase-containing ionene product

was precipitated in ethyl acetate and dried in vacuo (0.1 mmHg) for 24 h. Ionene homopolymers were synthesized in high yields (97%). ^{1}H NMR (400 MHz, CD_3OD) for adenine-containing ionene: 1.17-1.47 (m, 16H, H_b), 1.68-1.83 (m, 4H, H_c), 1.90 (t, 2H, H_d), 1.96-2.14 (m, 4H, $H_{e+e'}$), 2.44 (t, 2H, H_f), 3.00 (t, 2H, H_g), 3.06-3.16 (d, 12H, H_a), 3.32-3.55 (m, 12H, H_{K1-6}), 4.14 (t, 2H, H_i), 4.52 (t, 2H, H_h), 8.17 (s, 1H, H_{j2}), 8.21 (s, 1H, H_{j1}) (Figure S 3.4). ^{1}H NMR (400 MHz, CD_3OD) for thymine-containing ionene: 1.22-1.49 (m, 16H, H_b), 1.72-1.88 (m+s, 7H, H_{c+m}), 1.95 (t, 2H, H_d), 2.00-2.19 (m, 4H, H_e), 2.54 (t, 2H, H_f), 2.78 (t, 2H, H_g), 3.05-3.24 (d, 12H, H_a), 3.32-3.58 (m, 12H, H_{K1-6}), 4.00 (t, 2H, H_i), 4.17 (t, 2H, H_h), 7.55 (s, 1H, H_j) (Figure S 3.5).

3.3.7. Synthesis of non-segmented nucleobase-containing ionene (4-bond spacer)

Upon completion of polymerization, acrylamide-based ionene solution in DMF was charged with 1.5 eq of adenine and 0.5 eq of tBuOK for 10 d. Solution was decanted and precipitant was washed with DMF and then dried *in vacuo* (0.1 mmHg) overnight. Product was then dialyzed against water for 3 d and filtered to remove excess adenine. Product was dried by lyophilization over 3 d with 50% yield. ^{1}H NMR (500 MHz, CD_3OD): 1.26 (m, 16H, H_a), 1.69 (m, 4H, $H_{b+b'}$), 1.99 (m, 4H, $H_{c+c'}$), 3.03 (d, 12H, H_{d1-5}), 3.23-3.45 (m, 12H, H_{e1-6}), 3.92 (t, 2H, H_f), 7.47 (d, 2H, $H_{g+g'}$) (Figure S 3.8). For thymine-containing ionene, acrylic ionene solution in DMF was charged with 1.5 eq of thymine and 0.2 eq of tBuOK for 5 d. DMF was evaporated under reduced pressure followed by dialysis against water for 3 d. Precipitant was removed by filtration and product was dried in lyophilizer for 3 d and the yield was 90%. ^{1}H NMR (500 MHz, CD_3OD): 1.37 (m, 16H, H_a), 1.78 (m, 4H, $H_{b+b'}$), 1.84 (s, 3H, H_i), 2.04 (m, 4H, $H_{c+c'}$), 2.56 (t, 2H, H_h), 3.12 (d, 12H, H_{d1-4}), 3.34-3.53 (m, 12H, H_{e1-6}), 3.57 (t, 2H, H_f), 7.45 (s, 1H, H_g) (Figure S 3.9).

3.3.8. Preparation of ionene blends

A 1:1 solution of adenine-containing ionene in methanol and thymine-containing ionene in methanol were mixed and stirred for an hour. Films were cast into Teflon molds and the solvent was slowly evaporated over 2 days. The films were then annealed at 110 °C-130 °C in vacuum for 24 h and stored on drying agents (drierite) and kept inside the desiccator until prior to any characterization.

3.4. Results and Discussion

3.4.1. Synthesis of Non-segmented Nucleobase-Functionalized Ionene Homopolymers

Scheme 1 represents the synthesis of acrylate- and acrylamide-containing ditertiary amine monomers. The acrylate-containing monomer synthesis involved two steps (Scheme 3.1a). In the first step, ring opening of γ-butyrolactone occurred in the presence of DIBAL to produce OH-containing ditertiary amine monomer in high yields. In the second step, an acid-chloride reaction between the OH-containing amine and acryloyl chloride yielded acrylate-containing ditertiary amine monomer. The acrylamide-containing monomer synthesis involved a one-step acid-chloride reaction (Scheme 3.1b).

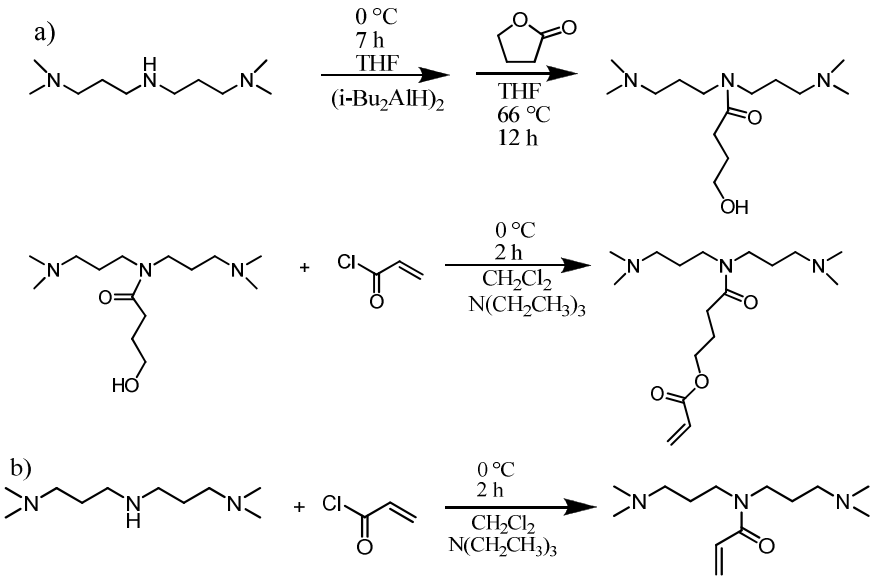

Scheme 3.1. Synthesis of acrylate-containing ditertiary amine monomer (a) and acrylamide-containing ditertiary amine monomer (b)

Upon the synthesis of ditertiary amine monomers in high purity, we synthesized two kinds of ionene homopolymers, one having longer spacer length (9-bond spacer) and one having shorter spacer length (4-bond spacer). Scheme 3.2 and Scheme 3.3 illustrate the polymerization of acrylamide-containing amine monomer and acrylate-containing amine monomer with 1,12-dibormododecane to yield 4-bond spacer and 9-bond spacer ionenes respectively. Both polymerizations occurred in polar DMF solvent and completed in 24 h. In our earlier report,[19] we monitored the reaction progress for the synthesis of non-segmented 12/6,12-ammonium ionenes, using the C-N^+ stretch at ≈905 cm^{-1} and confirmed the reaction completion within 24 h. Herein, we followed the reaction progress using ^{1}H NMR spectroscopy with monitoring the growth of methyl protons connected to quaternized nitrogens at *ca.* 3.10 ppm and subsequently confirmed the structures of ionene homopolymers upon completion of the polymerization (Figure S 3.3 & Figure S 3.7). Upon the synthesis of the ionene precursors, base-catalyzed

Michael addition occurred in the same reaction flask and yielded nucleobase-functionalized ionenes. It should be mentioned that based on ^{1}H NMR spectrum, there were no chemical degradation observed for ionenes in the presence of the base catalyst ($tBuO^-$) at 80 $^{\circ}$C. Regioselective base-catalyzed Michael addition promotes substitution of adenine and thymine units at *N9* and *N1* respectively.[20]

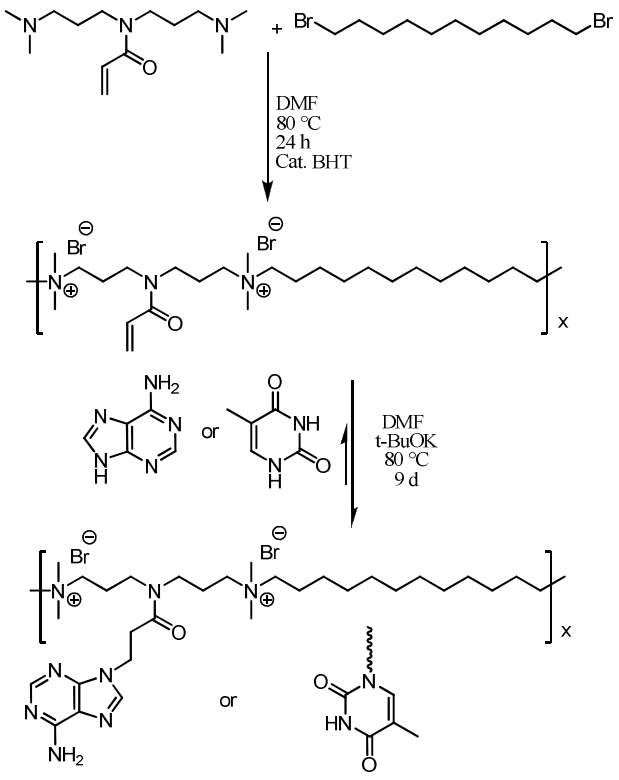

Scheme 3.2. Synthesis of nucleobase-containing ionenes having 4-bond spacer

Scheme 3.2 and Scheme 3.3 respectively illustrate the post-polymerization functionalization of nucleobase-containing ionenes having shorter spacer length (4-bond spacer) and longer spacer length (9-bond spacer). For the longer spacer ionene synthesis, the nucleobase Michael addition started heterogeneously and as the reaction preceded the reaction mixture became homogenous. We precipitated the adenine- and thymine-containing ionenes in ethyl acetate to remove both

DMF and the slight excess of adenine or thymine. For the shorter spacer ionene synthesis, the adenine-containing ionene precipitated upon production due to lower solubility in DMF. However, the thymine-containing ionene remained soluble in DMF throughout the reaction time due to better solubility of thymine unit compared to adenine in polar solvents. Both adenine- and thymine-containing ionenes having 4-bond spacer were dialyzed against water to remove DMF and excess adenine or thymine. Obtaining absolute molecular weights for the charged ammonium ionenes was challenging due to polymer-polymer and polymer-stationary phase interactions.

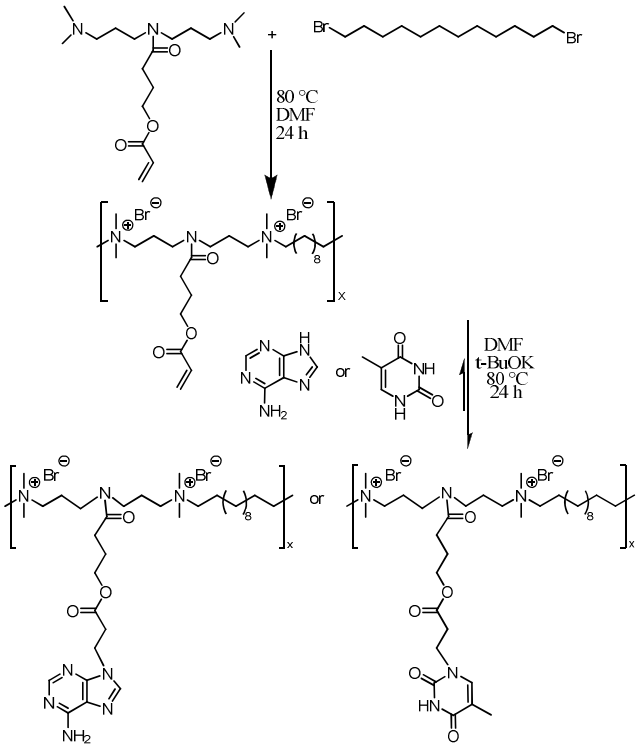

Scheme 3.3. Synthesis of nucleobase-containing ionenes having 9-bond spacer

3.4.2. Infrared Spectroscopy

One method to detect the intermolecular interaction between two polymers is to use FT-IR spectrometry. FT-IR monitors the thermoreversibility of hydrogen bonding interactions.[21, 22] We performed variable temperature FT-IR on the ionene blends having shorter and longer spacer length. Figure 3.1 represents the FT-IR spectrum (1550 cm^{-1}-1750 cm^{-1}) of both ionenes having a ratio of [A]:[T] = 1:1 at various temperatures (30 °C to 170 °C). The peak centered around 1590 cm^{-1} corresponded to the N–H bending/scissoring vibration of adenine. In the longer spacer ionene blend the band at 1590 cm^{-1} shifted to lower wavenumbers upon heating from 30 °C to 170 °C which indicated the dissociation of hydrogen bonds. However, for the shorter spacer ionene blend, we did not observe any significant shift for the N–H bending/scissoring vibration of adenine indicating little or no hydrogen bonding association present between chains. Another band at 1670 cm^{-1} attributed to the C=O stretching vibration of thymine unit. Upon heating, the C=O stretching vibration of thymine in the longer spacer ionene blend shifted to higher wavenumbers and did not change for the shorter spacer blend illustrating little or no complementary hydrogen bonding interaction. Therefore variable temperature FT-IR showed that the spacer length influences the complementary hydrogen bond association within the nucleobase pairs. The longer spacer is necessary to increase the distance between nucleobase units and the charged backbone to eliminate charge-charge repulsion between complementary chains and removes the steric hindrance between the nucleobase unit and the ionene backbone providing more flexibility for the complementary units to find each other and bind.

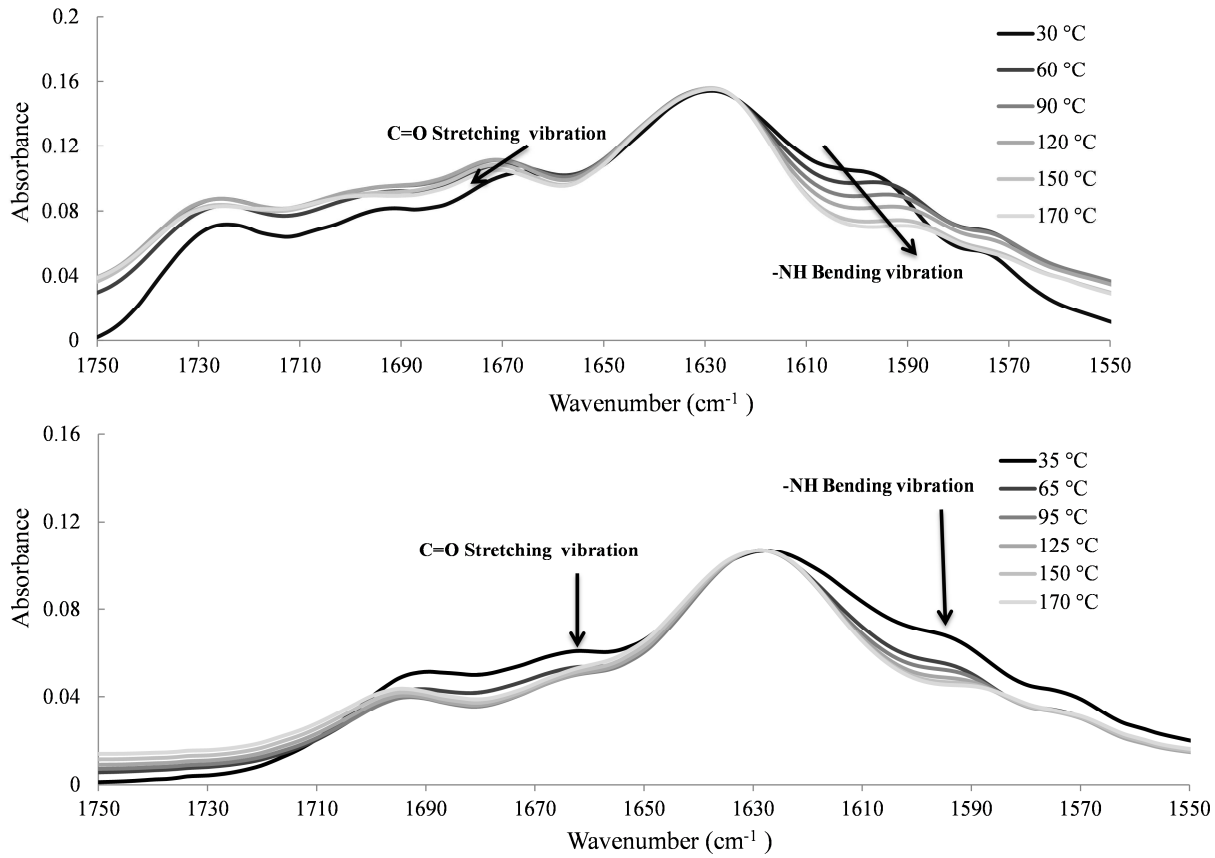

Figure 3.1. Variable temperature FT-IR spectra in the 1550-1750 cm^{-1} region for the longer spacer ionene blend (top) and shorter spacer ionene blend (bottom)

3.4.3. Thermal Transitions

In order to understand the effect of spacer length on the association of nucleobase-containing ionenes, we studied the thermal properties of ionene homopolymers as well as their blends. DSC analysis of all ionene homopolymers and blends with different spacer lengths showed a single glass transition temperature. The fact that the blends showed only a single glass transition temperature indicated that they are fully miscible and form a homogenous amorphous phase. The 4-bond spacer ionenes showed higher T_g's compared to the 9-bond spacer ionenes due to the sterically hindered ionene backbone and lower flexibility (Table 3.1). It is common to use Fox

equation to estimate the T_g for miscible polymer blends and copolymers.[23] The Fox equation assumes the blend is completely miscible and no intermolecular interaction is present. Therefore we prepared various [A]:[T] blends of ionenes having different spacer lengths and measured their T_g's. We observed a linear increase of T_g with an increase of adenine mole fraction for blends with the shorter spacer. The T_g's were well fitting within the Fox equation indicating that there are no intermolecular on intramolecular hydrogen bonding interaction present in the ionene blends having 4-bond spacer (Figure 3.2).

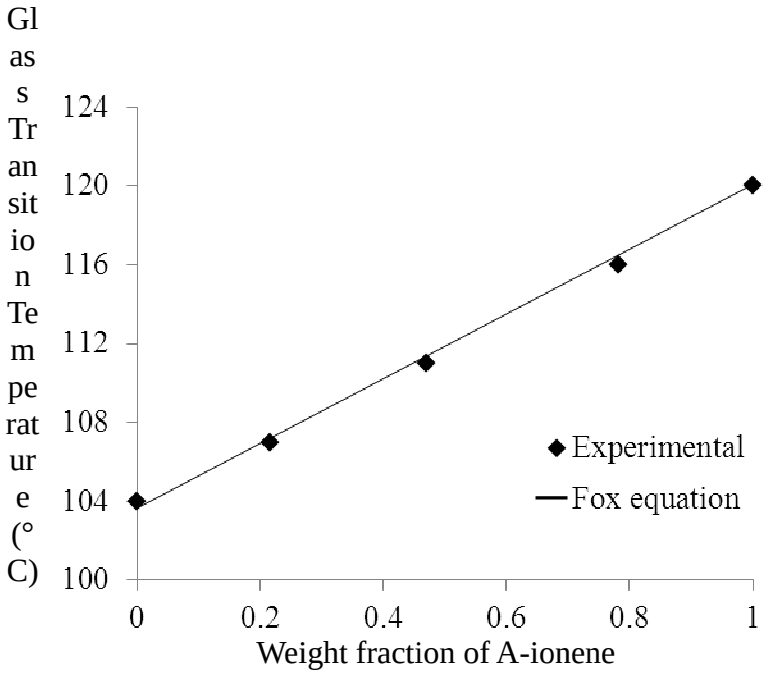

Figure 3.2. T_g versus composition curve of experimental data and Fox fitting equation for shorter spacer ionene blends

However, many polymer blends fail description by the Fox equation due to intermolecular interactions such as hydrogen bonding.[24, 25] Therefore researchers have developed equations to expand the Fox equation for T_g composition dependence of miscible polymer blends such as Gordon-Taylor,[26] Couchman,[27, 28] Kwei,[29] and Karasz.[30] In our system, the T_g's measured

for the 9-bond spacer ionene blends showed a significant negative deviation from the Fox equation. This deviation is attributed to the hydrogen bonding interactions. The most suitable equation for this system is the Kwei equation shown below. Previously Chang et al.[31-33] showed various systems having hydrogen bonding interactions and the T_gs of the blends either had positive or negative deviation from Fox equation and were well fit by the Kwei equation.

$$T_g = \frac{W_1 T_{g1} + k W_2 T_{g2}}{W_1 + k W_2} + q W_1 W_2$$

Where W_1 and W_2 are weight fractions of the compositions and T_{g1} and T_{g2} represent the corresponding glass transition temperatures, and k and q are fitting constants. This equation is applied to miscible polymer blends with specific interaction. The parameter q corresponds to the strength of hydrogen bonding in the blend reflecting a balance between the breaking of self-association and forming inter-association hydrogen bonding. In most systems, if the inter-association equilibrium constant is greater than the self-association equilibrium constant, the q value will be positive, whereas if the self-association equilibrium constant is greater than the inter-association, the q is negative. Figure 3.3 demonstrates the plots of the T_g of the blend versus its composition for cases where the experimental data did not fit well with either the Gordon-Taylor or Fox equations. However, the Kwei equation correlated well with the experimental data and based on the non-linear least squares "best-fit", k = 1 and q = -316. A negative q value of "-316" indicates that the intermolecular hydrogen bonding is weaker than intramolecular ones.

Table 3.1. Glass transition temperatures of ionenes with 4-bond spacer and 9-bond spacer

Sample	**T_g (°C) - shorter spacer**	**T_g (°C) - longer spacer**
Ionene-precursor	80	61
A-ionene	124	99
T-ionene	104	88

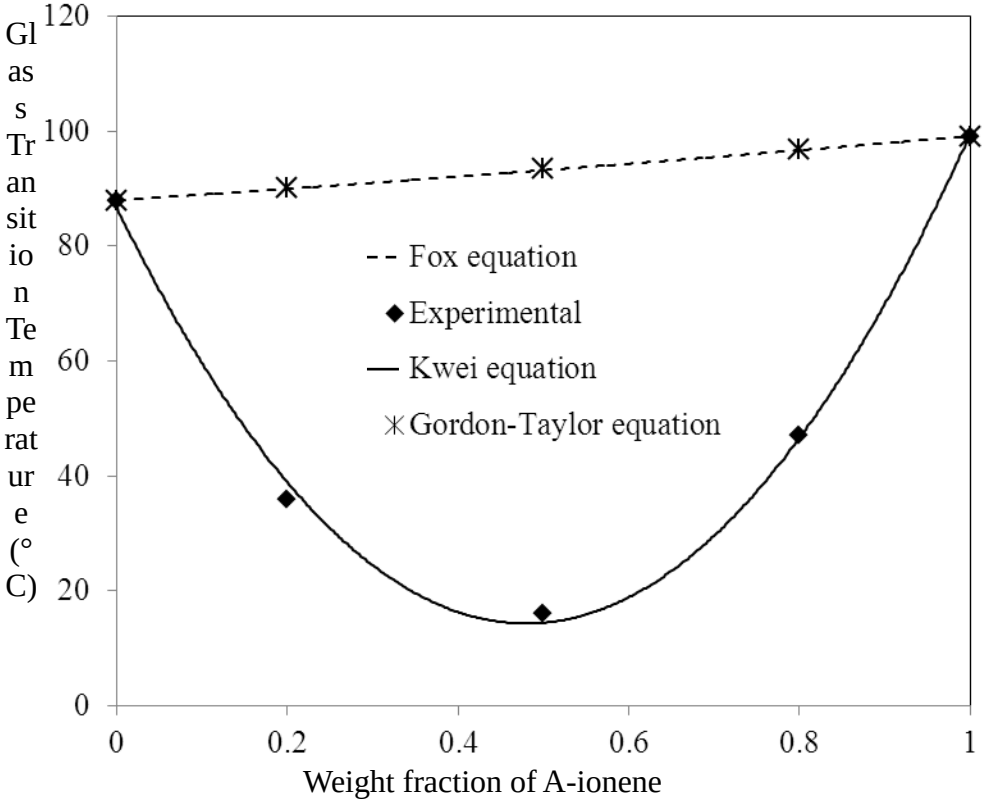

Figure 3.3. T_g versus composition curves from experimental data and different fitting equations for longer spacer ionene blends

3.4.4. Morphology

After annealing films of the ionene homopolymers and blends, AFM phase images of the free surface allowed us to study the surface texture of ionene structures (Figure 3.4). According to SAXS data, all of these systems are not microphase separated, however, what we are seeing is the contrast between hard and soft domains of the polymer backbone. The nucleobases and ions contributed to the brighter regions of the image and the methylene spacers in the backbone contributed to the darker regions of the image. The top images in Figure 3.4 show the phase images of ionenes with longer spacer length and the bottom images represent the ionenes with shorter spacer length. The longer spacer length ionenes lose their surface morphological texture upon 1:1 blending due to efficient formation of hydrogen bonds. Shorter spacer length ionenes keep their morphological texture upon 1:1 blending, which indicates no hydrogen bonds.

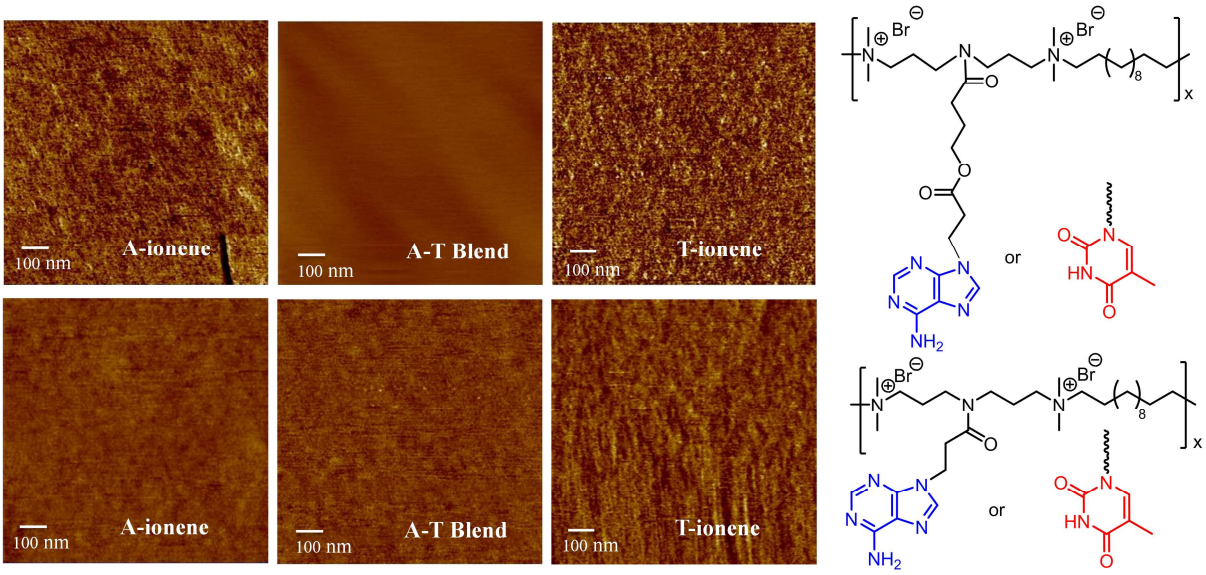

Figure 3.4. AFM phase images of ionene homopolymers and blends having shorter spacer (bottom image) and longer spacer (top image)

3.5. Conclusions

Using post-polymerization functionalization, we synthesized novel nucleobase-containing ionene homopolymers having two different spacer lengths and studied the effect of spacer length on the hydrogen bonding interactions in the blends. The shorter spacer ionene homopolymers and blends showed higher glass transition temperatures than longer spacer ionenes due to the closeness of the bulky nucleobase units to the backbone which hindered the segmental motion of the ionene backbone. We observed a single glass transition temperature for all ionenes having various spacer lengths. Each ionene blend showing a single T_g confirmed the miscibility of both blends. The glass transition temperatures of ionene blends with shorter spacer followed the Fox equation indicating no intermolecular interactions and with increasing the spacer length from 4-bonds to 9-bonds the T_gs of the blends deviated from both the Fox and Gordon-Taylor equations demonstrating a presence of hydrogen bonding interactions. The Kwei equation accurately predicted the T_gs from the experimental results. We did not calculate the self-association and inter-association equilibrium constants for these ionenes, however based on the negative deviation from Fox equation and a negative q value we were able to confirm that the average strength of inter-hydrogen bonding was weaker than the intra-hydrogen bonding in the adenine or thymine ionene homopolymers. The variable-temperature FT-IR confirmed the hydrogen bonding interactions for the longer spacer ionenes with NH_2 bending vibration shifting to lower wave numbers and C=O stretching vibration shifting to higher wave numbers with increasing temperature. AFM phase image of longer spacer ionene blend showed the disappearance of surface texture compared to the shorter spacer ionene blend.

3.6. References

(1) Gibbs, C. F.; Marvel, C. S. *J. Am. Chem. Soc.* **1934,** 56, 725-7.
(2) Abboud, J. L. M.; Notario, R.; Bertran, J.; Sola, M. *Progress in Physical Organic Chemistry* **1993,** 19, 1-182.
(3) Brunsveld, L.; Folmer, B. J. B.; Meijer, E. W.; Sijbesma, R. P. *Chem. Rev* **2001,** 101, 4071-4097.
(4) Ilhan, F.; Galow, T. H.; Gray, M.; Clavier, G.; Rotello, V. M. *J. Am. Chem. Soc.* **2000,** 122, 5895-5896.
(5) Yamauchi, K.; Lizotte, J. R.; Hercules, D. M.; Vergne, M. J.; Long, T. E. *J. Am. Chem. Soc.* **2002,** 124, 8599-8604.
(6) Sivakova, S.; Rowan, S. J. *Chem. Soc. Rev.* **2005,** 34, 9-21.
(7) Kyogoku, Y.; Lord, R. C.; Rich, A. *Proc. Natl. Acad. Sci. U. S. A.* **1967,** 57, 250-7.
(8) Rieth, S.; Baddeley, C.; Badjic, J. D. *Soft Matter* **2007,** 3, 137-154.
(9) Yamauchi, K.; Lizotte, J. R.; Long, T. E. *Macromolecules* **2002,** 35, (23), 8745-8750.
(10) Snip, E.; Shinkai, S.; Reinhoudt, D. N. *Tetrahedron Lett.* **2001,** 42, 2153-2156.
(11) Dankers, P. Y. W.; Harmsen, M. C.; Brouwer, L. A.; Van, L. M. J. A.; Meijer, E. W. *Nat. Mater.* **2005,** 4, 568-574.
(12) Mather, B. D.; Baker, M. B.; Beyer, F. L.; Berg, M. A. G.; Green, M. D.; Long, T. E. *Macromolecules* **2007,** 40, (19), 6834-6845.
(13) Shenhar, R.; Xu, H.; Frankamp, B. L.; Mates, T. E.; Sanyal, A.; Uzun, O.; Rotello, V. M. *J. Am. Chem. Soc.* **2005,** 127, 16318-16324.
(14) Binder, W. H.; Kluger, C.; Straif, C. J.; Friedbacher, G. *Macromolecules* **2005,** 38, 9405-9410.
(15) Lin, I. H.; Cheng, C.-C.; Yen, Y.-C.; Chang, F.-C. *Macromolecules* **2010,** 43, 1245-1252.
(16) Karikari, A. S.; Mather, B. D.; Long, T. E. *Biomacromolecules* **2007,** 8, 302-308.
(17) Rowan, S. J.; Suwanmala, P.; Sivakova, S. *J. Polym. Sci., Part A: Polym. Chem.* **2003,** 41, 3589-3596.
(18) De, G. T. F. A.; Kade, M. J.; Feldman, K. E.; Kramer, E. J.; Hawker, C. J.; Meijer, E. W. *J. Polym. Sci., Part A: Polym. Chem.* **2011,** 49, 4253-4260.
(19) Tamami, M.; Salas-de, l. C. D.; Winey, K. I.; Long, T. E. *Macromol. Chem. Phys.* **2012,** 213, 965-972.
(20) Lira, E. P.; Huffman, C. W. *J. Org. Chem.* **1966,** 31, 2188-91.
(21) Sivakova, S.; Bohnsack, D. A.; Mackay, M. E.; Suwanmala, P.; Rowan, S. J. *J. Am. Chem. Soc.* **2005,** 127, 18202-18211.
(22) Sijbesma, R. P.; Beijer, F. H.; Brunsveld, L.; Folmer, B. J. B.; Hirschberg, J. H. K. K.; Lange, R. F. M.; Lowe, J. K. L.; Meijer, E. W. *Science* **1997,** 278, 1601-1604.
(23) Fox, T. G. *Bull. Am. Phys. Soc.* **1956,** 1, 123.
(24) Coleman, M. M.; Xu, Y.; Painter, P. C. *Macromolecules* **1994,** 27, 127-34.
(25) Xu, H.; Hong, R.; Lu, T.; Uzun, O.; Rotello, V. M. *J. Am. Chem. Soc.* **2006,** 128, 3162-3163.
(26) Gordon, M.; Taylor, J. S. *J. Appl. Chem.* **1952,** 2, 493-500.
(27) Couchman, P. R. *Macromolecules* **1991,** 24, 5772-4.
(28) Couchman, P. R. *Polym. Eng. Sci.* **1984,** 24, 135-43.
(29) Kwei, T. K. *J. Polym. Sci., Polym. Lett. Ed.* **1984,** 22, 307-13.

(30) Couchman, P. R.; Karasz, F. E. *Macromolecules* **1978,** 11, 117-19.
(31) Kuo, S. W.; Chang, F. C. *Macromolecules* **2001,** 34, 5224-5228.
(32) Kuo, S. W.; Chang, F. C. *Macromol. Chem. Phys.* **2002,** 203, 868-878.
(33) Huang, M.-W.; Kuo, S.-W.; Wu, H.-D.; Chang, F.-C.; Fang, S.-Y. *Polymer* **2002,** 43, 2479-2487.

Supplemental ^{1}H NMR Figures:

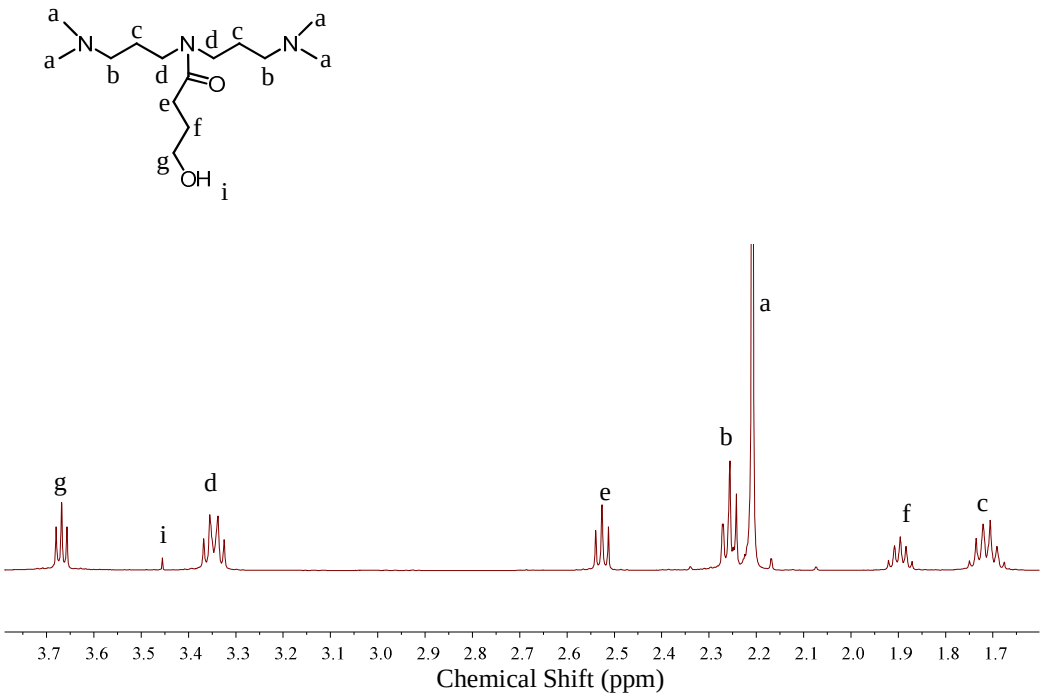

Figure S 3.1 ^{1}H NMR of *N*,*N*-bis(3-(dimethylamino)propyl)-4-hydroxybutanamide monomer

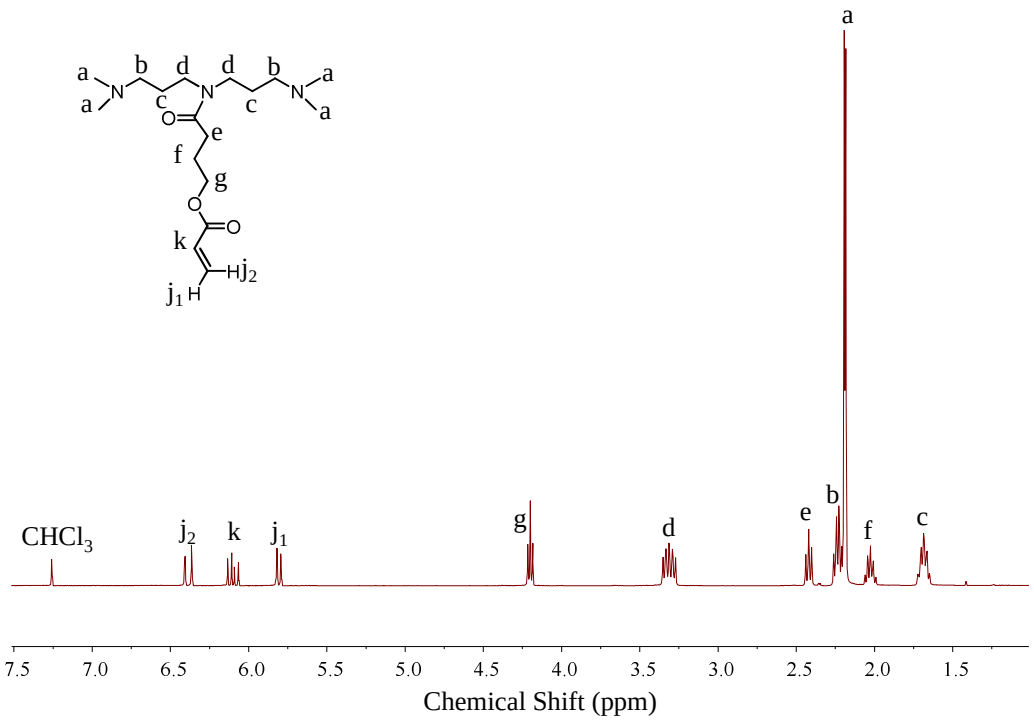

Figure S 3.2. [1]H NMR of 4-(bis(3-dimethylamino)propyl)amino)-4-oxobutyl acrylate monomer

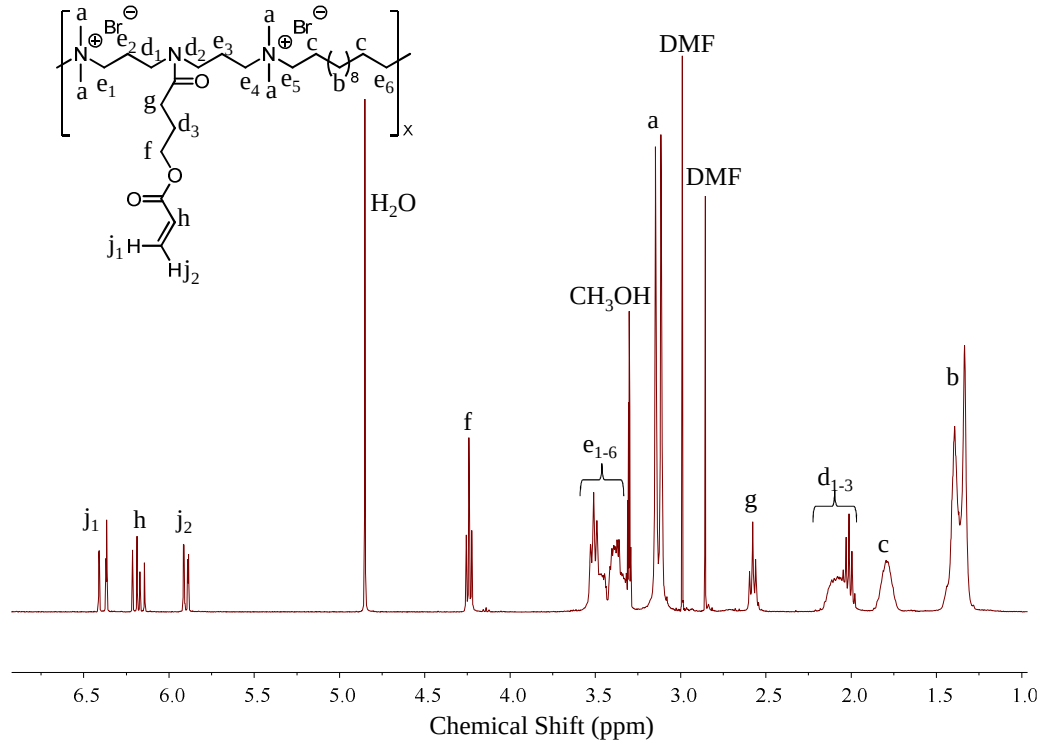

Figure S 3.3. [1]H NMR of acrylate-containing ionene (9-bond spacer)

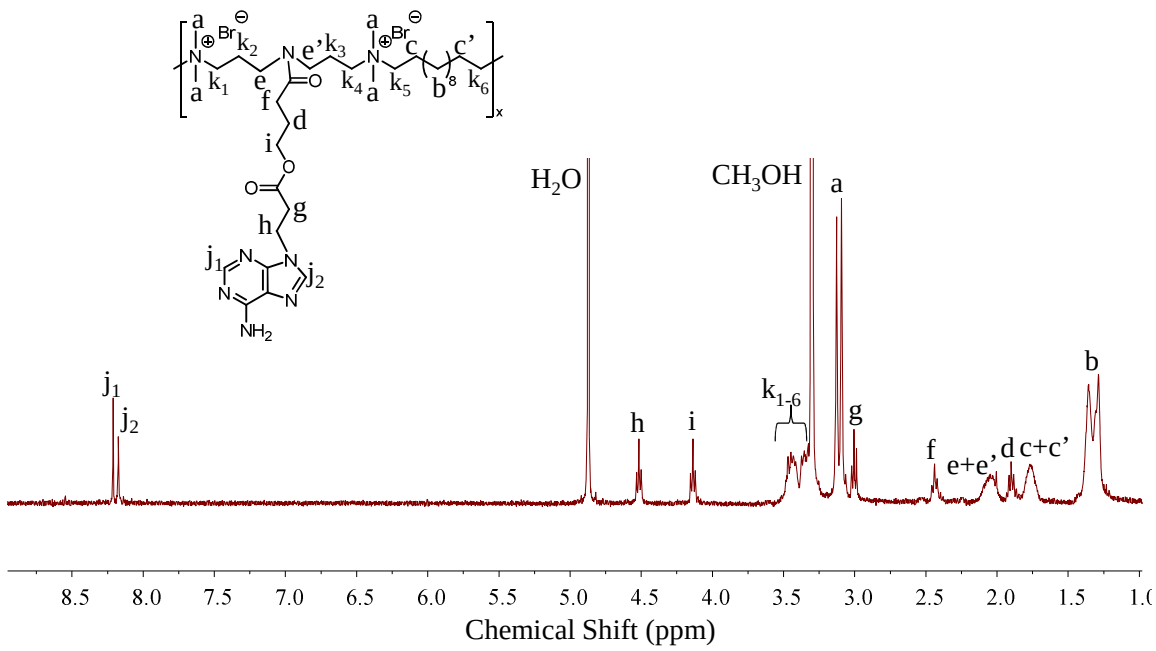

Figure S 3.4. [1]H NMR of adenine-containing ionene (9-bond spacer)

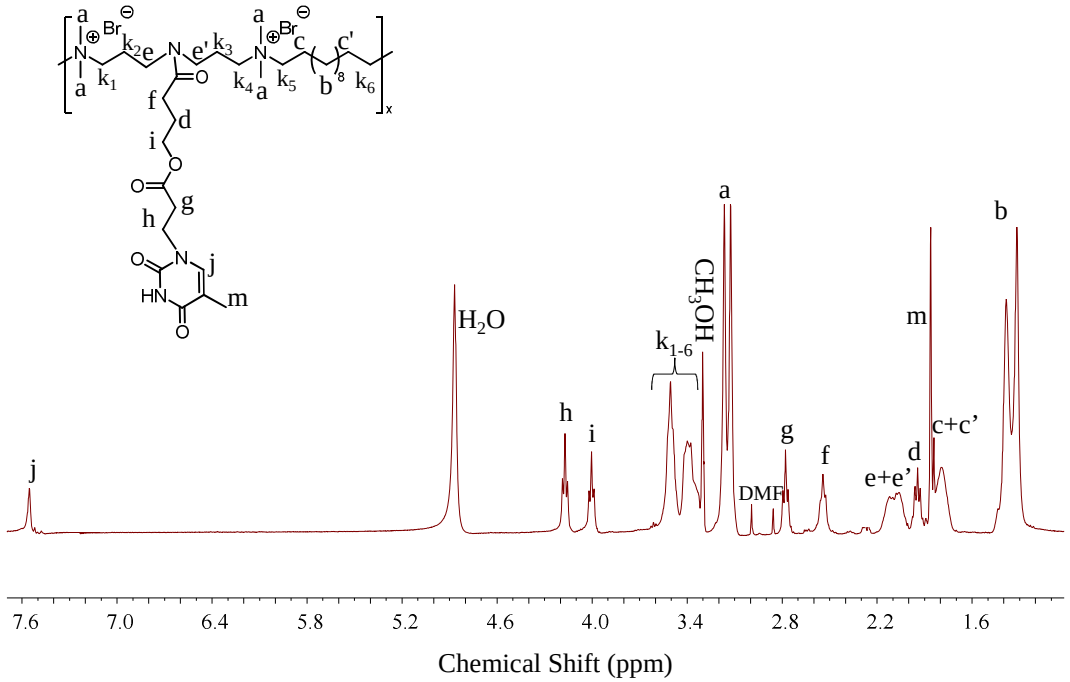

Figure S 3.5. [1]H NMR of thymine-containing ionene (9-bond spacer)

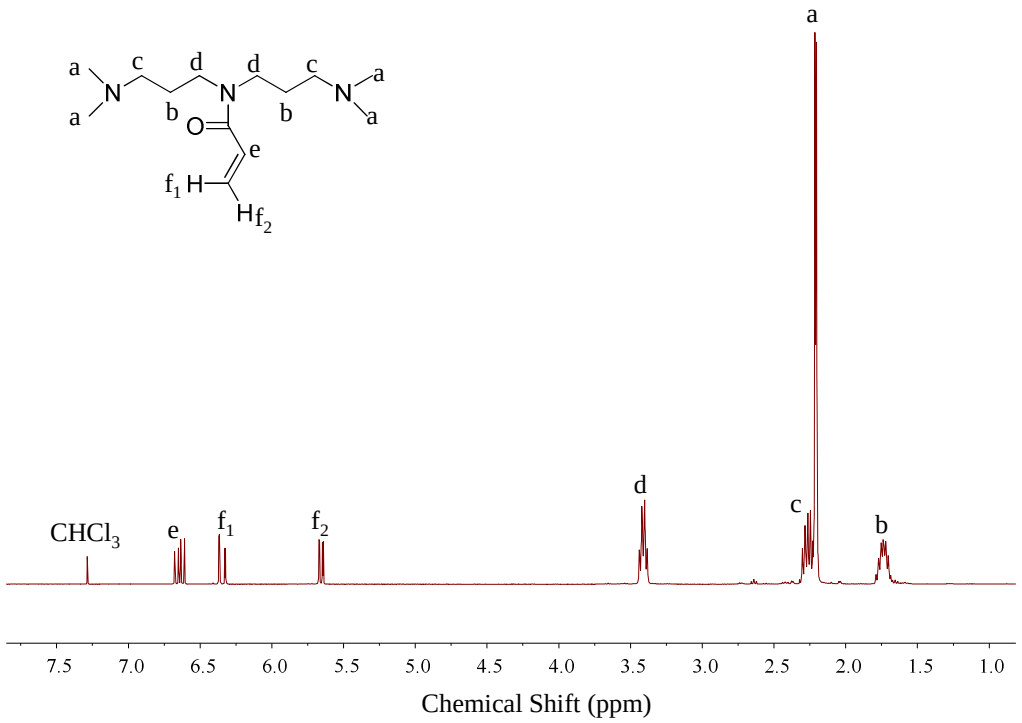

Figure S 3.6. ^{1}H NMR of *N*,*N*-bis(3-(dimethylamino)propyl)acrylamide monomer

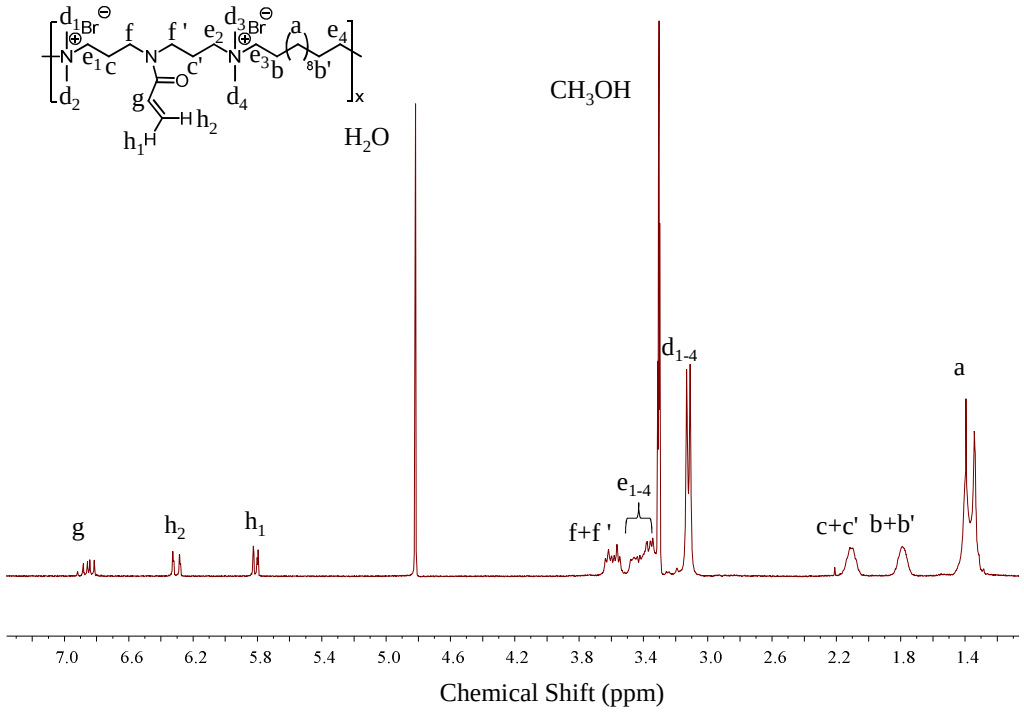

Figure S 3.7. ^{1}H NMR of acrylamide-containing ionene (4-bond spacer)

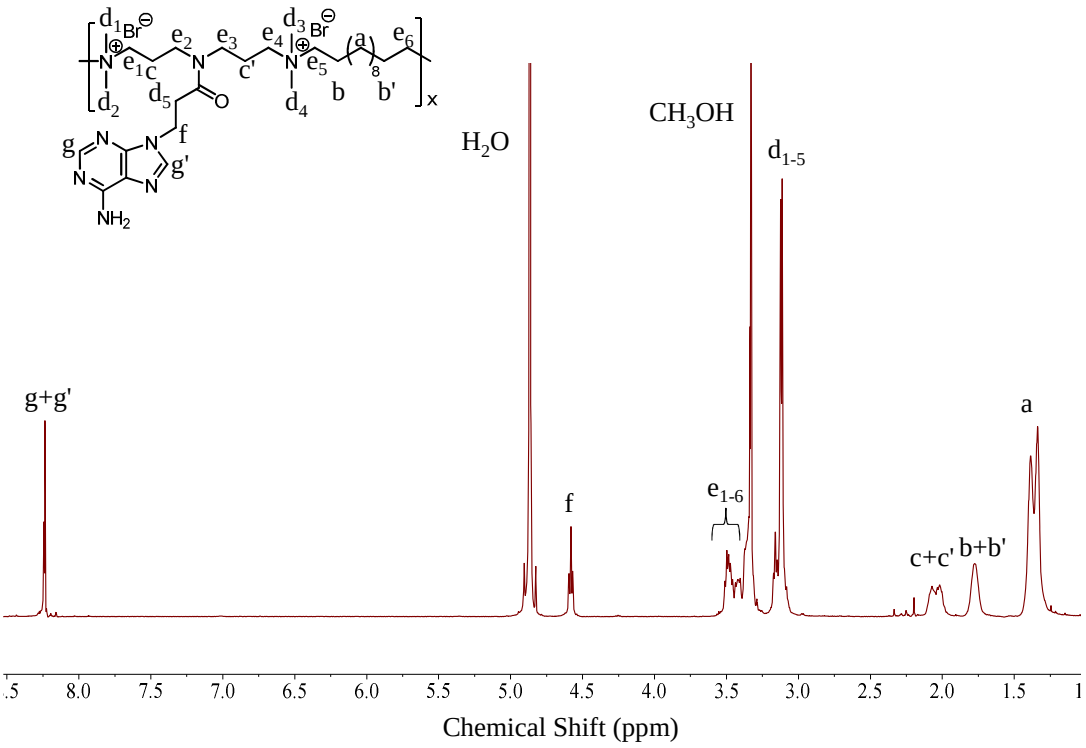

Figure S 3.8. ^{1}H NMR of adenine-containing ionene (4-bond spacer)

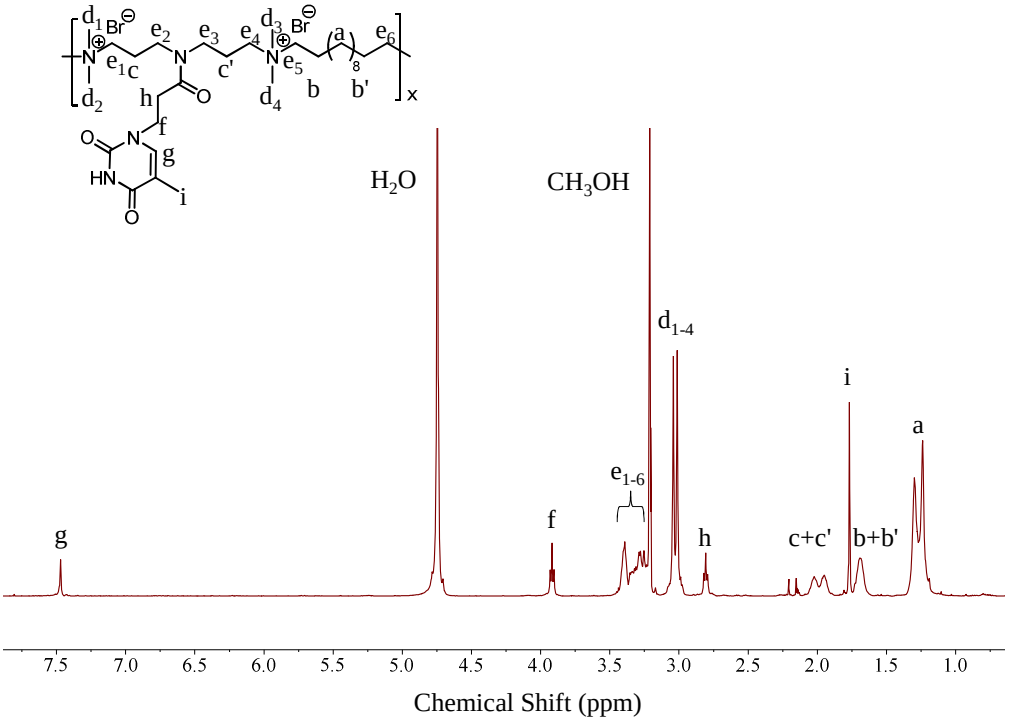

Figure S 3.9. ^{1}H NMR of adenine-containing ionene (4-bond spacer)

Chapter 4. Nucleobase Self-Assembly in Segmented Poly(ethylene glycol)-Based Ammonium Ionenes

Mana Tamami, Sean Hemp, Keren Zhang, Mingqiang Zhang, Robert B. Moore, and Timothy E. Long*

Macromolecules and Interfaces Institute, Department of Chemistry, Virginia Tech, Blacksburg, VA 24061, USA

*E-mail address: telong@vt.edu

4.1. Abstract

Novel adenine-functionalized ionene (ionene-A) and thymine-functionalized ionene (ionene-T) were synthesized using aza-Michael addition chemistry. Complexes of these ionenes with nucleobase-containing guest molecules (*n*-butyl thymine, *n*BT) and (*n*-butyl adenine, *n*BA) showed well-defined complementary hydrogen bonding interactions. Job's analysis revealed a 1:1 stoichiometry for the hydrogen-bonded complexes of [ionene-A]:[*n*BT], [ionene-T]:[*n*BA], and [*n*BA]:[*n*BT]. Fitting the chemical shifts to the Benesi-Hildebrand method, the calculated association constants were 94 M^{-1}, 130 M^{-1}, and 137 M^{-1} for complexes of [ionene-A]:[*n*BT], [ionene-T]:[*n*BA], and [*n*BA]:[*n*BT], respectively. Furthermore, the DSC thermograms of 1:1 [ionene-A/T]:[guest molecule] complexes showed the disappearance of the guest molecule's melting peak confirming no macrophase separation of the nucleobase guest from the polymer matrix. Morphological studies including atomic force microscopy (AFM) and small-angle X-ray scattering (SAXS) revealed a microphase-seperated morphology for the nucleobase-containing ionenes and demonstrated a reduced degree of microphase separation for the 1:1 complexes.

Keywords: segmented ionenes, nucleobases, ^{1}H NMR titration, guest molecule, microphase separation

4.2. Introduction

Current advances in polymer science involve the use of non-covalent interactions, such as hydrogen bonding, electrostatics, π-π interactions, metal coordination, and van der waals forces to develop supramolecular polymers for various applications. DNA utilizes complementary hydrogen bonding through nucleobases to generate complex structures and many polymer chemists have drawn inspiration from DNA to synthesize nucleobase-containing polymers.[1] Environmental parameters including temperature, solvent polarity, humidity, concentration, and pH readily control the strength of these interactions, thus leading to stimuli-responsive polymers.[2]

Ionenes are ion-containing polymers that contain quaternized nitrogens in their molecular backbone.[3] The step-growth polymerization of a ditertiary amine and a dihalide monomer synthesizes ionenes. The synthetic design of this reaction provides control over charge density and thus makes ionenes ideal models to investigate the structure-property relationships of well-defined cationic polymers. Due to the positive charge of the ammonium ionenes, they demonstrate many potential biomedical applications as gene transfection agents,[4, 5] components of cosmetics,[6] antimicrobial agents,[7] and flocculants for water treatments.[8]

Two general types of ionenes are segmented and non-segmented. These ionenes can have various topologies (linear, branched, etc). Segmented[9] ionenes have oligomeric, low T_g spacers between their charged sites and demonstrate enhanced mechanical properties compared to non-segmented[10] ionenes, which contain shorter distances between charges and therefore higher charge density along the backbone. Previous literature describes a wide variety of synthetic polymers functionalized with complementary adenine and thymine nucleobases.[11-16] However, few reports detail the incorporation of complementary hydrogen bonding along with ionic interactions. Rotello et al.[17] used orthogonal self-assembly of polymers and nanoparticles to micropattern surfaces.

However, the hydrogen bonding recognition units and charged species resided on separate polymer backbones. Weck et al.[18] first synthesized ammonium and 2,6-diamonopyridine (DAP)-functionalized norbornene diblock copolymers containing both electrostatic and hydrogen bonding interactions. Based on ^{1}H NMR titrations, they concluded that both non-covalent interactions were orthogonal with electrostatics causing no disruption of hydrogen bonding. Recently, Long et al.[19] copolymerized 9-vinylbenzyladenine (VBA) and 2-(dimethylamino)ethyl methacrylate (DMAEMA) with subsequent protonation to provide adenine-containing polyelectrolyte. Copolymers having 11, 22, and 35 mol% of VBA showed polyelectrolyte behavior in the dilute and semidilute regimes. Due to the hydrogen bonding association between adenine units, they did not observe polyelectrolyte behavior in the concentrated regime. In addition, the electrospinning behavior showed a strong dependence on the VBA incorporation. Another example that demonstrated the interplay between hydrogen bonding and electrostatic interactions in both solid state and solution state was the synthesis of poly(9-vinylbenzyladenine-*b*-*n*-butylacrylate-*b*-9-vinylbenzyladenine) triblock copolymer and the selective association of uracil-containing salt with adenine units in the hard phase.[20]

In this article, we discuss the synthesis of segmented 1000 g/mol poly(ethylene glycol) (PEG)-based ionenes that contain adenine or thymine units. The PEG segment enhanced the polymer solubility in organic solvents and increased chain mobility compared to its non-segmented ionene counterpart, leading to improved complementary hydrogen bonding interactions. For the first time, we report the synthesis and characterization of water-soluble, adenine (A) and thymine (T) functionalized (K_{AT} *ca*. 100 M^{-1} in $CDCl_3$) segmented PEG-based ammonium ionenes with supramolecular characteristics similar to the DNA molecule. Supramolecular assembly studies between the adenine and thymine nucleobases probed the influence of electrostatics on complementary hydrogen bonding. In the solution state, we performed ^{1}H NMR titration studies to

determine the stoichiometry as well as the association constants, K_a, between adenine- and thymine-containing PEG-ionenes with complementary guest molecules. In the solid state, we investigated the effect of self-complementary hydrogen bonds and complementary hydrogen bonds on thermal and morphological properties of adenine- and thymine-ionene homopolymers as well as their complexes with guest molecules.

4.3. Experimental

4.3.1. Materials

3,3-Iminobis(N,N-dimethylpropylamine) (DMPA, 97%), acryloyl chloride (97%), 6-bromohexanoyl chloride (97%), and triethylamine (TEA, 99%) were purchased from Aldrich and vacuum distilled prior to use. Potassium tert-butoxide (99.99%), adenine (A, 99%), thymine (T, 99%), poly(ethylene glycol) (PEG) with M_n = 1000 g/mol, sodium bicarbonate (99.7%), magnesium sulfate (99.5%), 1-bromobutane (99%), and potassium carbonate (>99%) were obtained from Sigma-Aldrich and used without further purification. γ-butyrolactone (+99%) and diisobutylalumium hydride 1.0 M solution in toluene were purchased from Aldrich and used as received. Dichloromethane (DCM, HPLC grade), tetrahydrofuran (THF, HPLC grade), and dimethyl formamide (DMF, HPLC grade) were passed through an alumina and molecular sieve column before use. Chloroform ($CHCl_3$, HPLC grade) and ethyl acetate (EtOAc, HPLC grade) were purchased from Fischer Scientific and were used as received.

4.3.2. Instrumentation

^{1}H NMR spectroscopic analyses were performed on a Varian Advance 500 MHz spectrometer to confirm the monomer and polymer composition at ambient temperature in $CDCl_3$ or CD_3OD. Fast

Atom Bombardment Mass Spectrometry (FAB-MS) was conducted in a positive ion mode on a JEOL HX110 dual focusing mass spectrometer. Differential scanning calorimetry (DSC) was conducted on a TA Instruments Q100 under a nitrogen purge of 50 mL/min at a heating rate of 10 °C/min. The glass transition temperatures were measured as the midpoint of the transition in the second heating scan. Thermogravimetric analysis (TGA) was conducted on a TA Instruments Hi-Res TGA 2950 under nitrogen at a heating rate of 10 °C/min. Atomic force microscopy (AFM) was performed using a Veeco MultiMode AFM equipped with (Veeco Instruments, Plainview, NYA). Samples were imaged at a set-point ratio of 0.70 with a magnification of 1 μm×1 μm. Veeco's Nanosensor silicon tips having a spring constant of 42 N/m were utilized for imaging. SAXS was performed using a Rigaku S-Max 3000 3 pinhole SAXS system, equipped with a rotating anode emitting X-ray with a wavelength of 0.154 nm (Cu Kα). Scattering from a Silver behenate standard was used to calibrate the sample-to-detector distance. For SAXS, the sample-to-detector distance was 1603 mm. Two-dimensional SAXS patterns were obtained using a fully integrated 2D multiwire, proportional counting, gas-filled detector, with an exposure time of 1 hour. All SAXD data were analyzed using the SAXSGUI software package to obtain radically integrated SAXS intensity versus the scattering vector q (SAXS), where $q=(4\pi/\lambda)\sin(\theta)$, θ is one half of the scattering angle and λ is the wavelength of X-ray profiles.

4.3.3. Synthesis of N,N-bis(3-(dimethylamino)propyl)-4-hydroxybutanamide

The acrylic monomer was synthesized using two steps. In the first step, a flame-dried, 2000-mL, three-neck, round-bottomed flask was attached to a 250-mL addition funnel and a condenser. The round-bottomed flask was charged with 50 mL (1.00 mol) of 3,3-iminobis(N,N-dimethylpropylamine) and 700 mL tetrahydrofuran (THF). The round-bottomed flask was purged with nitrogen. Diisobutylalumium hydride (1.0 M solution in toluene, 225 mL, 1.00 mol) was added

to the addition funnel and subsequently added to the reaction flask in a drop-wise fashion. The solution was stirred for 7 h at 0 °C. Subsequently, the reaction flask was warmed to room temperature and 17 mL (1.00 mol) of γ-butyrolactone was added to the reaction mixture and the solution was refluxed for 12 h. Water (10 mL) was added slowly to the cooled reaction flask and THF was evaporated under reduced pressure. A 15% sodium hydroxide solution (100 mL) was added and stirred for an hour. The aqueous layer was extracted three times with 100 mL dichloromethane and the organic fractions were combined. The solvent was concentrated *in vacuo* and the product was purified using Kugel-rohr distillation and yellow oil was obtained. An overall yield of 70% was obtained. ^{1}H NMR (500 MHz, $CDCl_3$): 1.71 (m, 4H, H_c), 1.90 (m, 2H, H_f), 2.21 (d, 12H, H_a), 2.26 (t, 4H, H_b), 2.52 (t, 2H, H_e), 3.35 (m, 4H, H_d), 3.67 (t, 2H, H_g), 3.45 (s, 1H, H_i). HRMS (ES+): m/z calcd for [M+H+] 273.24 g/mol, found 274.17 g/mol. (Figure S **4.1**).

4.3.4. Synthesis of 4-(bis(3-(dimethylamino)propyl)amino)-4-oxobutyl acrylate

In the second step, a flame-dried, 100-mL, round-bottomed flask was connected to a 50-mL addition funnel and was charged with dichloromethane (DCM) and 1.00 eq of hydroxyl-containing ditertiary amine monomer that was synthesized from the first step. The flask was cooled to 0 °C and acryloyl chloride (1.20 eq) was added to the addition funnel containing DCM and the solution was added drop-wise added to the reaction flask. The reaction was allowed to proceed for 12 h. Upon reaction completion, DCM was evaporated and the salt was dissolved in a mixture of saturated $NaHCO_3$ (aq) and saturated Na_2CO_3 (aq). The aqueous solution was extracted six times with DCM. The solution was concentrated *in vacuo* and the product was purified using Kugel-rohr distillation. A yellow oil with an overall yield of 30% was obtained. ^{1}H NMR (500 MHz, $CDCl_3$): 1.68 (m, 4H, H_c), 2.02 (m, 2H, H_f), 2.19 (d, 12H, H_a), 2.24 (t, 4H, H_b), 2.42 (t, 2H, H_e), 3.31 (m, 4H, H_d), 4.20 (t, 2H, H_g), 5.78-5.83 (m, 1H, H_{J1}), 6.05-6.14 (m, 1H, H_k), 6.35-6.42 (m, 1H, H_{J2}) (Figure S **4.2**).

4.3.5. Synthesis of Bromine End-Capped PEG (Br-PEG-Br)

The commercially available 1000 g/mol poly(ethylene glycol) (PEG) (10 g, 1.00 mol) was introduced to a 250-mL, two-neck, round-bottomed flask equipped with a magnetic stir bar, addition funnel, and nitrogen inlet. Anhydrous dichloromethane (100 mL) was added to the round-bottomed flask and 50 mL was added to the addition funnel. The flask was cooled to 0 °C and 6-bromohexanoyl chloride (2.20 eq) was added to the addition funnel with a syringe and subsequently added to the reaction flask in a drop wise fashion. The reaction was allowed to proceed for 24 h. Upon reaction completion, the reaction mixture was washed twice with saturated $NaHCO_3$ (aq) and twice with distilled water. The DCM layer was separated and dried over magnesium sulfate. The solution was concentrated *in vacuo* and dried under vacuum at 100 °C for 12 h (97% yield). The ^{1}H NMR number-average molecular weight was 1300 g/mol. The ^{1}H NMR (400 MHz, $CDCl_3$) spectroscopy for the bromine end-capped 1K PEG is as follows: δ = 1.47 ppm (m, 4H, per chain, H_c), 1.65 ppm (m, 4H, H_d), 1.87 ppm (m, 4H, H_b), 2.35 ppm (t, 4H, H_e), 3.40 ppm (t, 4H, H_a), 3.64 ppm (m, 76H, H_h), 3.69 ppm (m, 4H, H_g), 4.22 ppm (m, 4H, H_f) (Figure S 4.3).

4.3.6. Synthesis of n-Butyl thymine (nBT) Guest Molecule

Thymine (10.05 g, 80.0 mmol), potassium carbonate (11.06 g, 80.0 mmol), 1-bromobutane (3.67 g, 26.8 mmol), and DMSO (200 mL) were added to a 500-mL round-bottomed flask. The solution was heated to 50 °C for 8 h and then cooled. The resulting precipitate was removed through filtration and the DMSO solution was added to 600 mL water. The aqueous solution was extracted four times with 100 mL DCM and then the organic layer was washed four times with 300 mL water. The organic layer was dried over magnesium sulfate and then concentrated *in vacuo* to obtain a solid. The solid product was recrystallized from chloroform:hexanes to obtain a white solid with a yield of 51%. ^{1}H NMR (400 MHz, $CDCl_3$): 0.95 ppm (t, 3H, H_a), 1.36 ppm (m, 2H, H_b), 1.66 ppm

(p, 2H, H_c), 1.92 ppm (s, 3H, H_e), 3.69 ppm (t, 2H, H_d), 6.97 ppm (s, 1H, H_f), 8.65 ppm (s, 1H, H_g) (Figure S 4.4).

4.3.7. Synthesis of n-Butyl adenine (nBA) Guest Molecule

Adenine (6.05 g, 44.8 mmol), 1-bromobutane (6.16 g, 45.0 mmol), potassium carbonate (8.33 g, 60.3 mmol), and DMSO (60 mL) were added to a 250-mL round-bottomed flask. The resulting solution was stirred for 48 h at 23 °C and then poured into 600 mL water. The aqueous solution was extracted three times with 100 mL DCM and then the organic layer was washed three times with 100 mL water. The organic layer was dried over magnesium sulfate and concentrated *in vacuo* to obtain a solid. The product was obtained as a white solid after recrystallization from chloroform:hexanes. ^{1}H NMR (400 MHz, $CDCl_3$): 0.96 ppm (t, 3H, H_a), 1.37 ppm (m, 2H, H_b), 1.88 ppm (p, 2H, H_c), 4.20 ppm (t, 2H, H_d), 5.67 ppm (s, 2H, H_e), 7.79 ppm (s, 1H, H_f), 8.37 ppm (s, 1H, H_g) (Figure S 4.5).

4.3.8. Synthesis of Acrylate-Containing PEG-Based Ionene Precursor

Upon the synthesis of acrylic ditertiary amine monomer and bromine end-capped PEG, a 1:1 ratio of monomers were polymerized in DMF for 24 h at 80 °C in the presence of a catalytic amount of BHT. The polymer was stored in the DMF solution until the next synthetic step. ^{1}H NMR (400 MHz, CD_3OD):1.42 (m, 4H, H_m), 1.72 (m, 4H, H_n), 1.81 (m, 4H, H_i), 2.05 (m, 6H, H_d), 2.40 (m, 4H, H_p), 2.55 (t, 2H, H_e), 3.11 (d, 12H, H_a), 3.33-3.47 (m, 8H, H_{b+c}), 3.50 (t, 4H, H_g), 3.63 (s, 75H, H_{k1+k2}), 3.69 (t, 4H, H_l), 4.18-4.27 (m, 6H, H_f), 5.88-5.93 (dd, 1H, H_{j2}), 6.13-6.22 (m, 1H, H_h), 6.36-6.42 (dd, 1H, H_{j1}) (Figure S 4.6).

4.3.9. Synthesis of Nucleobase-Containing PEG-Based Ionene using Post-Polymerization Functionalization

After polymerization, the acrylic ionene solution in DMF was charged with 1.20 mol of adenine or thymine and 0.30 mol of tBuOK for 4 d. The nucleobase-containing ionene product was precipitated in ethyl acetate and dried in vacuo (0.1 mmHg) for 24 h (90% yield). ^{1}H NMR (400 MHz, CD_3OD) for adenine-containing ionene:1.42 (m, 4H, H_m), 1.70 (m, 4H, H_n), 1.81 (m, 4H, H_i), 1.91 (p, 2H, $H_{d'}$), 2.06 (m, 4H, H_d), 2.30 (t, 2H, H_e), 2.40 (m, 4H, H_p), 3.01 (t, 2H, H_h), 3.12 (d, 12H, H_a), 3.33-3.59 (m, 8H, H_{b+c+g}), 3.63 (s, 70H, H_{k1+k2}), 3.69 (t, 4H, H_l), 4.15 (t, 2H, H_q), 4.20 (m, 4H, H_f), 4.52 (m, 2H, H_j), 8.16 (s, 1H, H_s), 8.22 (s, 1H, H_r).^{1}H NMR (400 MHz, CD_3OD) for thymine-containing ionene: 1.44 (m, 4H, H_m), 1.71(m, 4H, H_n), 1.81 (m, 4H, H_i), 1.86 (s, 3H, H_s), 1.95 (p, 2H, $H_{d'}$), 2.08 (m, 4H, H_d), 2.32(t, 2H, H_e), 2.40 (t, 4H, H_p), 2.77 (t, 2H, H_h), 3.13 (d, 12H, H_a), 3.34-3.59 (m, 8H, H_{b+c+g}), 3.63 (s, 70H, H_{k1+k2}), 3.69 (t, 4H, H_l), 4.00 (t, 2H, H_q), 4.17 (t, 2H, H_j), 4.20 (t, 4H, H_f), 7.49 (s, 1H, H_r). (Figure S 4.7)

4.3.10. Preparation of Ionene Blend with Guest Molecules

The segmented adenine-containing ionene and thymine-containing ionene solutions in chloroform were mixed with *n*BT and *n*BA chloroform solutions in a 1:1 molar ratio respectively. The blends were stirred for an hour, and cast in Teflon® molds. The chloroform slowly evaporated at room temperature for 48 h and the films were then annealed at 100 °C for 24 hours *in vacuo*. Upon drying, the films were stored on drying agents (Drierite) and kept inside desiccator until further characterizations.

4.4. Results and Discussion

4.4.1. Synthesis of Nucleobase Functionalized PEG-Based Ionene Homopolymers

Synthesis of nucleobase functional PEG-based ionenes involved the synthesis of an acrylic ditertiary amine monomer and an oligomeric bromine-terminated PEG spacer. In the first synthetic step of the acrylic monomer synthesis, the secondary amine ring-opened the γ-butyrolactone in the presence of DIBAL, an efficient amidating agent for the conversion of lactones to amides.[21] Thus the reaction produced an OH-containing ditertiary amine monomer in high yields. In the second step, an acid chloride reaction between the primary alcohol and acryloyl chloride yielded an acrylic ditertiary amine monomer (Scheme 4.1a). We also used an acid chloride reaction to synthesize the difunctional bromine-terminated PEG (Scheme 4.1b). In our earlier work, we used similar reaction conditions to synthesize bromine end-capped poly(propylene glycol) oligomers and confirmed their difunctionalities with MALDI-TOF mass spectroscopy and titration analysis.[9]

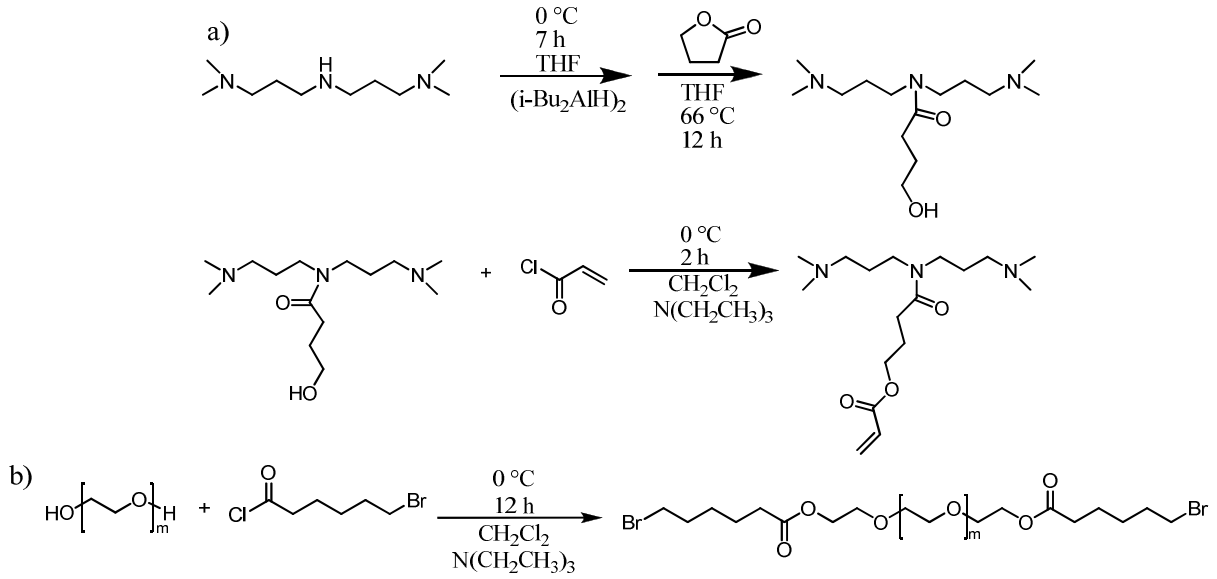

Scheme 4.1. Synthesis of acrylic ditertiary amine monomer (a), bromine end-capped 1000 g/mol PEG (b)

As shown in Scheme 4.2, the pure, difunctional tertiary amine and bromide monomers reacted under Menshutkin reaction conditions to provide acrylate-containing PEG-based ionene. In the same reaction flask, the post-polymerization functionalization using base-catalyzed Michael addition to the acrylate ionene precursor in DMF proceeded to yield the adenine-containing ionene (ionene-A) and thymine-containing ionene (ionene-T). The Michael addition reaction solution initially began heterogeneous and became homogeneous as it proceeded due to the enhanced solubility of the final nucleobase ionene product. The thermodynamically controlled base-catalyzed Michael addition promoted a regioselective substitution of adenine and thymine at the *N*9 and *N*1 positions, respectively.[22] Herein, we optimized the reaction conditions such as solvent, temperature, and base to obtain the regioselective nucleobase-containing ionenes. ^{1}H NMR spectroscopy confirmed successful incorporation of the heterocyclic base pairs. The disappearance of the olefinic protons at 5.8-6.6 ppm confirmed the quantitative Michael addition of the nucleobases to the acrylate ionene.

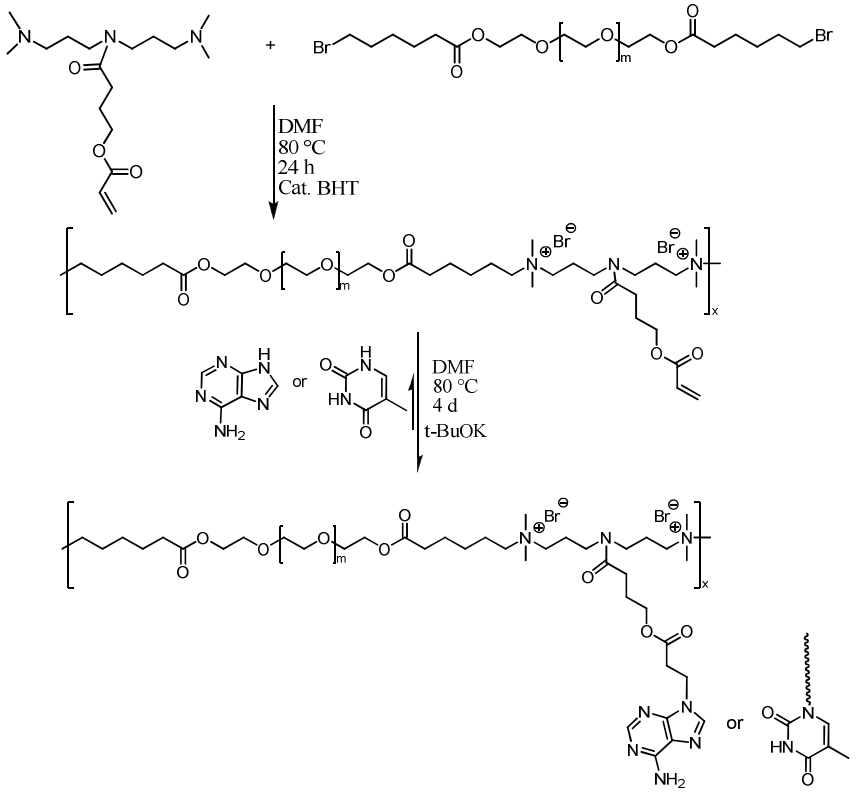

Scheme 4.2. Post-polymerization functionalization of PEG-based ionene

4.4.2. ^{1}H NMR Titrations

When adenine and thymine nucleobases form complementary hydrogen bonds, the chemical shift for the NH (thymine) and NH_2 (adenine) protons shift downfield compared to their original peak position. We prepared a 1:1 molar ratio blend of [ionene-A]:[ionene-T] at a 4 mM nucleobase in chloroform to investigate the formation of complementary multiple hydrogen bonds. However, ^{1}H NMR resonances of NH and NH_2 protons for the [ionene-A]:[ionene-T] blend had no significant change in their chemical shifts compared to the ionene homopolymers. In order for the side-group nucleobases to interact, PEG-based ionene chains must be in close affinity. However, due to the charged nature of the ionene backbone and steric hindrance between two bulky nucleobase-containing PEG chains, the formation of hydrogen bond between the complementary nucleobases

was restricted. In order to examine the effect of charge and the bulkiness of complementary nucleobase carriers, we introduced uracil octyl phosphonium salt (UOP^+) as a complementary small charged guest molecule to the [ionene-A]. For each repeat unit the charge ratio of [ionene-A] to [UOP^+] was two to one. Therefore not only we reduced the charge density per repeat unit but also we reduced the bulkiness of the complementary nucleobase carrier by using a low molecular weight guest molecule compared to the entangled PEG chains. Solutions of [ionene-A]:[UOP^+] complexes were prepared where the [ionene-A] concentration remained constant at 4 mM and the [UOP^+] concentration systematically increased. The position of the NH_2 resonance of ionene-A in the complex shifted down field (from 6.27 to 6.64 ppm) with the increase in [UOP^+] concentration. The association constant (K_a) based on Benesi-Hildebrand plot (Figure 4.1) was 19 M^{-1} which was in acceptable range (10-100 M^{-1}) but compared to the neutral guest molecules, studied in the following, was quite low. While charge-charge repulsion still reduced the strength of association between complementary bases, the less sterically hindered guest molecule promoted hydrogen bonding interaction. Thus, we synthesized neutral adenine and thymine-containing small guest molecules to examine the supramolecular assembly of the small molecule nucleobase guests and the nucleobase ionenes. These guest molecules are small ($M_w \approx 190$ g/mol), have no charge, and are highly soluble in chloroform, which makes them ideal candidates to interact with the complementary ionene homopolymers.

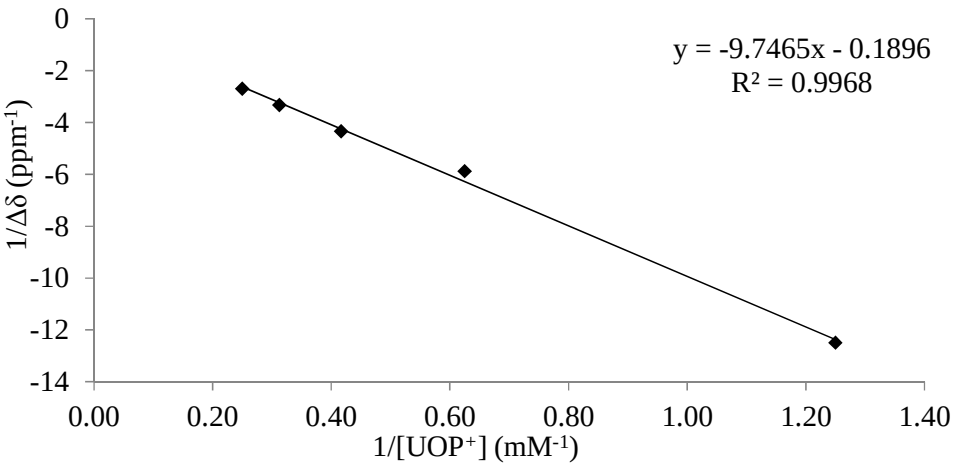

Figure 4.1. Benesi-Hildebrand plot of ionene-A and UOP^+ guest molecule association in $CDCl_3$

We first determined the stoichiometry of the host-guest complex, which is necessary before calculating their association constant (K_a).[23] Job's method, a continuous variation method, elucidates the host-guest stoichiometry using ^1H NMR spectroscopy.[24, 25] Solutions containing host nucleobase ionenes and small molecule nucleobase guest were prepared in chloroform. The total solution concentration maintained constant, while the molar ratios of the two components varied. We monitored the adenine NH_2 chemical shift at different mole fractions of [ionene-T]:[*n*BA], and [*n*BT]:[*n*BA] complexes and thymine NH chemical shift at different mole fractions of [ionene-A]:[*n*BT]. Figure 4.2 demonstrates Job's plots for [ionene-A]:[*n*BT], [ionene-T]:[*n*BA], and [*n*BT]:[*n*BA]. The x-axis value of the parabolic maximum of the Job's plot represents the stoichiometry of the complex. The fitting of the parabolic had R^2 value of *ca*. 0.9998 confirming a negligible error in Job's plots. All plots are symmetric and have a maximum at a 0.5 mole fraction, which means that the base pairing occurs in a 1:1 fashion. Therefore, the majority of the concentration in these complexes with various fractions contains 1:1 molar ratios of host and

guest.[26]

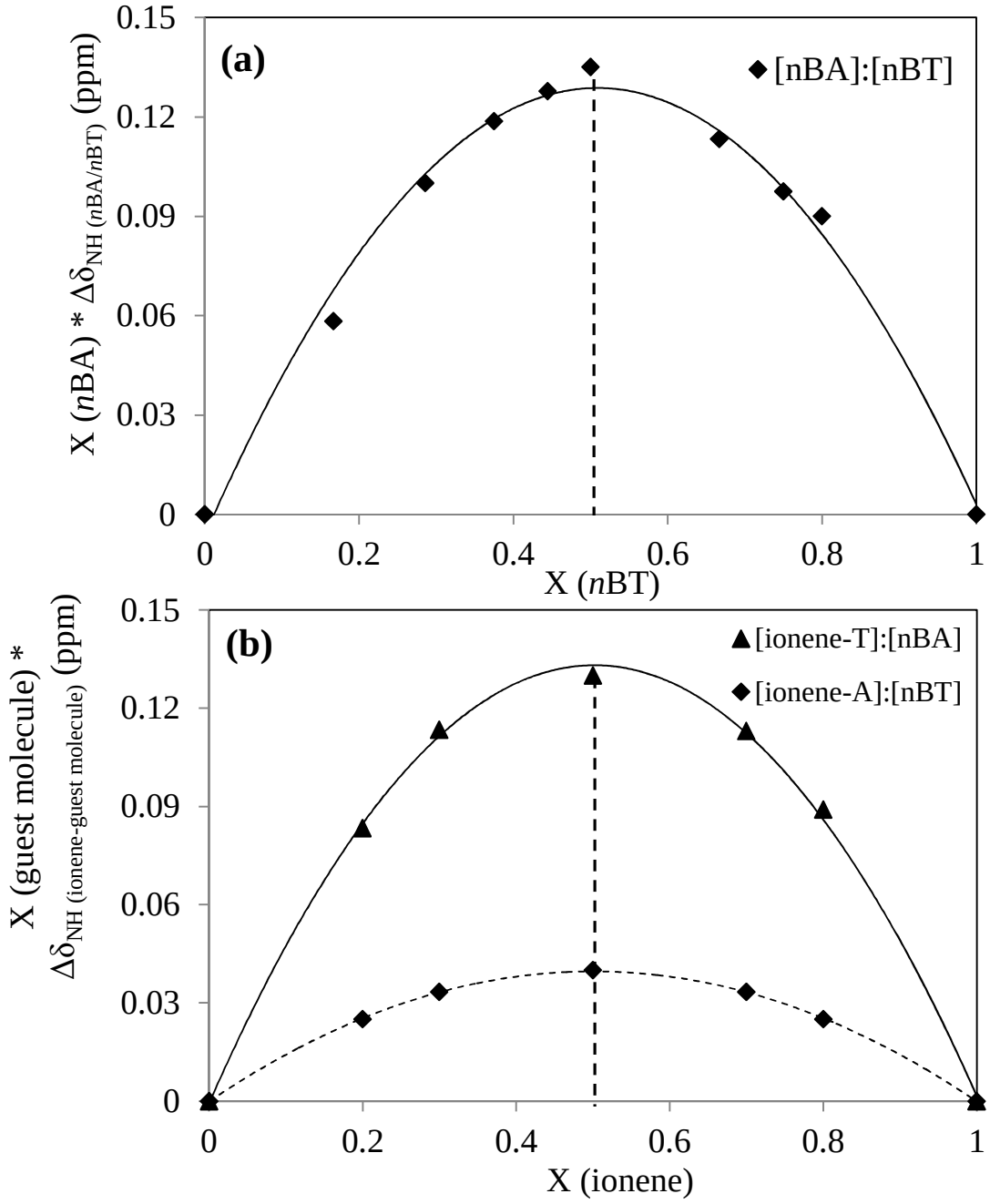

Figure 4.2. Job's plot to determine the stoichiometry of (a) [*n*BT]:[*n*BA], (b) [ionene-T]:[*n*BA] and [ionene-A]:[*n*BT] complexes in $CDCl_3$

^{1}H NMR titration experiments in chloroform, which favored hydrogen bonding interactions due to the relatively low dielectric constant, determined the association constants (K_a) between the adenine and thymine nucleobases. Solutions of [ionene-A]:[*n*BT] complexes were prepared where the [*n*BT] concentration remained constant at 4 mM and the [ionene-A] concentration systematically increased from 4 mM to 16 mM. The position of the NH resonance of *n*BT in the complex shifted down field (from 8.11 to 8.35 ppm) with the increase in [ionene-A] concentration. The curvature of chemical shift data with increasing adenine concentration remained consistent with typical ^{1}H NMR titration curves.[27] The change in chemical shift with complexation results from a faster exchange between the associated and dissociated A-T complex on the NMR time scale.[23, 28]

Figure 4.3 demonstrates a typical non-linear NMR titration curve of induced chemical shift versus solution concentration. The Benesi-Hildebrande model is a mathematical method to determine the association constant (K_a) from NMR titration experiments. This model fits the nonlinear chemical shift data for a dimeric hydrogen bond association assuming that the complex is formed in a 1:1 stoichiometry.[23, 29] Fitting of this data to the Benesi-Hildebrande method produces a linear double reciprocal plot based on the association of A-T complex, which further confirms the 1:1 stoichiometry (Figure 4.3). We calculated the association constant (K_a) from the Benesi-Hildebrand analysis using the equation: $1/\Delta\delta = 1/(K_a\Delta\delta_{max}[\text{ionene-A}])+ 1/\Delta\delta_{max}$. The $\Delta\delta_{max}$ is the maximum change of the chemical shift of the thymine NH proton. The slope of the double reciprocal plot is $1/K_a\Delta\delta_{max}$ and the intercept is $1/\Delta\delta_{max}$. The K_a for the supramolecular assembly of *n*BT and ionene-A was 94 M^{-1}, which was consistent with earlier reports on adenine-thymine base pair recognition (10-100 M^{-1} in $CDCl_3$).[26, 30, 31]

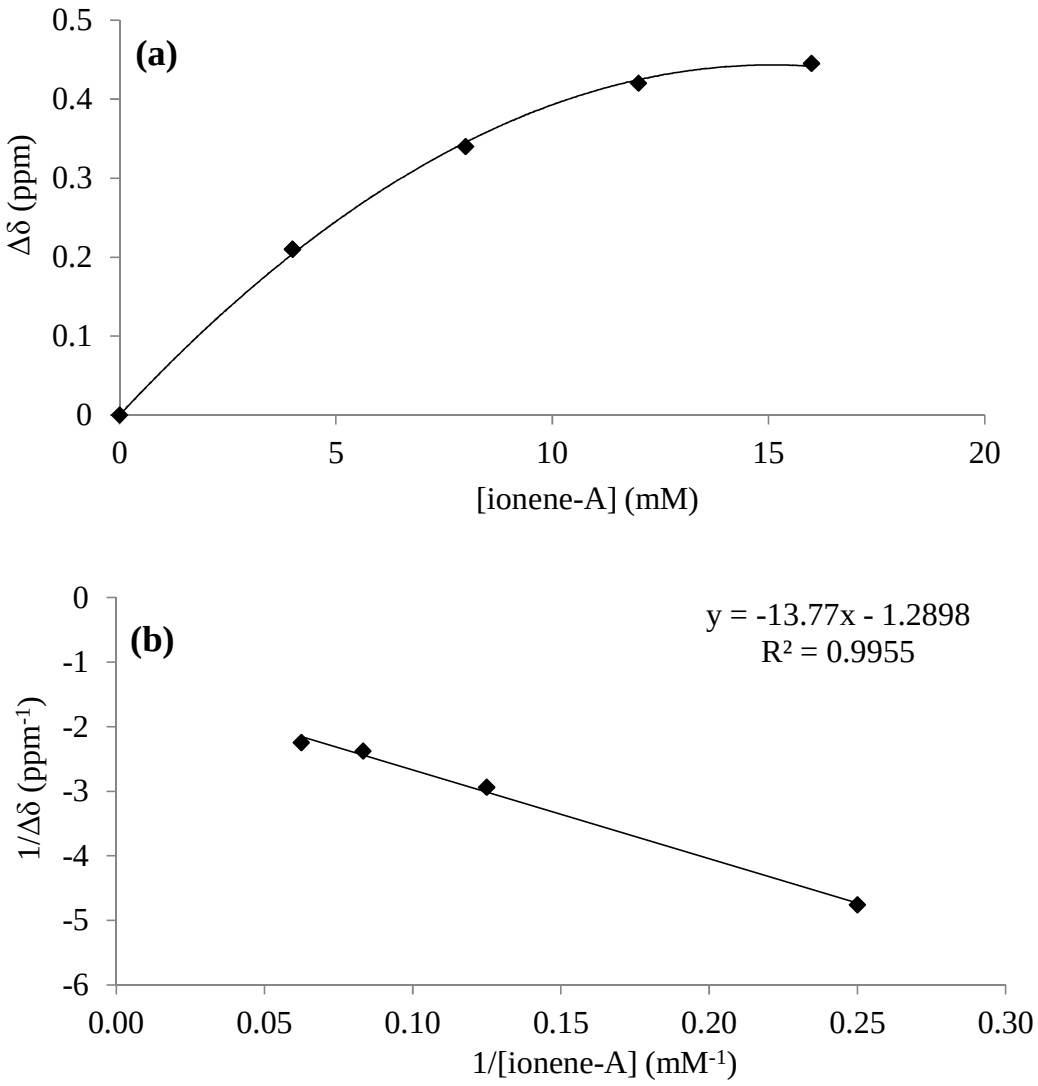

Figure 4.3. (a) Nonlinear relationship between induce change for thymine NH chemical shift and ionene-A concentration, (b) Benesi-Hildebrand plot of ionene-A and *n*BT guest molecule association in $CDCl_3$

We conducted similar ^{1}HNMR titration experiments for the [ionene-T]:[*n*BA] complex. The concentration of [*n*BA] was 4 mM and we systematically increased the [ionene-T] concentration from 4 mM to 16 mM. The position of the NH_2 resonance of *n*BA in the complex shifted down field (from 5.61 to 5.68 ppm) with the increase in [ionene-T] concentration. The linear fit to the Benesi-Hildebrand model also confirmed a 1:1 stoichiometry. Figure 4.4 depicts the double reciprocal plot

of Benesi-Hildebrand for the association of [ionene-T] and [*n*BA]. The K_a calculated from the slope of this plot is 130 M^{-1}.

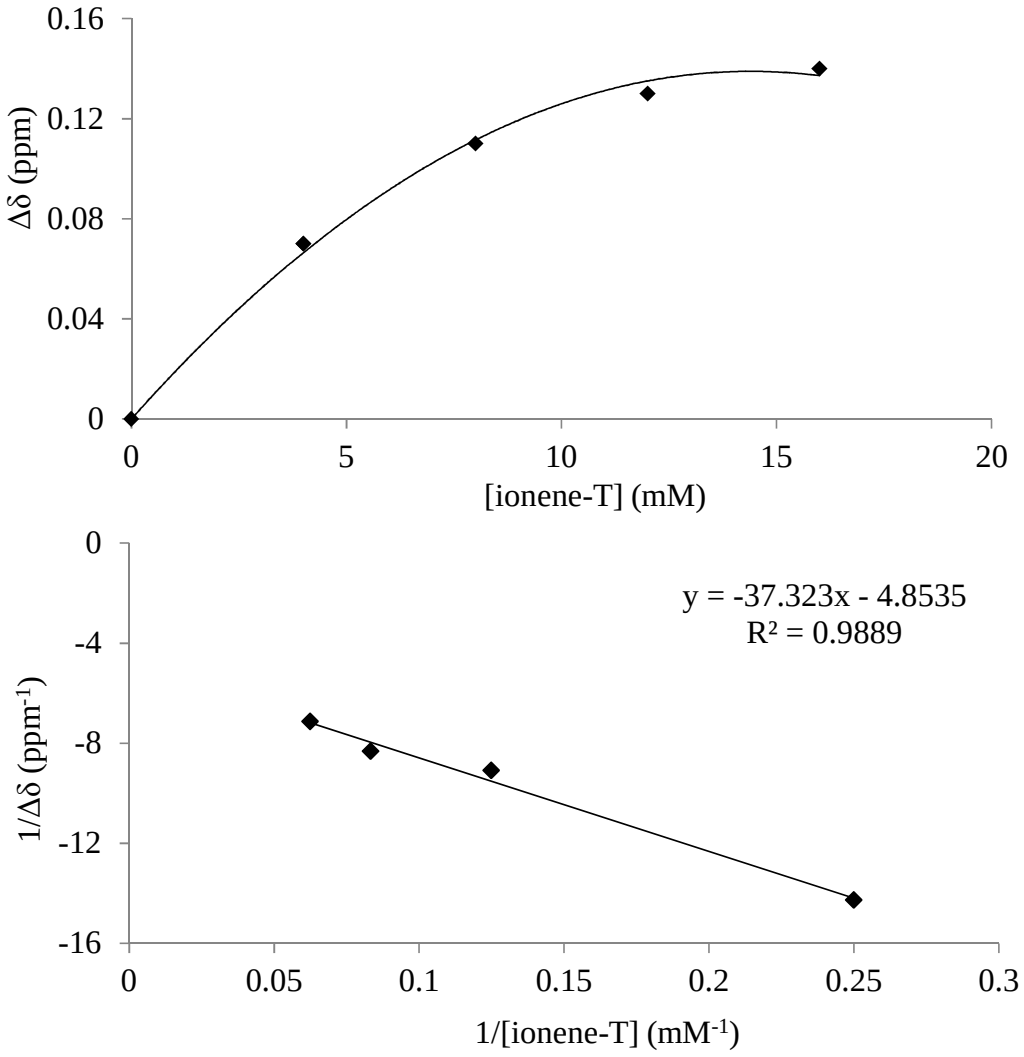

Figure 4.4. (a) Nonlinear relationship between induce change for adenine NH_2 chemical shift and ionene-T concentration, (b) Benesi-Hildebrand plot of ionene-T and *n*BA guest molecule association in $CDCl_3$

In order to have a control experiment, we also performed ^{1}H NMR titrations with the *n*BA and *n*BT guest molecules. The association constant K_a based on the slope of the plot represented in Figure 4.5 was 137 M^{-1}. Although the K_a values calculated for the three complexes are quite comparable and within acceptable range for adenine-thymine interaction, however the similarity of the K_a

values of 130 M^{-1} for [ionene-T]:[*n*BA] and [*n*BA]:[*n*BT] with K_a of 137 M^{-1} can be due to better solubility of ionene-T compared to ionene-A in $CDCl_3$. This can lead to efficient accessibility of nucleobases and stronger association between nucleobase pairs in solution.

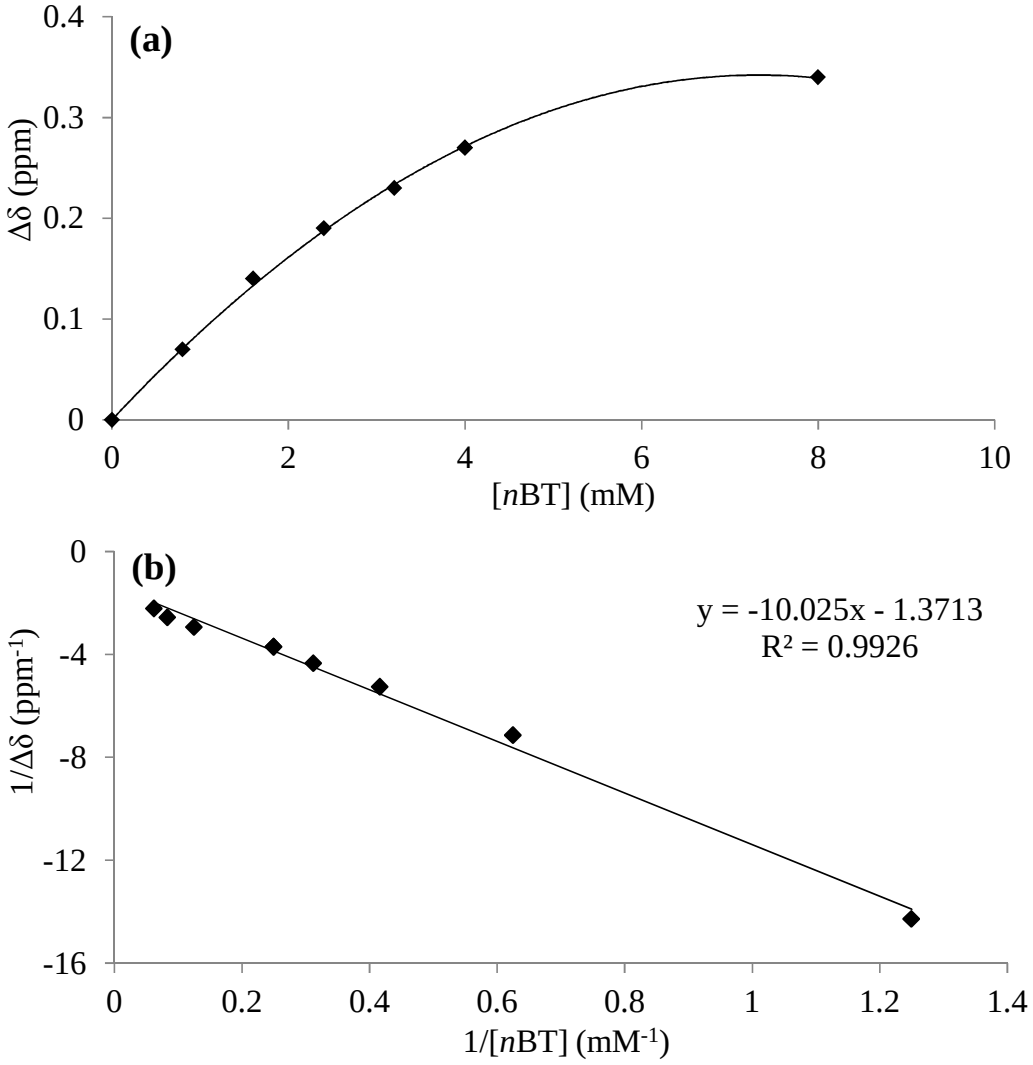

Figure 4.5. (a) Nonlinear relationship between induce change for adenine NH_2 chemical shift and *n*BT concentration, (b) Benesi-Hildebrand plot of *n*BT and *n*BA guest molecule association in $CDCl_3$

4.4.3. Thermal Transitions

Upon discovering the complementary behavior of nucleobase-containing ionenes with guest molecules in solution, we investigated the solid state properties of 1:1 molar ratios of ionene complexes with small guest molecules. To understand the association of nucleobase pairs, we studied the thermal properties of ionene-A, ionene-T and their complexes. All films were solution cast from chloroform and annealed at 100 °C for 24 h in vacuum. DSC curves for the nucleobase-functionalized ionene homopolymers and complexes showed a single glass transition temperature at roughly -40 °C. This transition corresponded to the T_g of the PEG soft segment (SS) (1000 g/mol) and confirmed a microphase separation of PEG SS from the ionic hard segment (HS). Since the nucleobases were incorporated into the hard phase, the hydrogen-bonding interactions did not significantly influence the T_g of the SS. In the solution-cast 1:1 blend of [ionene-A]:[*n*BT] and [ionene-T]:[*n*BA] from chloroform, the crystallization and melting peak of *n*BT and *n*BA were absent from the DSC thermograms (Figure 4.6) and the films were optically clear. Previously Long et al.[20] also showed that the addition of uracil-containing phosphonium salt to the adenine-containing triblock copolymers resulted in the disappearance of the phosphonium salt crystallization peak in the DSC thermograms. Thus, the absence of melting and crystallization peaks of the guest molecules indicates a well-defined hydrogen bonding interaction between the polymer and the guest molecule. Table 1 illustrates the thermal transitions of ionene homopolymers and ionene complexes.

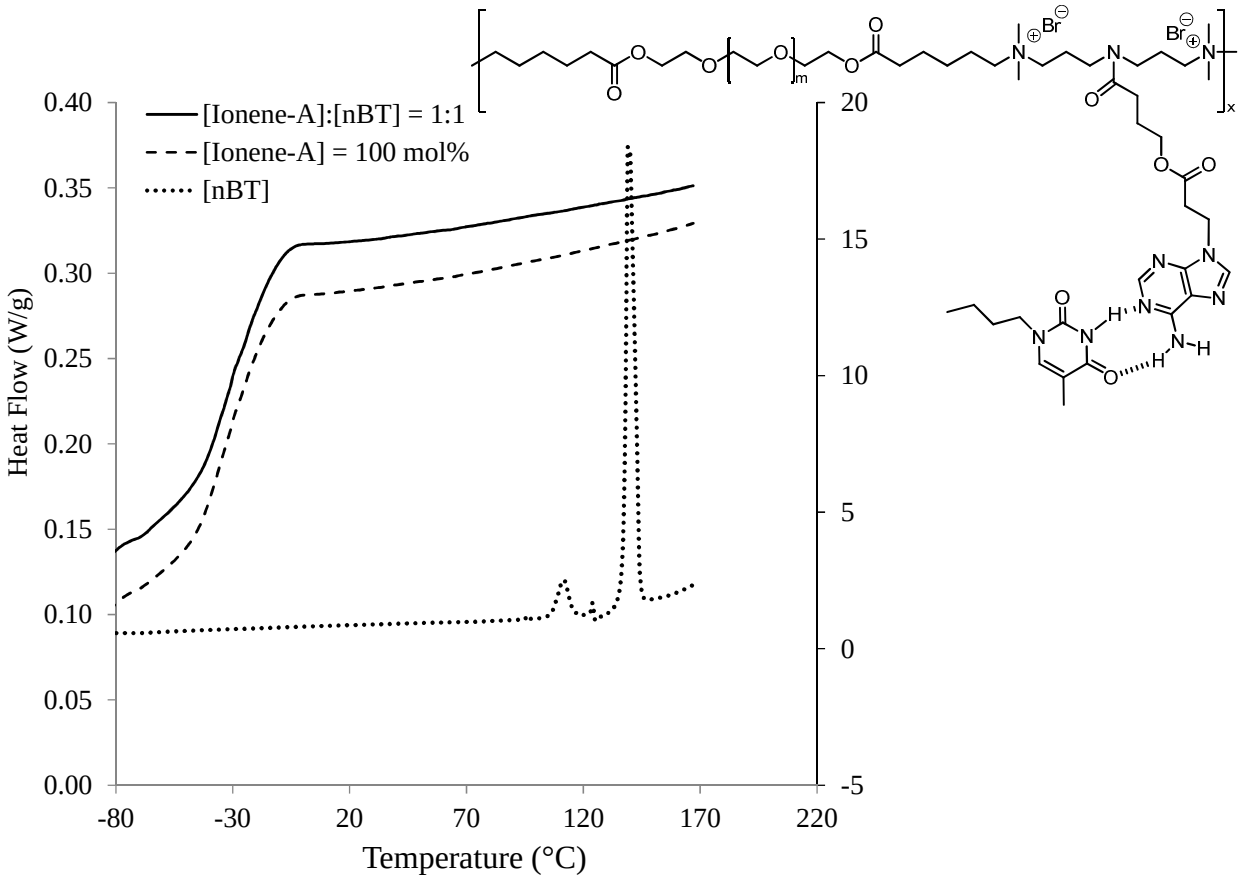

Figure 4.6. DSC thermograms of ionene-A homopolymer and 1:1 complex with *n*BT. Second heating cycle is shown.

Table 4.1. Thermal transitions of nucleobase-containing ionenes and their blends

Sample	T_g (°C) DSC	$T_{d5\%}$ (°C) TGA
Ionene-A	-36	246
Ionene-T	-40	248
[Ionene-A]:[*n*BT]	-31	243
[Ionene-T]:[*n*BA]	-48	222

4.4.4. Morphology

We conducted atomic force microscopy (AFM) and X-ray scattering on the films of ionene homopolymers and ionene complexes. Figure 4.7 represents the AFM phase images of ionene-A and ionene-T as well as their complexes. AFM images of ionene homopolymers revealed microphase-seperated morphology. The darker regions corresponded to the PEG SS (78 wt%) and the brighter regions corresponded to the harder ionic domains and heterocyclic nucleobases (22 wt%). Comparing the ionene homopolymers with the blends demonstrated a decreased phase contrast. This suggested the disruption of the adenine-adenine or thymine-thymine hard phase through incorporation of complementary small molecules. Figure 4.8 illustrates the corresponding SAXS data. Due to the difference in electron density of the HS relative to the SS, a single peak was observed in the SAXS profile of ionene homopolymers. The Bragg spacing, the distance between the ionic aggregates, of 5.75 nm for ionene-A was in agreement with our previous report on the 1k PPG-based ammonium ionenes having a Bragg spacing of 6.6 nm.[9] The SAXS data revealed that the addition of the *n*BT guest molecule resulted in a disruption of original morphology and led to a broad peak at shorter Bragg spacing of 4.62 nm.

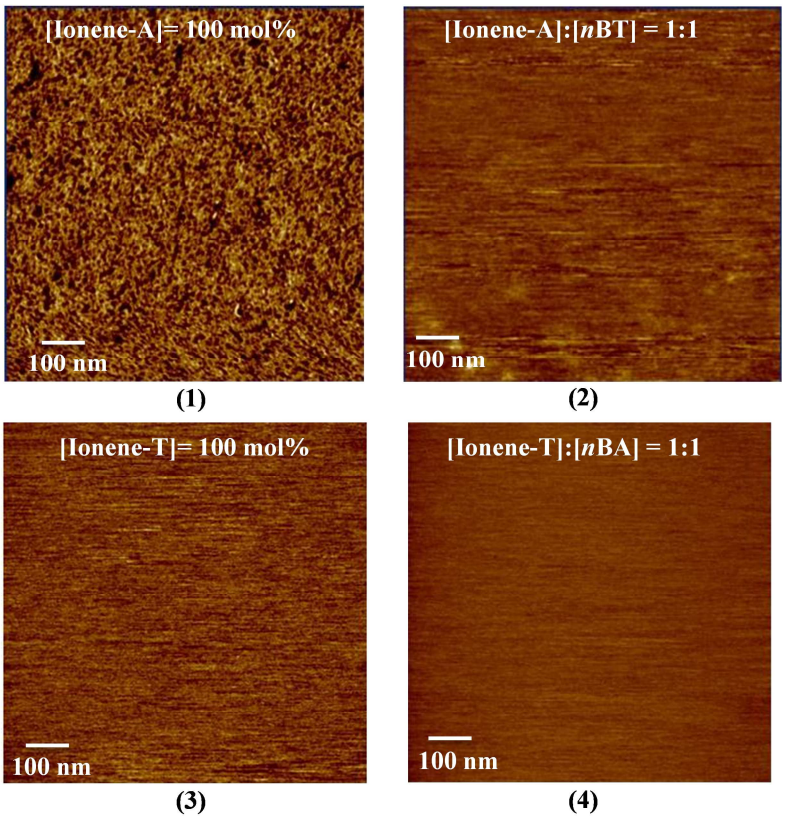

Figure 4.7. AFM phase images of nucleobase-containing ionene homopolymers (1,3) and their 1:1 complexes with *n*Bt and *n*BA (2,4)

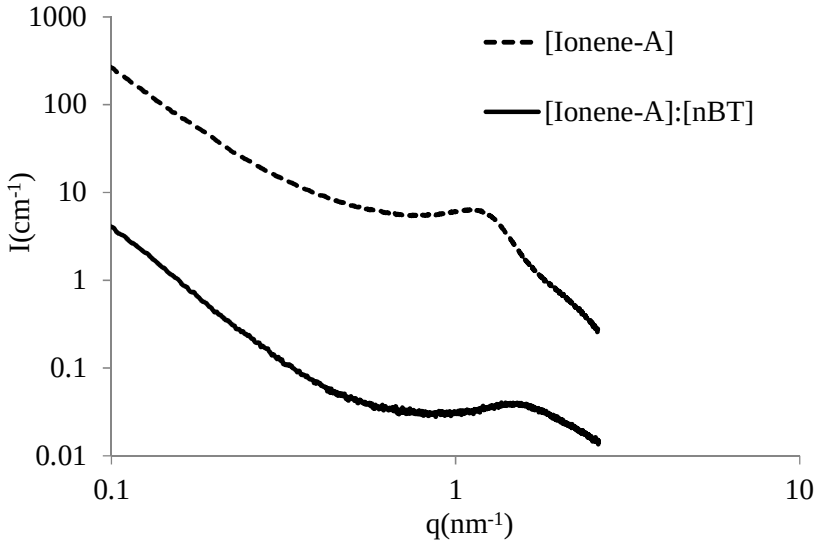

Figure 4.8. SAXS data for nucleobase-containing ionene homopolymers and blends

4.5. Conclusions

We synthesized and characterized nucleobase-containing ammonium ionenes using post-polymerization functionalization. The blends of the ionene homopolymers with complementary nucleobase-containing guest molecules resulted in efficient hydrogen bonding interactions. Job's plots and Benesi-Hildebrand analyses revealed 1:1 complexation between ionene homopolymers and guest molecules. The K_a for [ionene-A]:[*n*BT], [ionene-T]:[*n*BA], and [*n*BT]:[*n*BA] complexes were 94, 130, and 137 M^{-1} respectively. Ionene homopolymers and complexes showed a single T_g at -40 °C that corresponded to the T_g of PEG soft segment due to the microphase separation. The AFM and SAXS further confirmed a microphase-separated morphology for ionene homopolymers.

4.6. References

(1) Lutz, J.-F.; Thuenemann, A. F.; Rurack, K. *Macromolecules* **2005,** 38, 8124-8126.
(2) Mather, B. D.; Baker, M. B.; Beyer, F. L.; Berg, M. A. G.; Green, M. D.; Long, T. E. *Macromolecules* **2007,** 40, (19), 6834-6845.
(3) Williams, S. R.; Long, T. E. *Prog. Polym. Sci.* **2009,** 34, (8), 762-782.
(4) Ramirez, S. M.; Layman, J. M.; Long, T. E. *Macromol. Biosci.* **2009,** 9, 1127-1134.
(5) Trukhanova, E. S.; Izumrudov, V. A.; Litmanovich, A. A.; Zelikin, A. N. *Biomacromolecules* **2005,** 6, (6), 3198-3201.
(6) Jacquet, B.; Lang, G. Quaternized polymer for use as a cosmetic agent in cosmetic compositions for the hair and skin. US4217914A, 1980.
(7) Narita, T.; Ohtakeyama, R.; Nishino, M.; Gong, J. P.; Osada, Y. *Colloid. Polym. Sci.* **2000,** 278, (9), 884-887.
(8) Factor, A.; Heinsohn, G. E. *J. Polym. Sci., Part C: Polym. Lett.* **1971,** 9, (4), 289-95.
(9) Tamami, M.; Williams, S. R.; Park, J. K.; Moore, R. B.; Long, T. E. *J. Polym. Sci., Part A: Polym. Chem.* **2010,** 48, (19), 4159-4167.
(10) Tamami, M.; Salas-de, l. C. D.; Winey, K. I.; Long, T. E. *Macromol. Chem. Phys.* **2012,** 213, 965-972.
(11) Cheng, S.; Zhang, M.; Dixit, N.; Moore, R. B.; Long, T. E. *Macromolecules* **2012,** 45, 805-812.
(12) Lin, I. H.; Cheng, C.-C.; Yen, Y.-C.; Chang, F.-C. *Macromolecules* 43, (3), 1245-1252.
(13) Lo, P. K.; Sleiman, H. F. *J. Am. Chem. Soc.* **2009,** 131, 4182-4183.
(14) Spijker, H. J.; van, D. F. L.; van, H. J. C. M. *Macromolecules* **2007,** 40, 12-18.
(15) Lutz, J.-F.; Pfeifer, S.; Chanana, M.; Thuenemann, A. F.; Bienert, R. *Langmuir* **2006,** 22, 7411-7415.
(16) Bazzi, H. S.; Sleiman, H. F. *Macromolecules* **2002,** 35, 9617-9620.

(17) Xu, H.; Hong, R.; Lu, T.; Uzun, O.; Rotello, V. M. *J. Am. Chem. Soc.* **2006,** 128, 3162-3163.
(18) Nair, K. P.; Weck, M. *Macromolecules* **2007,** 40, 211-219.
(19) Hemp, S. T.; Hunley, M. T.; Cheng, S.; DeMella, K. C.; Long, T. E. *Polymer* **2012,** 53, 1437-1443.
(20) Mather, B. D.; Baker, M. B.; Beyer, F. L.; Green, M. D.; Berg, M. A. G.; Long, T. E. *Macromolecules* **2007,** 40, 4396-4398.
(21) Huang, P.-Q.; Zheng, X.; Deng, X.-M. *Tetrahedron Lett.* **2001,** 42, 9039-9041.
(22) Lira, E. P.; Huffman, C. W. *J. Org. Chem.* **1966,** 31, 2188-91.
(23) Fielding, L. *Tetrahedron* **2000,** 56, 6151-6170.
(24) Job, P. *Ann. Chim. Appl.* **1928,** 9, 113-203.
(25) Sahai, R.; Loper, G. L.; Lin, S. H.; Eyring, H. *Proc. Nat. Acad. Sci. U. S. A.* **1974,** 71, 1499-503.
(26) Nowick, J. S.; Chen, J. S.; Noronha, G. *J. Am. Chem. Soc.* **1993,** 115, 7636-44.
(27) Karikari, A. S.; Mather, B. D.; Long, T. E. *Biomacromolecules* **2007,** 8, 302-308.
(28) Park, T.; Zimmerman, S. C. *J. Am. Chem. Soc.* **2006,** 128, 11582-11590.
(29) Mesplet, N.; Morin, P.; Ribet, J.-P. *Eur. J. Pharm. Biopharm.* **2005,** 59, 523-526.
(30) Sivakova, S.; Bohnsack, D. A.; Mackay, M. E.; Suwanmala, P.; Rowan, S. J. *J. Am. Chem. Soc.* **2005,** 127, 18202-18211.
(31) Kyogoku, Y.; Lord, R. C.; Rich, A. *Biochim. Biophys. Acta, Nucleic Acids Protein Synth.* **1969,** 179, 10-17.

Supplemental ^{1}H NMR Figures:

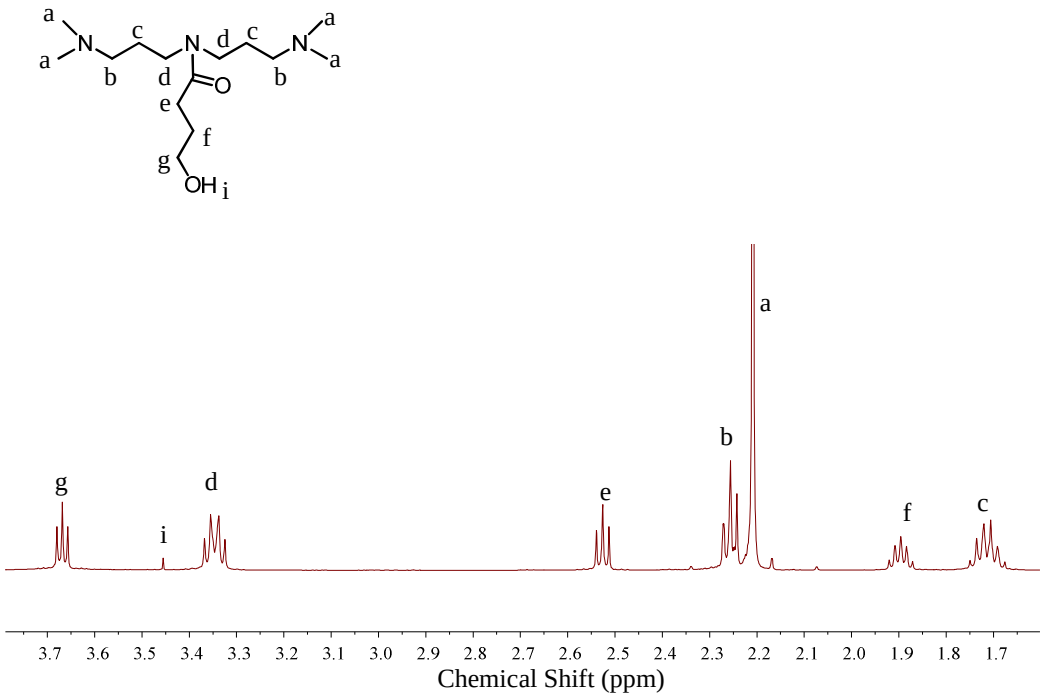

Figure S 4.1. ^{1}H NMR of *N*,*N*-bis(3-(dimethylamino)propyl)-4-hydroxybutanamide

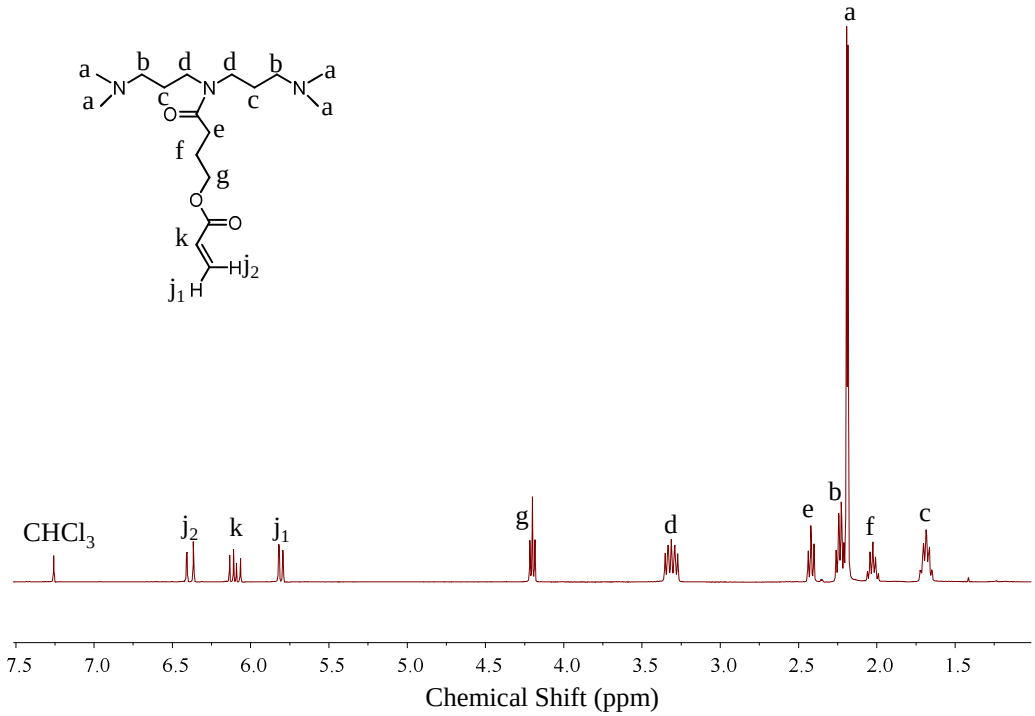

Figure S 4.2. ^{1}H NMR of 4-(bis(3-(dimethylamino)propyl)amino)-4-oxobutyl acrylate

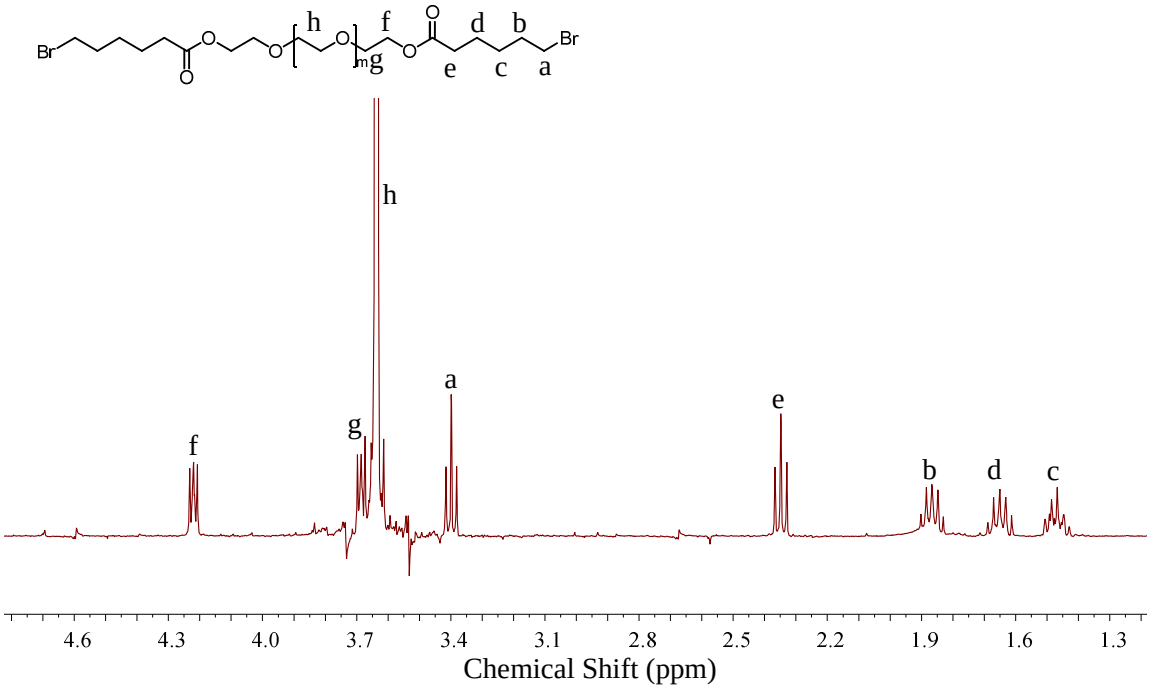

Figure S 4.3. ^{1}H NMR of bromine end-capped PEG (Br-PEG-Br)

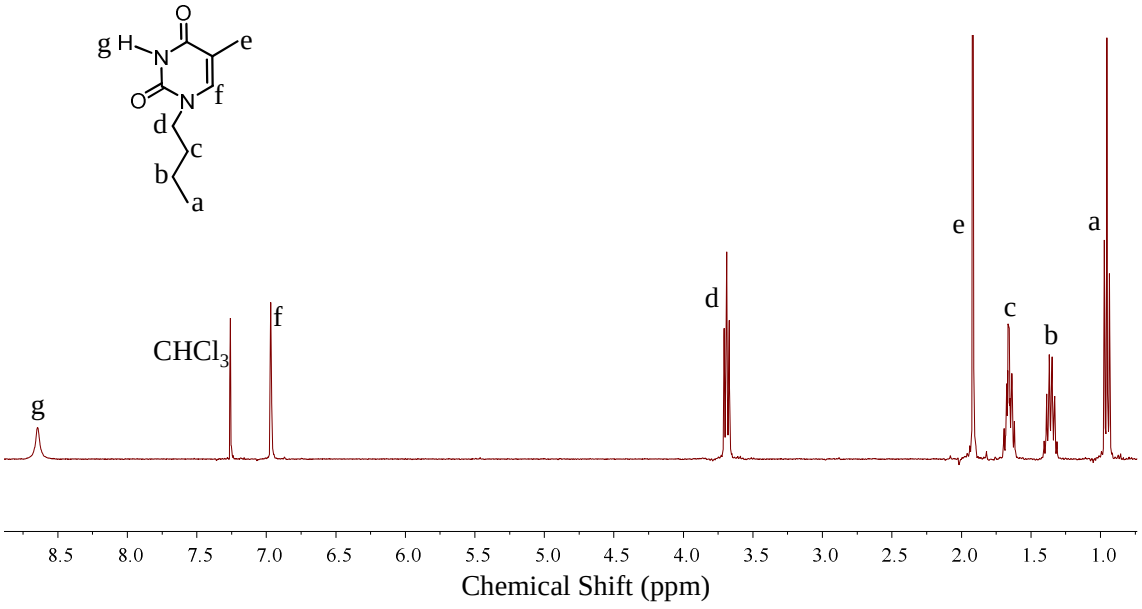

Figure S 4.4. ^{1}H NMR of *n*-butyl thymine guest molecule (*n*BT)

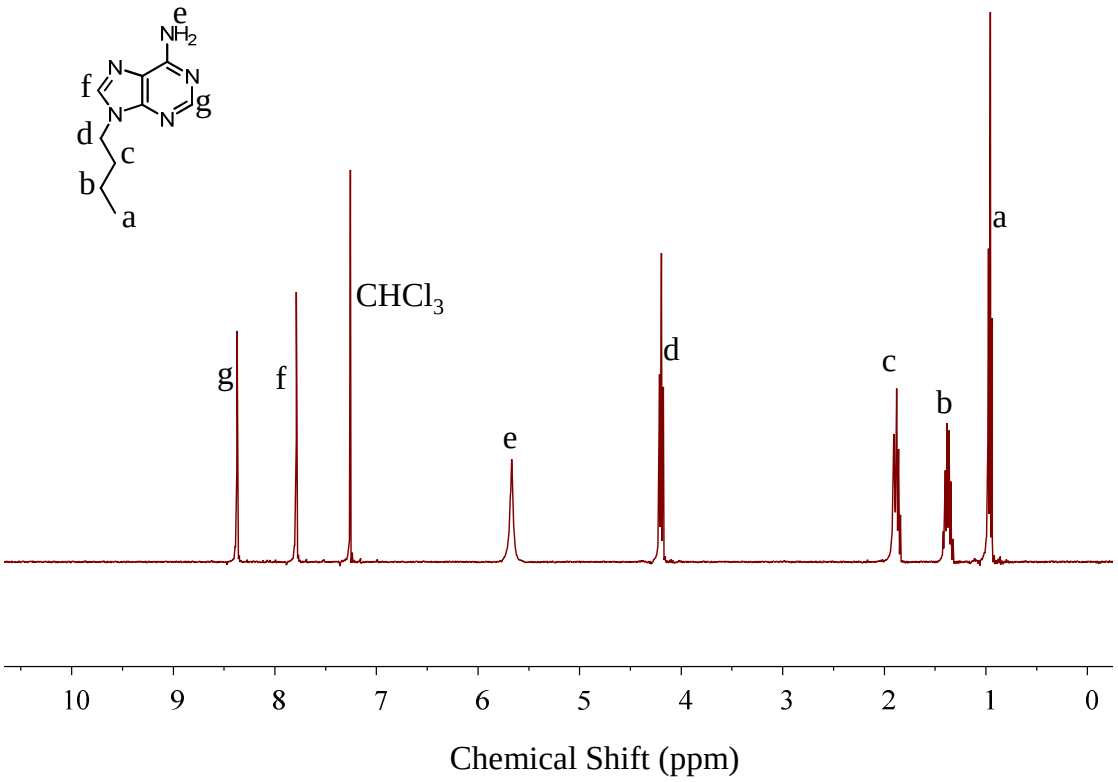

Figure S 4.5. ^{1}H NMR of *n*-butyl adenine guest molecule (*n*BA)

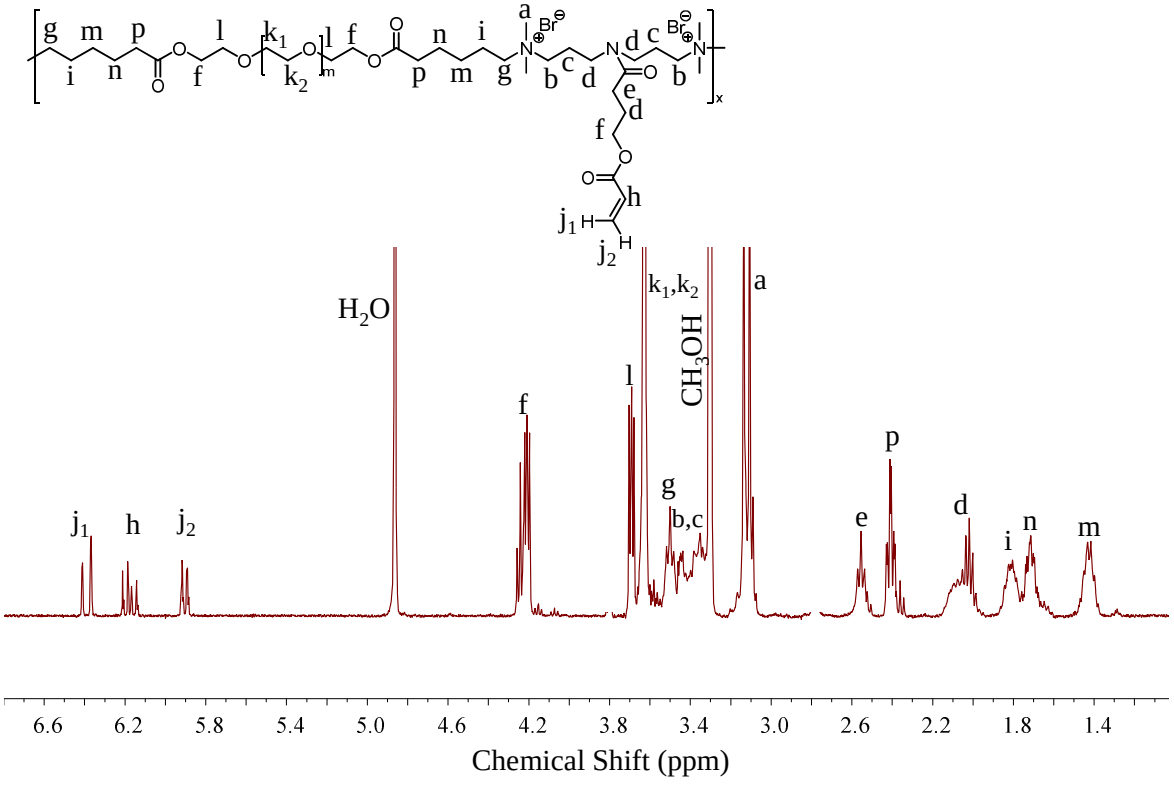

Figure S 4.6. ^{1}H NMR of acrylate-containing PEG-based ionene precursor

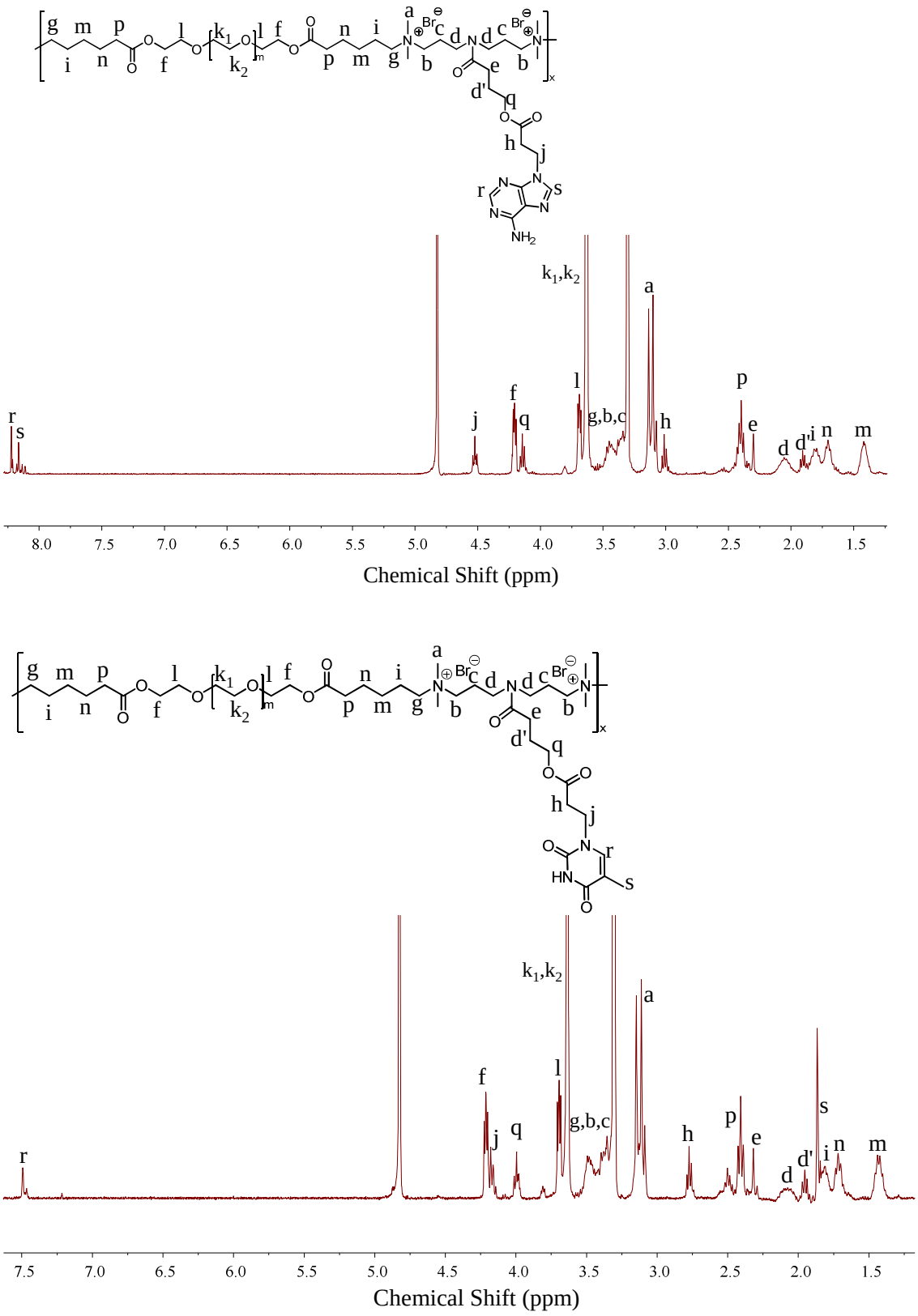

Figure S 4.7. [1]H NMR of nucleobase-containing ionenes: adenine-ionene (top), thymine-ionene (bottom)

Chapter 5. Synthesis and Characterization of Silicone-Based Ammonium Ionenes as Candidates for Self-Healing Polymers

Mana Tamami and Timothy E. Long*

Macromolecules and Interfaces Institute, Department of Chemistry, Virginia Tech, Blacksburg, VA 24061, USA

*E-mail address: telong@vt.edu

5.1. Abstract

We used Menshutkin reaction to synthesize PDMS-based ionenes having various hard segment contents. The effect of hard segment content on thermal, mechanical, rheological, and gas permeability was investigated. DSC showed one transition at -120 °C corresponding to the T_g of PDMS and upon 30 wt% HS a melting transition appeared for PDMS-ionenes. Mechanical properties of PDMS-ionenes were dependent on the amount of hard segment content. DMA confirmed microphase separation and showed that the rubbery plateau modulus extended to higher temperatures (from 87 °C to 164 °C) with increase in hard segment content (from 5 wt% to 15 wt%). Tensile analysis demonstrated systematic increase in modulus for PDMS-ionenes with increasing hard segment content. The melt viscosity of 5 wt% HS PDMS-based ionene was more temperature dependent compared to 15 wt% HS ionene. The OTR values for virgin PDMS-ionenes decreased linearly from 60000 to 15000 cc/m^2/day as the wt% hard segment increased.

Keywords: poly(dimethyl siloxane)-ionene, oxygen transmission rate, melt viscosity, self-healing, microphase separation

5.2. Introduction

Self-healing polymers have the ability to recover their strength and properties after damage. Since self-healing materials will not require replacement after damage or wear, this characteristic is very attractive especially for conservation purposes. Over the years, many self-healing materials have been invented.[1] Based on the self-healing process, the self-healing materials can be divided into two categories: self-healing based on covalent interactions which require carbon-carbon bond formation and self-healing driven by non-covalent interactions which require heat or light to stimulate the responsive polymer. Non-covalent interactions such as electrostatics[2, 3] and hydrogen bonding[4] not only improve thermal and mechanical properties of polymers, but also impart stimuli responsiveness that leads to self-healing.

Ionomers or ion-containing polymers are macromolecules that contain less than 15 mol% of ionic groups.[5, 6] The incompatibility of ionic groups and the organic polymer matrix causes ionic aggregation. Eisenberg et al.[5, 7, 8] proposed a model to describe the structure of ionic aggregates. They defined a multiplet as “an aggregate consisting of several ion pairs with a diameter of 5-10 Å”. Multiplets act as physical crosslinks and restrict the mobility of surrounding polymer chains. Upon increasing the ionic content, more multiplets form close to each other. Increase in charge density restricts the mobility surrounding each multiplet and causes it to overlap into continuous phase known as clusters. It is reported in the literature that ionic aggregates have drastic effect on mechanical[9, 10] and thermal properties.[11]

Recently the application of ionomers in self-healing materials has been explored. The copolymers of ethylene and methacrylic acid (EMAA) neutralized to a certain extent to form their salt form have shown self-healing behavior. Among these copolymers, Surlyn® manufactured by DuPont is a semicrystalline copolymer of ethylene and methacrylic acid. It has

been shown that Surlyn® heals through a viscoelastic healing process.[12] It is proposed that upon puncture, heat that is generated melts the ethylene crystallites in the damaged area. The clusters disorder and reaggregate to provide molten polymer with sufficient energy to bounce back. The polymer chains interdiffuse together and heal the hole. The neighboring polymer chains that remained at room temperature acted as an anchor for the mobile chains to pull against.

Ionenes are ion-containing polymers that have quaternized nitrogen atoms along the polymer backbone and are synthesized using step-growth polymerization of a ditertiary amine monomer with an alkyl dihalide monomer.[13] This polymerization is straight forward and there are no byproducts generated. The synthetic design of this reaction provides control over charge density and we can explore novel topologies using various monomer architectures. Our group has extensively synthesized ionenes having different chemical structures and investigated the effect of charge density on thermal, mechanical, rheological, and morphological properties.[14-17] We demonstrated that electrostatic interactions significantly influenced the ionene properties compared to their non-ionic counterparts. However, ionenes compared to ionomers have not been investigated for their self-healing properties. It is anticipated that the melt-elastic behavior of ionenes above their ionic dissociation temperature will assist in self-healing. The morphology of ionenes, unlike Surlyn®, can be more easily tailored for a targeted ionic dissociation temperature and tuned to have a programmed heal temperature as demanded by an application.

Herein, we report the synthesis of poly(dimethyl siloxane)-based ammonium ionenes adapted from our earlier research in collaboration with Wilkes et al.[18] we synthesized a series of PDMS-based ionenes in order to investigate the effect of HS content on ionic dissociation temperature, thermal, mechanical, and gas permeation properties.

5.3. Experimental.

5.3.1. Materials

α,ω-Amino propyl-polydimethylsiloxane (PDMS) oligomer with number-average molecular weight of 2500 g/mol was purchased from Gelest and dried *in vacuo* (0.1 mm Hg) for 24 h prior to use. 1,12-Dibromododecane (Aldrich, 98%) and 1,4-diazabicyclo[2.2.2]octane (DABCO, 98%) were sublimed before use. 6-bromohexanoyl chloride (97%) was purchased from Aldrich and used as received. Triethylamine (TEA, Aldrich, 99%) was distilled prior to use. Sodium bicarbonate ($NaHCO_3$) (99.7%) and magnesium sulfate (99.5%) were obtained from Sigma-Aldrich and used without further purification. Methanol (MeOH, Fisher, HPLC grade) was passed through alumina and molecular sieves columns. Chloroform ($CHCl_3$, Fisher, Optima grade) was distilled from calcium hydride.

5.3.2. Instrumentation

^1H NMR was utilized to determine monomer and polymer composition in $CDCl_3$ or CD_3OD at 23 °C with a 400 MHz Inova spectrometer. Thermogravimetric analysis (TGA) was conducted on a TA Instruments Hi-Res TGA 2950 with a temperature ramp of 10 °C/min in a nitrogen atmosphere. Differential scanning calorimetry (DSC) was performed using a TA Instruments Q100 differential scanning calorimeter under a nitrogen flow of 50 mL/min.

Dynamic mechanical analysis (DMA) was conducted on a TA Instruments Q800 dynamic mechanical analyzer in tension mode at a frequency of 1 Hz and temperature ramp of 3 °C/min. Tensile tests were performed on a 5500R Instron universal testing instrument with a cross-head speed of 50 mm/min using manual grips at ambient temperature. Melt rheology experiment was conducted on a TA Instruments G2 Rheometer in parallel-plate geometry with a diameter of 8

mm and a gap distance of 1mm. Strain amplitude was 1%. Oxygen transmission rate was measured using Illinois Instruments Model 8001 Oxygen Permeation Analyzer at 23 °C.

5.3.3. Synthesis of bromine end-capped poly(dimethyl siloxane) (Br-PDMS-Br)

A literature procedure was used to synthesize Br-PDMS-Br.[18] The commercially available amine-terminated PDMS (20.00 g, 1 eq) was added to a two-neck, round-bottomed flask equipped with a magnetic stir bar, addition funnel, nitrogen inlet, and 250 mL dichloromethane (DCM). Distilled triethylamine (2.2 eq) was added to the flask with a syringe. The flask was cooled to 0 °C. 6-Bromohexanoyl chloride (2.2 eq) was added to the addition funnel containing 50 mL DCM and subsequently added to the reaction flask in a drop wise fashion. The reaction was allowed to proceed for 24 h. Triethylamine salt was filtered through a fritted funnel. The product in DCM was introduced into a separatory funnel and washed twice with saturated $NaHCO_3$(aq) and twice with distilled water. The DCM layer was separated and dried over magnesium sulfate, filtered, and evaporated. The product was further dried under vacuum and the yield was 97%. The ^{1}H NMR number average molecular weight for Br-PDMS-Br was 3052 g/mol. ^{1}H NMR (400 MHz, $CDCl_3$): δ = 0.00 (m, 230H, H_a), 0.46 (m, 4H, H_b), 1.43 (m, 8H, H_c), 1.60 (p, 4H, H_d), 1.81 (p, 4H, H_e), 2.10 (t, 4H,H_f), 3.17 (q, 4H, H_g), 3.33 (t, 4H, H_h), 5.37 (s, 2H, H_i) (Figure 5.1).

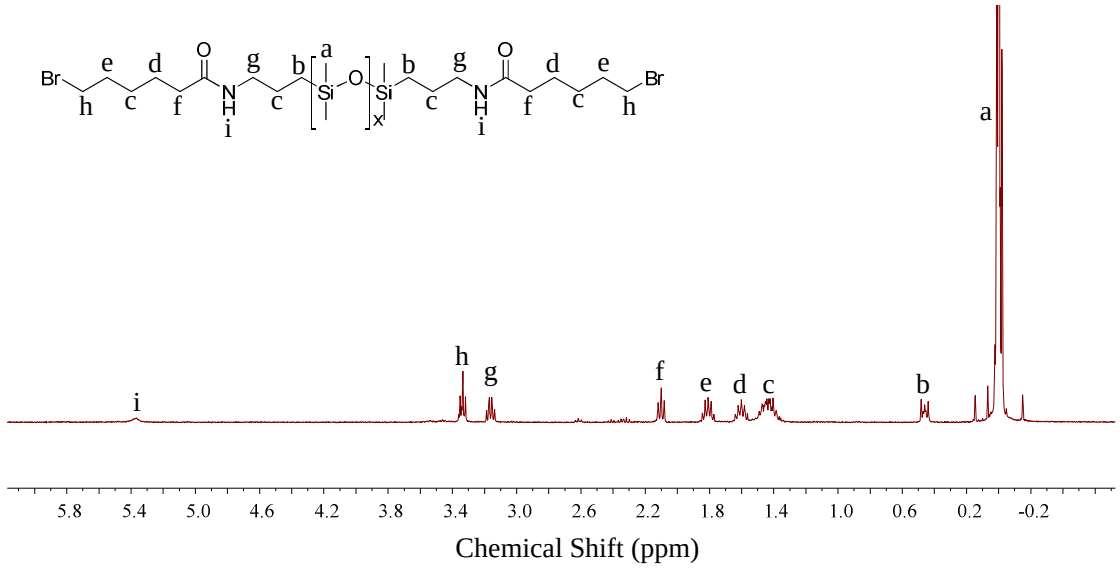

Figure 5.1. ^{1}H NMR spectrum of bromine-terminated PDMS

5.3.4. Synthesis of poly(dimethyl siloxane)-based ionene homopolymer

Upon the synthesis of difunctional Br-PDMS-Br, the commercially available cyclic ditertiary amine monomer (DABCO) was sublimed for further purification and dryness. Then a 1:1 molar ratio of Br-PDMS-Br (5.6 g, 2.6 mmol) with DABCO (0.29 g, 2.6 mmol) were introduced to a flame-dried round-bottom flask equipped with a condenser. The dried chloroform (15 mL) was added to the flask and the reaction was refluxed for 24 h at 65 °C. Upon reaction completion no further purification was needed. The excess solvent was removed and the rest of reaction solution was cast in Teflon mold. The films were slowly air-dried for 48 h and were then annealed at 100 °C for 24 h. The ionene films were then stored on drying agents (drierite) and inside the desiccator until analyzed. ^{1}H NMR (400 MHz, CD_3OD): δ = 0.00 (m, 304H, H_a), 0.48 (m, 4H, H_b), 1.24-1.87 (m, 16H, H_c), 2.16 (m, 4H, H_d), 3.07 (m, 4H, H_e), 3.52 (m, 4H, H_f), 3.93 (s, 12H, H_g) (Figure 5.2).

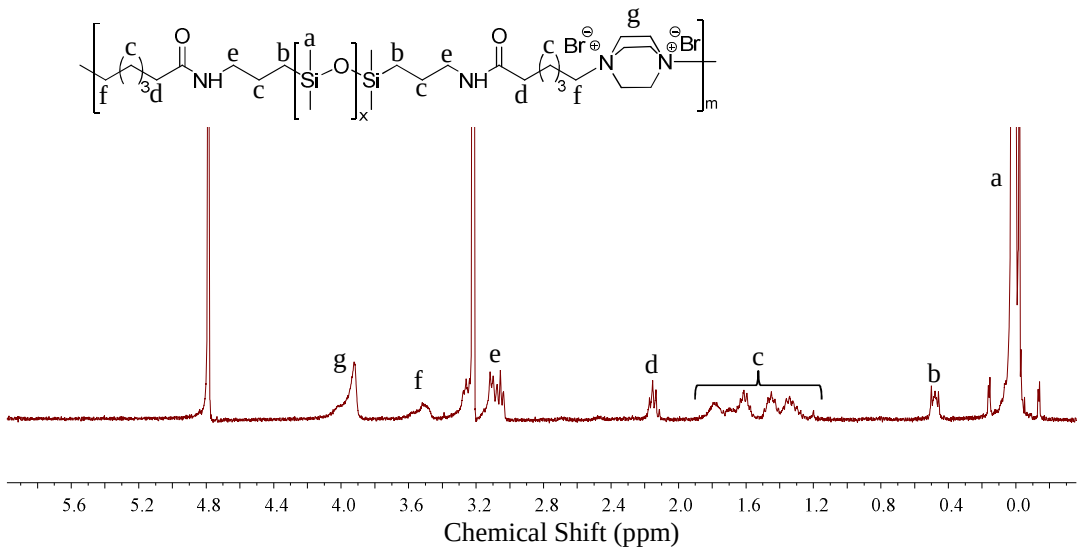

Figure 5.2. [1]H NMR spectrum of PDMS-based ionene homopolymer

5.3.5. Synthesis of poly(dimethyl siloxane)-based ionene random copolymer

The copolymer containing 15 wt % hard segment is used as an example; however, all copolymers were prepared in a similar fashion. 1,12-dibromododecane (1.08 g, 3.28 mmol), Br-PDMS-Br (10.00 g, 3.28 mmol), and DABCO (0.74 g, 6.55 mmol) were added to a two-neck, round-bottomed flask equipped with a stir bar, condenser, and nitrogen inlet. Dry chloroform (20 wt % solids) was added to the flask via syringe. The reaction was allowed to proceed for 24 h at 65 °C and upon completion, the polymer was cast into a film. The films were slowly air-dried for 48 h and were then annealed at 100 °C for 24 h. The ionene films were then stored on drying agents (drierite) and inside the desiccator until analyzed. [1]H NMR confirmed the structures of PDMS-based ionene random copolymers.

5.4. Results and Discussion

5.4.1. Synthesis of PDMS-based ionenes

We synthesized soft segment precursor, bromine-terminated PDMS, using quantitative derivatization of 2.5k g/mol aminopropyl-terminated PDMS with 6-bromohexanoyl chloride to yield an oligomeric dibromide (Scheme 5.1). Previously we reported the bromine functionalization of poly(propylene glycol) and poly(tetramethylene oxide) using the same procedure.[15, 17] ^{1}H NMR confirmed the structure of this oligomer (Figure 5.1). The number average molecular weight based on ^{1}H NMR was 3052 g/mol. Scheme 5.2 shows the synthesis of PDMS-based ionenes. We varied the amount of soft segment (SS) and hard segment (HS), while maintaining the 1:1 molar ratio of DABCO:dibromide. In order to obtain high molecular weight step-growth polymer, a 1:1 molar ratio of monomers is critical.[19] As shown in Table 5.1, five compositions were synthesized and ^{1}H NMR spectroscopy confirmed their structures. The resonance at 2.8 ppm in the ^{1}H NMR spectrum due to protons from DABCO ring shifted to 3.9 ppm after polymerization, confirming the quaternization of tertiary amine nitrogens within the ring. The total amount of 1,12-dibromododecane and DABCO corresponded to the HS content; the HS content varied from 5-60 wt%. Ionenes containing 5-60 wt% HS formed uniform solvent-cast films, however, due to the increase in HS content, the films of 50 and 60 wt% HS were very tacky and brittle

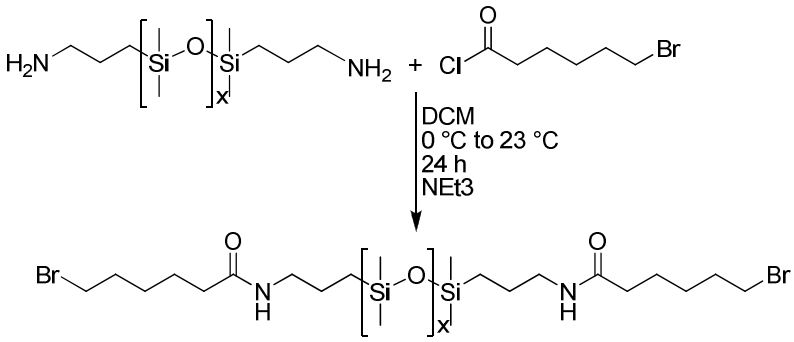

Scheme 5.1. Synthesis of bromine terminated PDMS

Table 5.1. Segmented copolymer compositions based on molar equivalents of monomer and HS/SS content

Br-PDMS-Br (mole eq.)	1,12-dibromododecane (mole eq.)	DABCO (mole eq.)	HS (wt%)	SS (wt%)
1.00	0.00	1.00	5	95
0.50	0.50	1.00	15	85
0.24	0.76	1.00	30	70
0.12	0.88	1.00	50	50
0.08	0.92	1.00	60	40

5.4.2. Thermal Transitions

The effect of hard segment content on thermal transitions was investigated using TGA and DSC. We used TGA to measure the thermal stability of all ionenes. TGA indicated that the ionic content within the polymer backbone dictates the thermal degradation behavior. The thermal degradation temperature at 5% weight loss (T_D) decreased from 273 °C to 170 °C with

increasing ionic content. The actual mechanism of thermal degradation is complex. Chen et al.[20] and Jerome et al.[21] proposed dequaternization of nitrogens according to the Hoffman elimination pathway. The Hoffman elimination reaction depends on the basicity of the anion.[22] At higher temperatures, the bromine counterion acts as a strong base and can dequaternize nitrogens, leaving tertiary amine and alkene chain ends. Herein, as the ionic content increases, the number of quaternized nitrogens increase along the backbone and therefore the degradation occurs earlier at lower temperatures. All ionenes revealed glass transition temperatures (T_g) of -123 °C, which corresponded to the T_g of the PDMS soft segment. Upon 30 wt% hard segment content the melting temperature (T_m) appeared which demonstrated an ordered crystalline phase within the soft PDMS amorphous phase. The data in Table 5.2 strongly suggest that these PDMS-based ionenes were microphase separated.

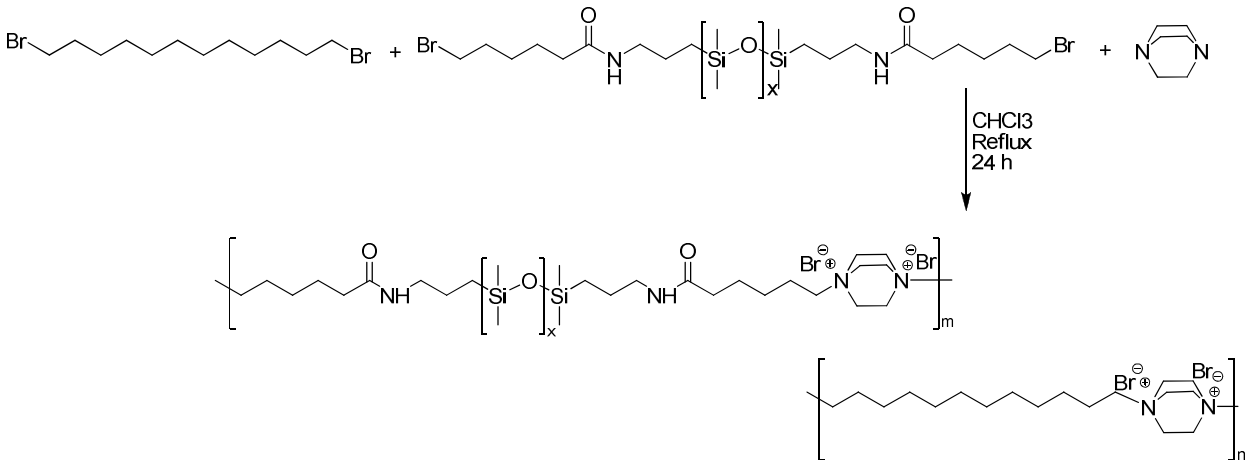

Scheme 5.2. Synthesis of PDMS-based segmented ionene copolymers

Table 5.2. TGA and DSC results of segmented PDMS-based ionenes

HS (wt%)	SS (wt%)	$T_{d5\%}$ (°C)	T_g (°C)	T_m (°C)
5	95	273	-123	NA
15	85	242	-123	NA
30	70	209	-123	-48
50	50	190	-123	-50
60	40	170	-123	-46

5.4.3. Dynamic Mechanical Analysis (DMA)

PDMS-based ionenes having 5 and 15 wt% HS formed homogenous and elastomeric films that were ideal candidates to measure their temperature-dependent moduli using DMA. The films were stored in desiccator after annealing and were quickly removed from desiccator and loaded on to the DMA clamps to prevent absorption of moisture. Figure 5.3 shows the DMA analysis for 5 wt% HS-ionene as an example. DMA confirmed microphase separation in these systems. Ionene showed high moduli (>10^3 MPa) in glassy state and a drastic drop in modulus occurred at -120 °C due to the glass transition temperature of PDMS soft segment. The rubbery plateau modulus for 15 wt% HS-ionene was higher than 5 wt% HS and it also extended to higher temperatures compared to 5 wt% HS-ionene (from 87 °C and 164 °C). This shows the dependency of rubbery plateau modulus on the charge density and hard segment content. As the charge density increased along the ionene backbone, stronger physical crosslinks occurred which led to an extension of rubbery plateau modulus. Therefore controlling the hard segment content

can tune the ionic dissociation temperature and moduli. Similarly, we reported the effect of charge density and soft segment molecular weight on poly(propylene glycol)-based ionenes.[17] As shown in Figure 5.3, both ionenes showed three transitions; first transition at -120 °C corresponded to the T_g of 2.5k PDMS, the second transition at *ca*. 20 °C corresponded to the melting of PDMS crystallites, and the third transition which occurred at 87 °C for 5 wt% HS-ionene and at 164 °C for 15 wt% HS-ionene attributed to the ionic dissociation temperature followed by the flow. The upward storage modulus for 15 wt% HS-ionene between 50 °C and 150 °C is not real and is due to an extreme softness of the sample at those high temperatures.

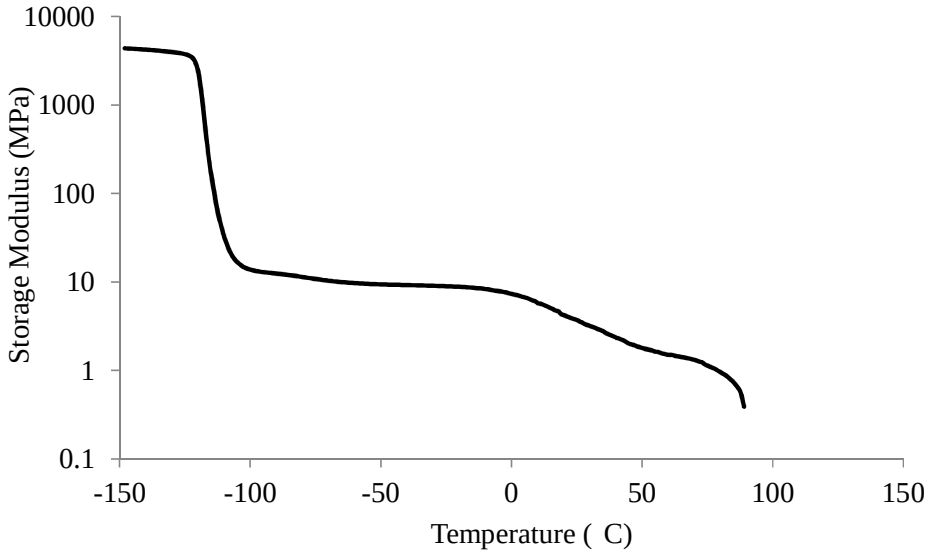

Figure 5.3. DMA of PDMS-based ionene having 5 wt% HS

5.4.4. Tensile test

We performed tensile analysis at ambient conditions for PDMS-ionenes having 5 and 15 wt% HS content (Figure 5.4). The 15 wt% HS ionene showed an ultimate tensile strength of 0.52 MPa and elongation at break of 151%. Due to increased wt% HS and stronger physical crosslinks, the 15 wt% HS-ionene showed higher modulus, tensile strength, and elongation compared to 5 wt%

HS-ionene (Table 5.3). It should be mentioned that the tensile moduli of both ionenes were comparable with moduli observed at ambient condition using DMA.

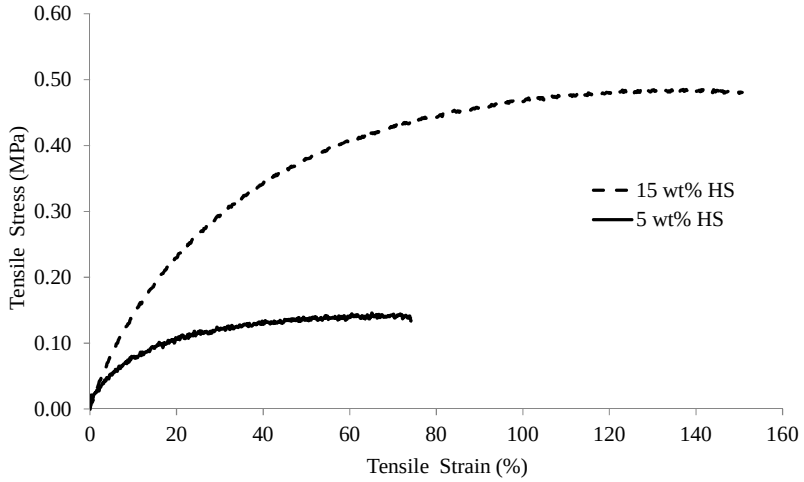

Figure 5.4. Tensile analysis of PDMS-based ionene having 5 wt% and 15 wt% HS

Table 5.3. Tensile data for PDMS-ionene films as a function of wt% HS

PDMS-ionenes	Tensile Stress at Break (MPa)	Tensile Strain at Break (%)	Young's Modulus (MPa)
5 wt% HS	0.13 ± 0.01	85.76 ± 7.17	0.70 ± 0.30
15 wt% HS	0.52 ± 0.04	150.66 ± 5.64	1.65 ± 0.11

5.4.5. Rheology

It is important to understand the effect of hard segment content on viscosity. In the healing event the material must flow to reach intimate contact. In order for the healing to occur, the viscosity of the polymer must be reduced by increasing the heat. This allows the polymer to reach a low enough viscosity to flow and then heal. Therefore upon film preparation of PDMS-based ionenes (5 and 15 wt% HS), we investigated the viscosity of the polymer melt as a function of temperature. It is illustrated in Figure 5.5 that melt viscosity of 5 wt% HS PDMS-ionene is

decreasing with temperature and in comparison the 15 wt% HS PDMS-ionene is independent of temperature. In addition, master curve of the storage and loss modulus versus frequency was generated for 5 wt% HS PDMS-ionene to estimate the changes in modulus over decades in time. Master curve of storage modulus versus frequency was referenced to 90 °C. As shown in Figure 5.6, time-temperature superposition was satisfied for the PDMS-ionene having 5 wt% HS.

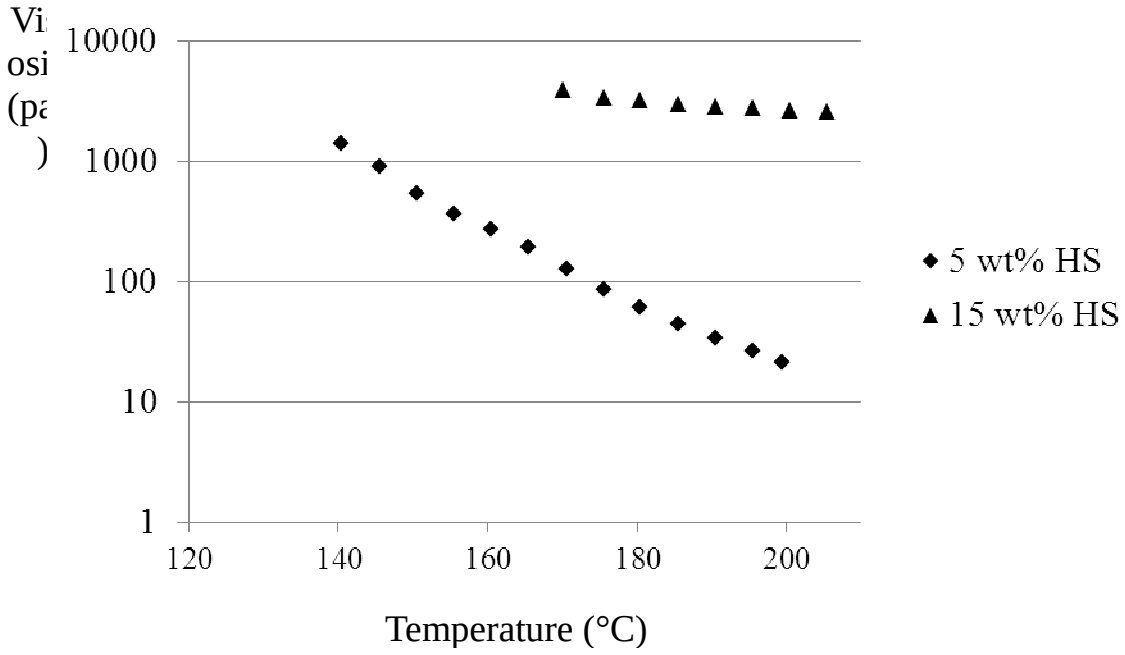

Figure 5.5. Melt viscosity of PDMS-based ionenes having 5 wt% and 15 wt% HS

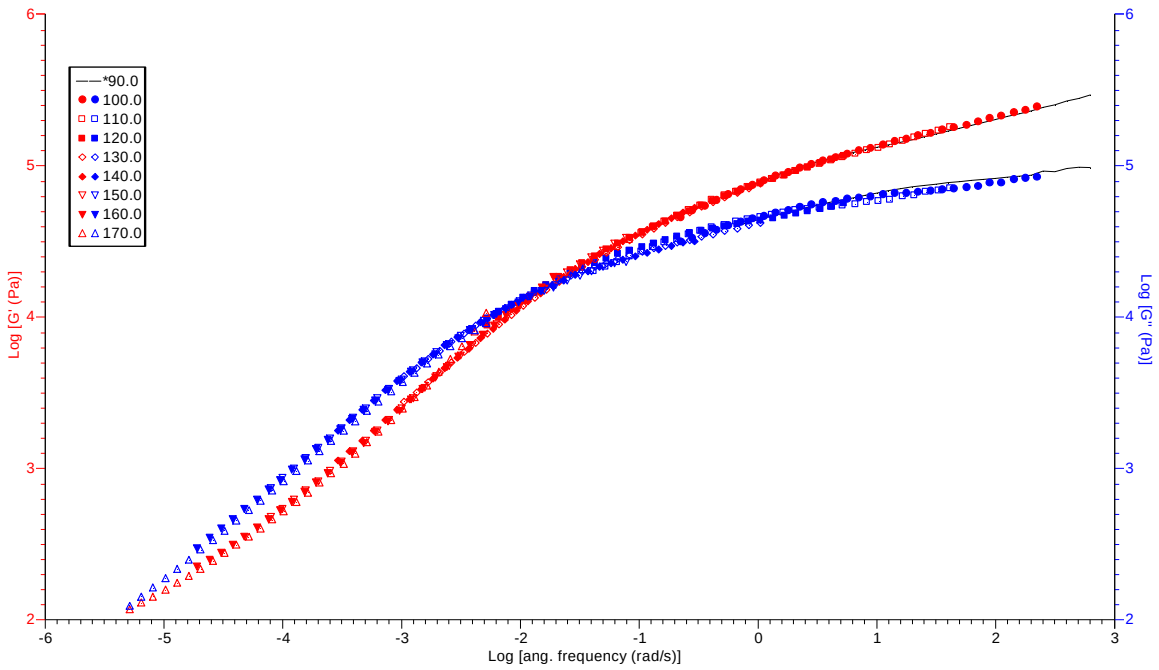

Figure 5.6. Master curve of PDMS-based ionene with 5wt% HS

5.4.6. Oxygen Transmission Rate

One technique to determine the efficiency of healing process is to measure and compare oxygen transmission rate (OTR) of virgin and healed samples. If the sample has healed successfully, the OTR values for the virgin sample and healed sample must be quite comparable. Therefore we measured the OTR values for virgin PDMS-based ionenes as a starting point. Although PDMS is well-known for its high oxygen permeation, however, the synthetic strategy and its modular nature will allow facile extension to other soft segments, including high oxygen barrier segments. Figure 5.7 demonstrates OTR values for virgin PDMS-ionenes with 5, 15, and 30 wt% hard segment content. The OTR values decreased linearly from 60000 to 15000 cc/m^2/day as the wt% hard segment increased. This indicates that the composition of the continuous phase influenced permeation, and higher ionic concentrations impeded efficient gas transport. The next step is to damage the samples and perform healing above the ionic dissociation temperature of

each sample (The healing studies will be performed in collaboration with Virginia Common Wealth University). Upon healing the OTR values will be determined and compared with virgin samples to study the healing efficiency.

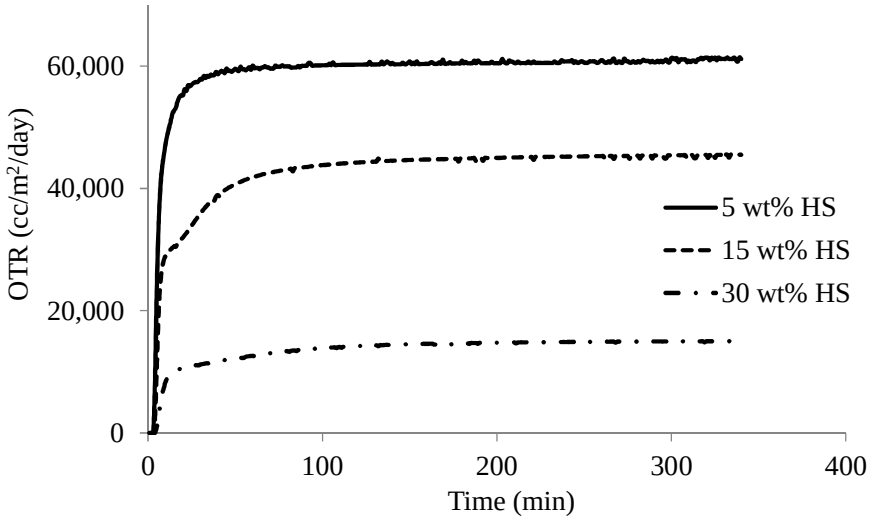

Figure 5.7. OTR values of PDMS-based ionenes with various HS contents

5.5. Conclusions

PDMS-based ionenes having various hard segment content were synthesized using Menshutkin reaction. The thermal analysis of PDMS-ionenes using DSC showed that they have one transition at -120 °C corresponding to the T_g of PDMS, further confirming microphase separation. Upon 30 wt% HS a melting transition appeared for PDMS-ionenes, corresponding to crystalline phase within the soft PDMS amorphous phase. DMA confirmed microphase separation and showed that the breadth of rubbery plateau moduli and their final softening temperatures change with the nature and content of hard segment. As the hard segment content increased from 5 wt% to 15 wt%, the rubbery plateau modulus extended from 87 °C to 164 °C due to higher physical

crosslinking. Tensile analysis demonstrated systematic increase in modulus of PDMS-ionenes with increasing hard segment content. The viscosity of polymer melt as a function of temperature showed that the viscosity of 5wt% HS PDMS-based ionene is more temperature dependent compared to 15 wt% HS PDMS-based ionene. OTR analysis revealed that OTR values for virgin PDMS-ionenes decreased linearly from 60000 to 15000 $cc/m^2/day$ as the wt% hard segment increased, indicating the influence of hard segment continuous phase on gas permeation.

Acknowledgements

The authors would like to acknowledge the financial support for this work through NASA STTR program administered by Johnson Space Center under the Contract No. NNX11CI22P for the project titled "Self-healing Inflatable Extraterrestrial shieLD (SHIELD)"

5.6. References

(1) Bergman, S. D.; Wudl, F. *J. Mater. Chem.* **2008,** 18, (1), 41-62.
(2) Kalista, S. J., Jr.; Ward, T. C.; Oyetunji, Z. *Mech. Adv. Mater. Struct.* **2007,** 14, 391-397.
(3) Kalista, S. J., Jr.; Ward, T. C. *J. R. Soc. Interface* **2007,** 4, 405-411.
(4) Sijbesma, R. P.; Beijer, F. H.; Brunsveld, L.; Folmer, B. J. B.; Hirschberg, J. H. K. K.; Lange, R. F. M.; Lowe, J. K. L.; Meijer, E. W. *Science* **1997,** 278, 1601-1604.
(5) Eisenberg, A.; Hird, B.; Moore, R. B. *Macromolecules* **1990,** 23, 4098-107.
(6) Tant, M. R.; Wilkes, G. L. In *Structure and properties of hydrocarbon-based ionomers,* 1997; Blackie: 1997; pp 261-289.
(7) Eisenberg, A. *Macromolecules* **1970,** 3, 147-54.
(8) Marx, C. L.; Caulfield, D. F.; Cooper, S. L. *Macromolecules* **1973,** 6, 344-53.
(9) Bellinger, M.; Sauer, J. A.; Hara, M. *Macromolecules* **1994,** 27, 1407-12.
(10) Hara, M.; Sauer, J. A. *J. Macromol. Sci., Rev. Macromol. Chem. Phys.* **1994,** C34, 325-73.
(11) Tadano, K.; Hirasawa, E.; Yamamoto, H.; Yano, S. *Macromolecules* **1989,** 22, 226-33.
(12) Varley, R. J.; Shen, S.; van, d. Z. S. *Polymer* **2010,** 51, 679-686.
(13) Williams, S. R.; Long, T. E. *Prog. Polym. Sci.* **2009,** 34, (8), 762-782.
(14) Williams, S. R.; Borgerding, E. M.; Layman, J. M.; Wang, W.; Winey, K. I.; Long, T. E. *Macromolecules* **2008,** 41, (14), 5216-5222.
(15) Williams, S. R.; Salas-de la Cruz, D.; Winey, K. I.; Long, T. E. *Polymer* **2010,** 51, (6), 1252-1257.
(16) Tamami, M.; Salas-de, l. C. D.; Winey, K. I.; Long, T. E. *Macromol. Chem. Phys.* **2012,** 213, 965-972.
(17) Tamami, M.; Williams, S. R.; Park, J. K.; Moore, R. B.; Long, T. E. *J. Polym. Sci., Part A: Polym. Chem.* **2010,** 48, (19), 4159-4167.
(18) Das, S.; Goff, J. D.; Williams, S.; Salas-De, L. C. D.; Riffle, J. S.; Long, T. E.; Winey, K. I.; Wilkes, G. L. *J. Macromol. Sci., Part A: Pure Appl. Chem.* **2010,** 47, 215-224.
(19) Odian, G., *Principles of polymerization*. Fourth ed.; John Wiley & Sons, Inc., Hoboken: New Jersey, 2004.
(20) Ruckenstein, E.; Chen, X. *Macromolecules* **2000,** 33, (24), 8992-9001.
(21) Yano, S.; Tadano, K.; Jerome, R. *Macromolecules* **1991,** 24, (24), 6439-42.
(22) March, J., *Advanced organic chemistry: Reactions, mechanims, and structure*. 3rd ed.; Wiley: New York: 1985.

Chapter 6. Overall Conclusions

The synthesis and characterization of novel architectures of ion-containing polymers named ionenes were described. The synergistic effect of non-covalent interactions including nucleobase hydrogen bonding and electrostatics were investigated on the properties of segmented and non-segmented ammonium ionenes.

With regard to non-segmented ionene systems, novel adenine and thymine functionalized ionene homopolymers having two different side chain spacer lengths were synthesized using Menshutkin reaction and subsequent post-polymerization functionalization was conducted via Michael addition chemistry. The effect of spacer length on hydrogen bonding interactions in 1:1 blends was studied. The shorter spacer ionene homopolymers and blends showed higher glass transition temperatures than longer spacer ionenes due to closeness of the bulky nucleobase units to the backbone and hindering the segmental motion in the ionene backbone. A single glass transition temperature confirmed the miscibility of ionene blends. The glass transition temperatures of ionene blends with shorter spacer followed the Fox equation indicating no hydrogen bonding interactions. The glass transition temperatures of the blends with longer spacer lengths deviated from both Fox and Gordon-Taylor equations, demonstrating a presence of hydrogen bonding interactions. The variable-temperature FT-IR (30 °C to 170 °C) confirmed the hydrogen bonding interactions for the longer spacer ionenes with NH_2 bending vibration shifting to lower wave numbers and C=O stretching vibration shifting to higher wave numbers with increasing temperature.

Regarding segmented nucleobase-containing ionene systems, similar post-polymerization functionalization was applied to synthesize poly(ethylene glycol)-based adenine and thymine

containing ionenes. The blends of the ionene homopolymers with complementary nucleobase-containing guest molecules resulted in efficient hydrogen bonding interactions. Job's plots and Benesi-Hildebrand analyses revealed 1:1 complexation between ionene homopolymers and guest molecules. The association constants for nucleobase-containing ionenes with complementary guest molecules were in the order of 100 M^{-1} which was in agreement with literature values. Ionene homopolymers and complexes showed a single glass transition temperature at -40 °C which corresponded to the T_g of PEG soft segment and confirmed the microphase separation.

The synthesis of silicone containing ionene copolymers was achieved through the use of PDMS dibromide oligomers, 1,12-dibromododecane, and DABCO. Hard segment contents ranged from 5-60 wt%, and structure-property relationships were established as a function of hard segment content. Thermal properties were measured via TGA and DSC. Film formation characteristics varied as a function of hard segment content, and free-standing elastic films were obtained for 5 and 15 wt% hard segment content. DMA confirmed microphase separation and showed that the breadth of rubbery plateau moduli and their final softening temperatures change with the nature and content of hard segment. As the hard segment content increased from 5 wt% to 15 wt%, the rubbery plateau modulus extended from 87 °C to 164 °C due to higher physical crosslinking. The viscosity of polymer melt as a function of temperature showed that the viscosity of 5 wt% HS PDMS-based ionene is more temperature dependent compared to 15 wt% HS ionene. Oxygen transmission rates for PDMS-ionenes decreased linearly from 60000 to 15000 $cc/m^2/day$ as the wt% hard segment increased, indicating the influence of hard segment continuous phase on gas permeation.

Chapter 7. Suggested Future Work

7.1. Synthesis and characterization of PEG-based cytosine and guanine-containing ammonium ionenes

Deoxyribose nucleic acid (DNA) structure includes four nucleobases, pyrimidines (thymine and cytosine) and purines (adenine and guanine). DNA with its supramolecular characteristics has inspired us along with many other researchers to utilize these features and develop polymers that can exhibit similar supramolecular properties. Chapter three and four of this thesis were focused on the synthesis and characterization of non-segmented and segmented adenine and thymine-containing ammonium ionenes. We studied the synergistic effect of complementary hydrogen bonding and electrostatics on various properties of ammonium ionenes. Future efforts should focus on the synthesis and characterization of cytosine and guanine-containing ammonium ionenes. Cytosine and guanine base pair interact via three hydrogen bonds with stronger degree of interaction (K_{CG} *ca.* 10^4-10^5 M^{-1}in $CDCl_3$) compared to adenine and thymine base pair with two hydrogen bonds (K_{AT} *ca.* 10^2 M^{-1} in $CDCl_3$). Therefore synthesizing polymers that contain cytosine-guanine hydrogen bonding motifs are attractive for their enhanced supramolecular characteristics. However, the synthesis of these polymers can be more challenging due to reduced solubility of these nucleobases compared to adenine and thymine. Figure 7.1 represents the proposed synthesis of cytosine and guanine-containing PEG-based ionene.

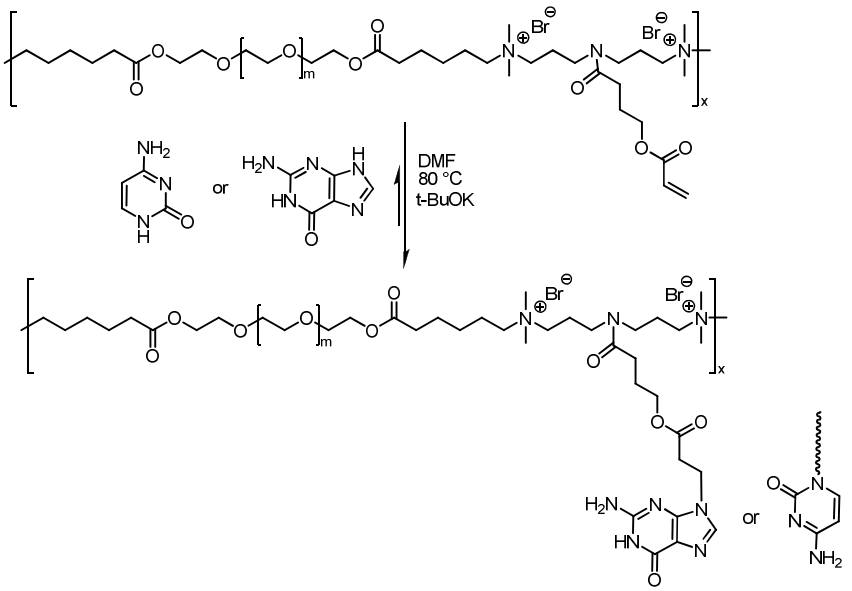

Figure 7.1. Synthesis of cytosine and guanine-containing poly(ethylene glycol)-based ammonium ionenes

7.2. Synthesis and characterization of ionenes with potential application in adhesives

As mentioned in chapter two, non-covalent interactions such as van der Waals, hydrogen bonding and electrostatics can provide physical adhesion. Hydrogen bonded polymers are specially used to prepare pressure sensitive adhesives (PSAs). Although, there have been extensive studies on the application of hydrogen bonded polymers in adhesive design, but not enough literature is present on the application of polymers that contain both hydrogen bonding and electrostatics in adhesives. Therefore, one of the future directions in the field of ionenes is to design novel architectures that have hydrogen bonding groups or moieties and measure their adhesive properties. These architectures can be linear, star-shaped, hyper-branched, and comb ionenes. For example, the synthesis of linear PEG-based ionene containing hydroxyl side groups is demonstrated in Figure 7.2. This polymer has shown potential in adhesive application.

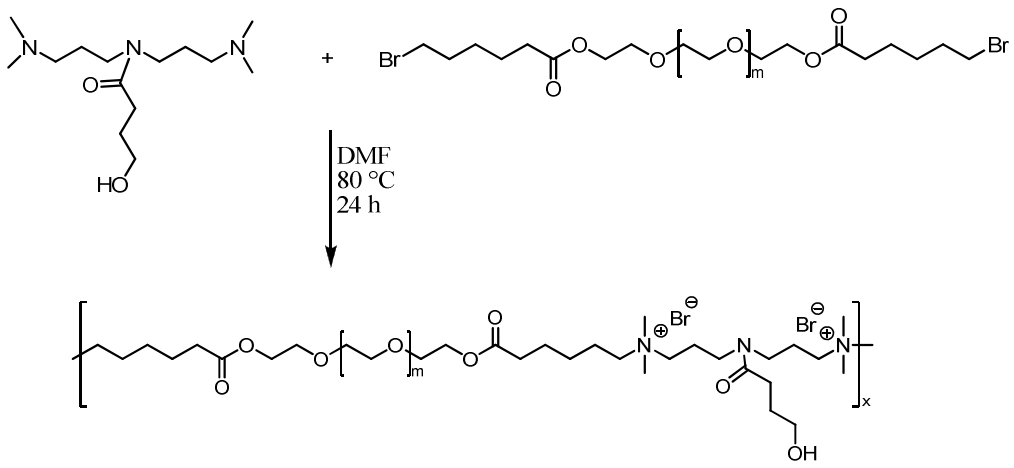

Figure 7.2. Synthesis of OH-containing PEG-based ammonium ionene

7.3. Synthesis and characterization of self-healing ammonium ionenes

Self-healing is a behavior in which a material detects its damage and heals itself either spontaneously (autonomic) or with the aid of a stimulus (non-autonomic). One series of non-autonomic materials are ionomers. Recently the application of ionomers in self-healing materials has been explored. The copolymers of ethylene and methacrylic acid (EMAA) such as Surlyn® manufactured by DuPont have shown promising self-healing behavior. In chapter five, the synthesis and structure-property relationships of silicone-based ammonium ionenes as an alternative candidate to Surlyn® were discussed. The future direction in this field is to design ionene systems that contain multiple hydrogen bonding motifs throughout the ionene backbone and investigate the effect of electrostatics and supramolecular association on self-healing behavior.